INVESTIGATING THE ROLE OF ELASTIN IN TENDON FUNCTION

Marta Sofia da Conceição Godinho

Submitted in partial fulfilment of the requirements of the Degree of Doctor of Philosophy

Supervisors: Professor Hazel Screen
Professor Steve Greenwald

Queen Mary University of London
School of Engineering and Materials Science

September 2018

Project funded by the Institute of Bioengineering (QMUL) - Bonfield Scholarship

Statement of Originality

I, Marta Sofia da Conceição Godinho, confirm that the research included within this thesis is my own work or that where it has been carried out in collaboration with, or supported by others, that this is duly acknowledged below and my contribution indicated. Previously published material is also acknowledged below.

I attest that I have exercised reasonable care to ensure that the work is original, and does not to the best of my knowledge break any UK law, infringe any third party's copyright or other Intellectual Property Right, or contain any confidential material.

I accept that the College has the right to use plagiarism detection software to check the electronic version of the thesis.

I confirm that this thesis has not been previously submitted for the award of a degree by this or any other university.

The copyright of this thesis rests with the author and no quotation from it or information derived from it may be published without the prior written consent of the author.

Signature:

Date:

Details of publications

Journal Publications

Godinho, M. S. C. et al. “Regional Specific Effect of Elastin Depletion on the Mechanical Properties of Tendon”. (For submission – Chapter 4)

Godinho, M. S. C. et al. (2017) ‘Elastin is Localised to the Interfascicular Matrix of Energy Storing Tendons and Becomes Increasingly Disorganised With Ageing’, Scientific Reports. Springer US, 7(1), p. 9713. (Chapter 3)

Thorpe, C. et al. (2015) ‘The interfascicular matrix enables fascicle sliding and recovery in tendon, and behaves more elastically in energy storing tendons’, Journal of the Mechanical Behavior of Biomedical Materials. Elsevier, 52, pp. 85–94. (Chapter 4 Protocols)

Conference Abstracts

“Regional Specific Effect of Elastin Depletion on the Mechanical Properties of Tendon”, M S C Godinho, C T Thorpe, S E Greenwald, H R C Screen. BioMedEng18, September 2018, London, UK – Oral Presentation

“Elastin is Localised to the Interfascicular Matrix of Energy Storing Tendons and Becomes More Disorganised With Ageing”, M S C Godinho, C T Thorpe, S E. Greenwald, H R. C. Screen. SB3C, June 2017, Tucson, Arizona – Oral Presentation

“Elastin is More Abundant in Energy Storing Tendons and is Localised to the Tendon Interfascicular Matrix”, M S C Godinho, H R C Screen, S E Greenwald, C T Thorpe. BSMB Spring Meeting 2016, Chester, UK – Oral & Poster Presentations

“The Interfascicular Matrix Allows Fascicle Sliding and Recoil in Tendon and Exhibits Greater Elasticity in Energy Storing Tendons”, M S C Godinho, C T Thorpe, G P Riley, H L Birch, P D Clegg, H R C Screen. BSMB Satellite Meeting “Advances in tendon research – From Bench to Bedside” September 2015, London, UK – Poster Presentation

Conference Awards

BioMedEng18, September 2018 - ARUK Travel Awards

The Armourers & Brasiers Gauntlet Trust Research Student Travel Grant, July 2017 - Armourers & Brasiers Materials Science Scheme

The Physiological Society Travel Grant, May 2017 - The Physiological Society Travel Grant Scheme.

The British Society of Matrix Biology Reporter Bursary, April 2017 - The British Society of Matrix Biology Bursary Scheme

Acknowledgments

Firstly, I would like to thank my supervisor, Professor Hazel Screen for her support, guidance, and friendship throughout these years. I could not have had a more dedicated, enthusiastic, hardworking supervisor, who always sees the positive side of all things. Definitely the person who inspires me the most in work and life.

Further, thanks to my supervisor Professor Steve Greenwald for his support and guidance, and for helping me expand my selection of special English words.

I would also like to thank Dr Chavaunne Thorpe for her support, patience and for answering all of my questions, and teaching me most of the lab skills and techniques that I know. Thanks to Dr Steven Thorpe for helping me so many times in the lab and also with my data analysis. I would also like to thank David Crane, Susan Crane, Rebecca Norton and Pedro Santos for all the help with my image scoring.

Further, thanks to Professor William Bonfield and the Institute of Bioengineering for funding this research.

I would also like to thank my friends at QM who made these 4 years really enjoyable, in particular to Daniel, Kathrin, Sheetal and Servann, it would not have been the same without them.

A big thank you to my amazing parents and sisters who have always supported me in this big adventure. Finally, I would like to thank my fiancé, Pedro Trepa for constantly pulling me up in difficult times, but most importantly for his love, patience, constant support, encouragement and belief that I could do this, and always being there when I needed.

Abstract

Tendon is composed of fascicles bound together by interfascicular matrix (IFM). Energy storing tendons are more elastic and extensible than positional tendons; behaviour provided by specialisation of the IFM to enable repeated interfascicular sliding and recoil. With ageing, IFM becomes stiffer and less fatigue resistant, potentially explaining why older tendons become more injury-prone. Recent data indicates enrichment of elastin within the IFM, but this has yet to be quantified and the role of elastin in IFM mechanics remains unknown. This thesis aims to quantify elastin content, organisation and fragmentation, and its influence on tendon mechanics, in both fascicular matrix (FM) and IFM of functionally distinct tendons, and how this changes with ageing.

It was hypothesised that elastin is mainly localised to the IFM of energy storing tendons and becomes increasingly disorganised with ageing. Further, it was hypothesised that elastin depletion affects the mechanical properties of IFM, specifically fatigue resistance and recoil ability, but will not affect fascicles.

Biochemical analyses and immunohistochemical techniques were used to determine elastin content and organisation in young and old equine energy storing and positional tendons. Elastase treatments were conducted in young and old IFM and fascicle samples from energy storing tendons to deplete elastin, after which failure, fatigue and recovery mechanical tests were performed, comparing IFM and fascicle mechanical properties before and after elastase treatment.

Supporting the hypothesis, elastin localises to the IFM of energy storing tendons, reducing in quantity and becoming increasingly disorganised with ageing. Further, elastin depletion did not affect fascicle mechanics, but lead to reduced mechanical properties and fatigue resistance in the IFM. These changes may contribute to the increased injury risk in aged energy storing tendons. Full understanding of the processes leading to loss of elastin and its disorganisation with ageing, may aid in the development of treatments to prevent age related tendinopathy.

Contents

List of Figures

List of Tables

Abbreviations

A	Alanine
AFM	Atomic Force microscopy
APEDS	Activated papain enzyme digestion solution
CDET	Common Digital Extensor Tendon
COMP	Collagen Oligomeric Matrix Protein
CRISPR	Clustered Regularly Interspaced Short Palindromic Repeats
DIC	Digital Image Correlation
EBP	Elastin Binding Protein
ECM	Extracellular Matrix
ES	Energy-Storing
ESWT	Extracorporeal Shock Wave Therapy
FBN-1	Fibrillin-1
FBN-2	Fibrillin-2
FM	Fascicular Matrix
GAG	Glycosaminoglycan
Gly	Glycine
I	Isoleucine
IFM	Interfascicular Matrix
L	Leucine

LCM	Laser Capture Microdissection
MCL	Medial Collateral Ligament
NSAIDS	Nonsteroidal Anti-Inflammatory Medication
P	Proline
PBE	Papain Buffer Extract
PBS	Phosphate-Buffered Saline
PGs	Proteoglycans
ROI	Region of Interest
ROS	Reactive Oxygen Species
SDFT	Superficial Digital Flexor Tendon
SEM	Standard Error from the Mean
SLRPs	Small Leucine Rich Proteoglycans
TEM	Transmission Electron Microscopy
V	Valine

Chapter 1 - Introduction

1.1. General Introduction

Tendons provide an attachment from muscle to bone, playing an important role in locomotion. Their primary function is to transfer the force generated by muscle contraction to the skeleton, facilitating movement around joints and positioning limbs (Alexander 1991, Benjamin & Ralphs 1997).

For efficient function, tendons must be strong and stiff under uniaxial tension but, at the same time, incorporate some viscoelasticity to optimize their stiffness to meet different loading conditions (Kubo et al., 2002, Ker 2007). These properties are conferred by the molecular composition of tendon and the interaction of structural molecules in the extracellular matrix (ECM). Tendons are comprised mainly of hierarchically organised type I collagen molecules, which results in high tensile strength. In addition to transferring force, some tendons have an additional role, in energy storage (Alexander, 1991), acting as a spring to store and release energy as they stretch during stance phase and recoil during the flight phase, reducing the energy cost of locomotion (Figure 1) (Alexander, 1991).

The human Achilles tendon and the equine superficial digital flexor tendon (SDFT) (Figure 1) are two examples of energy-storing (ES) tendons. These tendons experience high forces during locomotion, acting with low safety margins. Thus, ES tendons are more compliant than the positional tendons, storing considerable potential energy in their elongated state (Alexander 1991, Batson et al., 2003, Lichtwark & Wilson 2007). On the other hand, tendons such as the human anterior tibialis and equine common digital extensor tendon (CDET) (Figure 1) are examples of positional tendons. These tendons are loaded predominantly by muscular contraction and are subjected to lower strains compared to ES tendons (Kear & Smith 1975). Exercise – induced injury of positional tendons is subsequently rare (Ely et al., 2009, Markarian et al., 1998).

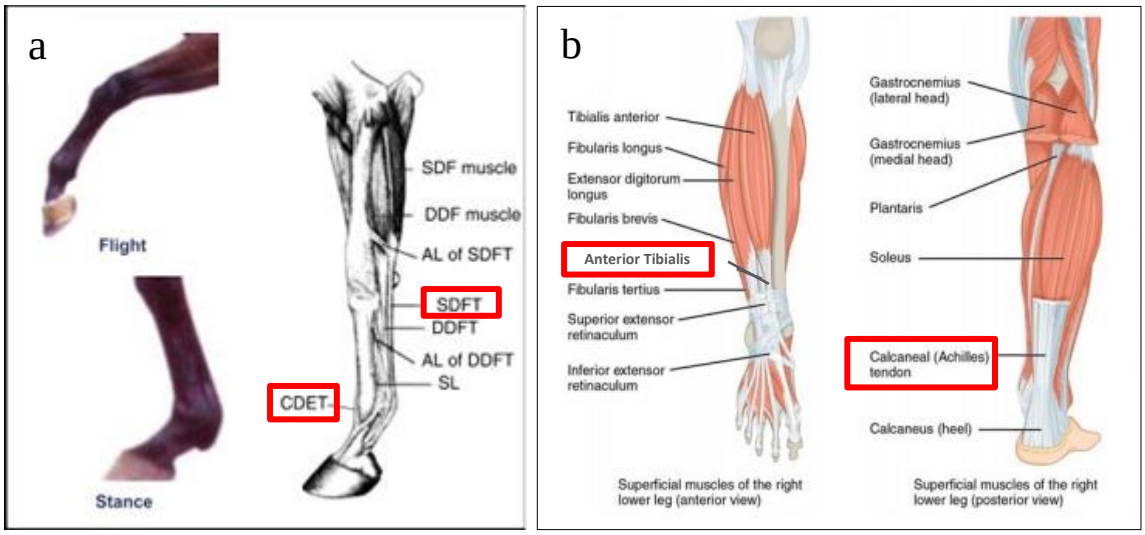

Figure 1: Illustration of the equine forelimb (a) and human leg (b). The superficial digital flexor tendon and common digital extensor tendon are identified in the equine forelimb (a). The positioning of the limb during movement is shown, highlighting how the SDFT is stretched during stance phase, and recoils during the flight phase. In the flight phase, the CDET undergoes much lower strains to position the limb. The equivalent energy storing Achilles tendon and positional anterior tibialis tendon, are indicated in the human leg (b). Adapted from Birch (2007), Betts et al., (2013).

The mechanical properties of tendon tissue vary according to its function, and so, reflect different functional behaviour between tendon types. Despite a great variation in SDFT strength and stiffness between individual horses (Birch 2007), the SDFT consistently fails at significantly higher strains than the CDET (Batson et al., 2003). In vivo, strains of up to 16.6 per cent have been recorded in the equine SDFT during galloping (Stephens et al., 1989), and strains that exceed 10.3 per cent have been recorded during hopping in the Achilles tendon (Lichtwark & Wilson 2005). In positional tendons, maximum strains of 2.5 per cent have been estimated in the CDET (Batson et al., 2003, Birch et al., 2008b) and strains up to 3.1 per cent have been measured in the human anterior tibialis tendon (Maganaris & Paul 1999). Reflecting these different functional demands, in vitro mechanical testing to failure has shown that the SDFT fails at approximately 23 per cent strain (Dowling et al., 2002, Gerard et al., 2005, Thorpe et al., 2012). By contrast, maximum in vitro failure strains have been estimated at 18 per cent in the CDET (Thorpe et al., 2012). Data highlighted that ES tendons function with a far smaller safety margin (Batson et al., 2003).

The SDFT has a lower elastic modulus and failure stress when compared to the CDET, enabling it to stretch to store (Batson et al., 2003). By contrast, the CDET requires greater stiffness in order to efficiently reduce the muscular work required to keep tendon tension (Batson et al., 2003).

Previous studies indicate that the differences in the material properties of each tendon type are determined by the compositional and organisational variations in the matrix (Birch et al., 2008a, Birch 2007). However, specifically how some of the matrix structural components influence the functionality and mechanical properties of specific tendons is yet to be determined.

The high strains energy storing tendons must withstand make them more prone to highly debilitating and painful injuries, compared to tendons that function purely to position the limb (positional tendons) (Shepherd & Screen 2013).

Tendon injuries, known as tendinopathies, are increasingly prevalent but extremely difficult to treat, mainly as we have very limited understanding of the aetiology and pathophysiology of these conditions (Riley 2008). It is known that the incidence of injury increases with age (Kannus et al., 1989), and is a recurrent problem, likely due to the slow and inadequate tendon healing response. The healing tendon tissue has a different structure, which is likely to be weaker than the original tissue (Corr et al., 2009).

Recent studies have focused on understanding the contribution of individual structural molecules to whole tendon mechanics, which have been useful in order to better understand and treat tendon disorders. This is important as tendon injury is one of the most common musculoskeletal injuries both in athletes and the general population, affecting up to one in three adults over the age of 50 (Järvinen et al., 2005, Tempelhof et al., 1999).

1.2. Epidemiology of Tendon Injuries

Tendon injury is one of the most common musculoskeletal injuries that occur both to athletes and the general population (Clayton & Court-Brown 2008). However, it is also the most common form of musculoskeletal injury in horses (Ely et al., 2009). A survey of thoroughbred injuries and fatalities at British racecourses found that injuries to the musculoskeletal system account for 82 per cent of all injuries to racehorses and, of these, 46 per cent involved the flexor tendon or the suspensory apparatus (Williams et al., 2001). Tendons in the horse forelimbs are the most affected, accounting for 97-99 per cent of the tendon injuries, with the energy storing SDFT being injured the most (Kasashima et al., 2004).

Humans and horses have a similar mechanism for the initiation and progression of tendon injury (Lui et al., 2011, Innes & Clegg 2010). The human Achilles tendon is the most commonly injured tendon in runners, in the same manner as the SDFT in horses (Knobloch et al., 2008, Thorpe et al., 2010a). On the other hand, the CDET and human anterior tibialis are rarely injured; this may be due to the fact that positional tendons experience much lower strains than those that act as energy stores. It is proven that the risk of tendinopathies increases significantly with ageing in both human and equine ES tendons (Knobloch et al., 2008, Hess 2010, Kasashima et al., 2004) and is more common in males (Clayton & Court-Brown 2008, Kannus et al., 1989).

It is not fully clear why ageing is a crucial factor that predisposes humans and animals to tendon injuries. Some studies have suggested that this may happen due to an accumulation of micro-damage within the tendon ECM or may be due a reduction in the ability of cells in aged tendons to maintain and repair the matrix (Smith et al., 2002a).

Tendinopathy is the generic name for a variety of painful conditions developing in and around tendons in response to overuse. It is usually associated with histopathologic changes such as degeneration and disorganization of collagen fibres, increased cellularity and minimal inflammation (Khan et al., 1999, Soslowsky et al., 2000). The recurrence of tendon injury is very common and, in some cases, the symptoms can last for several years. Traditional treatments for tendinopathy are focussed on reducing inflammation; however, these may not be the most effective option. Nonsteroidal anti-inflammatory medication (NSAIDS) and corticosteroids, used to control inflammation, purport to provide some pain relief in short term,

although their effectiveness is not proved in the long term (Andres & Murrell 2008, Almeikinders & Temple 1998). A vast range of other treatments are used to treat tendinopathy, such as eccentric strengthening exercises, glyceryl trinitrate patches and extracorporeal shock wave therapy (ESWT), however most current treatment options are neither effective nor evidence-based (Andres & Murrell 2008, Riley 2008). In fact, there is remarkably little evidence that any therapies are effective. The relationship between basic tendon structure and function in different tendon types is not yet understood. Also, little is known about how tendon mechanical properties are affected by ageing and injury and also by some ECM components. Such understanding is a fundamental first step towards understanding healthy function and the aetiology of tendinopathy, and thus, developing treatments able to prevent or reverse the degenerative process of tendinopathy and maybe even regenerate healthy tendon.

Various animal models have been developed in order to study the aetiology of tendinopathy. Most in vivo animal models available at present are small animal, and rely on either prolonged mechanical stimuli to induce overuse injury to the tissue (Huang et al., 2004, Jelinsky et al., 2008) or inflammatory drug treatments (Sullo et al., 2001). An in vivo approach provides the ability to examine how various repair mechanisms and signals from other areas of the body interact with the injured tendon. However, the interaction of all factors is very complex, and it is very difficult to investigate some of the basic molecular biology. Furthermore, reproducibility of the injuries provoked in small animals, such as rats, rabbits and mice, is variable between different animals, and dependent on the tendons used. Also, particularly in rodent models, damaged tendons seem to heal when overuse training is interrupted, in contrast with what happen in human clinical situations (Sullo et al., 2001, Huang et al., 2004, Jelinsky et al., 2008). In contrast, in vitro models of tendinopathy have utilised tendon explants from a wider variety of species and investigated the influence of mechanical or chemical injury in culture. Such models are generally easier to control and the molecular mechanisms occurring in response to injury are more easily investigated (Spiesz et al., 2015). However, whilst a simpler investigation of many different cellular processes, such as DNA synthesis, mitosis, gene expression, and cell differentiation is enabled, the study of cells outside their normal environment ultimately limits the translatability of the findings. Taken together, it has become clear that one perfect model of tendinopathy does not exist. Instead, finding appropriate treatments for

tendinopathy will likely arise from a culmination of experiments carried out in these models, which can then be applied to patients based on their unique characteristics.

1.3. Tendon Composition and Structure

Tendon has often been used as a model for structure-function studies because of its simple and highly ordered structure (Kastelic et al., 1978). Its specialised organisation and molecular composition result in a high strength structure, able to bear uni-directional forces (Kastelic et al., 1978).

Tendon is a fibrous connective tissue, composed predominantly of type I collagen interspersed with tenocytes (tendon cells) and non-collagenous matrix, such as proteoglycans (Benjamin & Ralphs 1997). Tropocollagen molecules are grouped together to form fibrils, connected by intermolecular chemical crosslinks, resulting in high tensile strength (Avery & Bailey 2005, Birch et al., 1999). In turn, these fibrils, which are generally aligned along the long axis of the tendon (Kastelic et al., 1978), group together in order to form fibres, fascicles and finally the entire tendon, which is surrounded by a connective tissue sheath called the epitenon (Kastelic et al., 1978) (Figure 2).

Tendon is composed of three main components: water, which makes up approximately 70% of the wet weight, extracellular matrix (ECM) and tenocytes (Elliott, 1965). The ECM consists predominantly of collagen type I molecules, constituting approximately 75 per cent of the dry tissue weight (Kjaer, 2004). In addition to type I collagen, which makes up approximately 95% of the total collagen content in tendon, a few other different types of collagen have also been identified, such as collagen types III, V, XII and XIV. The ECM also contains a small percentage of non-collagenous proteins, such as glycoproteins, proteoglycans (PGs) and a varying amount of elastin (Kannus, 2000). Approximately 10% of the tendon is cellular, and the major cell type is the tenocyte (Elliott, 1965).

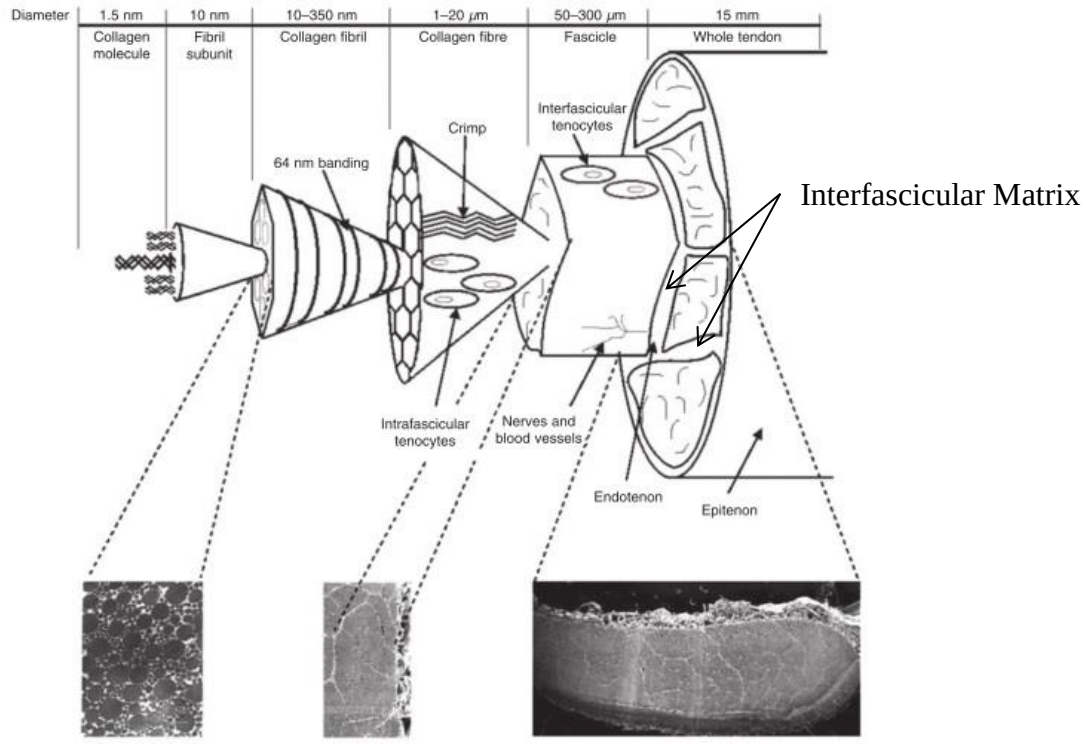

Figure 2: Schematic of the tendon hierarchical structure. The organisation of tendon structure from collagen fibrils to the entire tendon is illustrated. The differences between each level of the hierarchy are demonstrated in the schematic and the diameter of each structure is indicated. Adapted from Thorpe et al., (2010a).

1.3.1. Collagen Structure

Collagen is a fibrous protein, and the most abundant protein in mammals. To date, at least 28 different types of collagen have been identified, although most connective tissues are composed predominantly of collagen types I, II or III (Burgeson, 1988). The most abundant collagen in tendon and ligament is type I. The fibril forming type I collagen is responsible for the tendon's high tensile strength. The second most abundant collagen in tendon is another fibrillar collagen – type III – which constitutes up to 10% of the total collagen, depending on tendon type and age (Birch et al., 1999). This collagen seems to play an important role in fibrillogenesis and the regulation of the type I collagen fibrils, and has been identified in immature and healing tendons (Banos et al., 2008). Collagen type V, is another fibrillar collagen in tendon, and is commonly found in the core of type I fibrils, where it is also important in the fibrillogenesis process (Riley 2004). The other types of collagen are characterised as

non-fibrillar collagens. Type IX, XII and XIV are examples of fibril-associated collagens with interrupted triple helices (Burgeson 1988, Banos et al., 2008), which play an important role by providing a molecular bridge between fibrillar collagens and the rest of the ECM and also maintaining the tensile integrity of the tendon.

1.3.2. Collagen Synthesis

Collagen synthesis is the responsibility of fibroblasts and other connective tissue cells. The collagen molecule is composed of three wound polypeptide α chains, which form a rope-like super helix. The three individual chains, known as pro-α chains, coil together to form a slow right-handed helix with a length of approximately 300 nm (Kastelic et al., 1978), known as procollagen molecule.

The procollagen molecule consists of a triple helical region with non-helical amino (N-) and carboxy (C-) terminal telopeptides at each end (Figure 3) (Canty & Kadler 2005). Each polypeptide chain that forms the triple helical procollagen molecule has a repeating Glycine (Gly)-X-Y triplet, where X and Y are normally proline and hydroxyproline, respectively (Canty & Kadler 2005). Glycine (Gly) is the smallest amino acid, and in this case the one that permits the procollagen molecule to form a helical structure, which is stablished by hydrogen bonds (Canty & Kadler 2005).

Several post-translational modifications occur to the polypeptide chains, including hydroxylation of proline and lysine residues. After the formation of the procollagen triple helix, the assembled polypeptide chains are transported to the Golgi apparatus, where the N- and C- propeptides are removed, resulting in collagen molecules, which are then able to assemble into fibrils (Canty & Kadler 2005).

This process of assembling procollagen to form fibrils, is known as fibrillogenesis. Collagen type III, XII, XIV and Small Leucine Rich Proteoglycans (SLRPs) are thought to be involved in the regulation of fibrillogenesis, however there are other molecules which may help in this process as well (Banos et al., 2008). Fibrils in tendon are tightly packed and aligned along the long axis of the tissue. However, fibrils do not run perfectly straight and, in some areas, they present a crimped or kinked configuration (Franchi et al., 2010), which tends to disappear when they are under tension (Franchi et al., 2007). The crimp arrangement is dependent on the way the

tropocollagen was formed into fibrils, and is thought to relate to the variations in crimp morphologies seen between species and with tendon type (Franchi *et al.*, 2010).

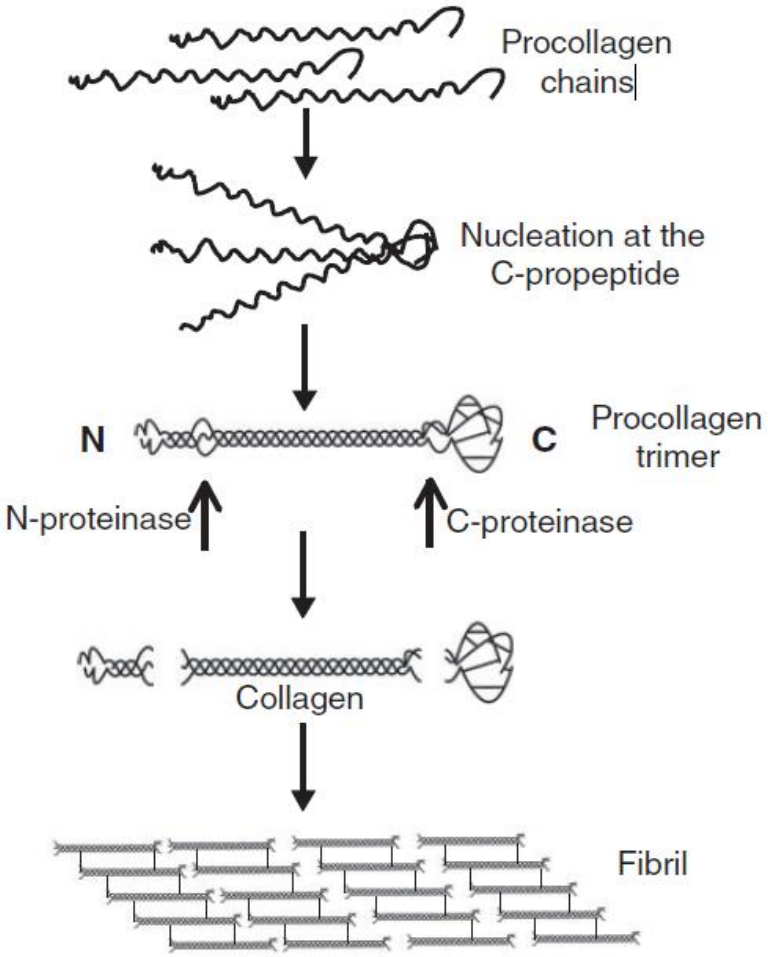

Figure 3: Schematic image showing the overview of the steps involved in the synthesis of collagen fibrils by fibroblasts. Adapted from Canty and Kadler, (2005)

1.3.3. Collagen Cross-linking

Fibrils are joined together by the formation of crosslinks between them, which help increase the tendon tensile strength. There are two different types of crosslinks formed in collagenous tissue: enzymatic and non-enzymatic adventitious crosslinks. The enzymatic crosslinks occur during the growth of immature tendons and are initiated by lysyl oxidase. On the other hand, non-enzymatic crosslinks are characterized by spontaneous reactions with sugars that happen to be present in the matrix.

1.3.4. Proteoglycans and Glycoproteins

Proteoglycans (PGs) are composed of a varying number of glycosaminoglycan (GAG) chains, covalently attached to a protein core. The proteoglycan core protein binds to the collagen fibril at specific sites, and the GAG side-chains interact with side-chains from other PGs, holding the fibrils at defined distances from each other (Scott, 1995). Thus, it is thought that PGs may influence directly the mechanical properties of tendon, improving the resistance to tensile loading (Scott 1995, Screen et al., 2005).

The most abundant proteoglycans found in tendon are the small leucine rich proteoglycans (SLRPs): decorin (the predominant PG in the proximal/tensional regions of the tendon and the one with the smallest core protein), biglycan, fibromodulin, lumican and also a small amount of aggrecan (Rees et al., 2000). The structure and function of proteoglycans found in tendons are described in Table 1. Glycosaminoglycans (GAGs) are long polysaccharide chains, composed of repeating disaccharide units. These hydrophilic chains are highly negatively charged, due to the sulphate or carboxyl group attached to the sugar residues. Also, as a result of their negative charge, they increase water absorption. In terms of glycoproteins, the most abundant in tendon tissue is cartilage oligomeric matrix protein (COMP), which is thought to play an important role in the fibrillogenesis and tendon development (Smith et al., 2002b).

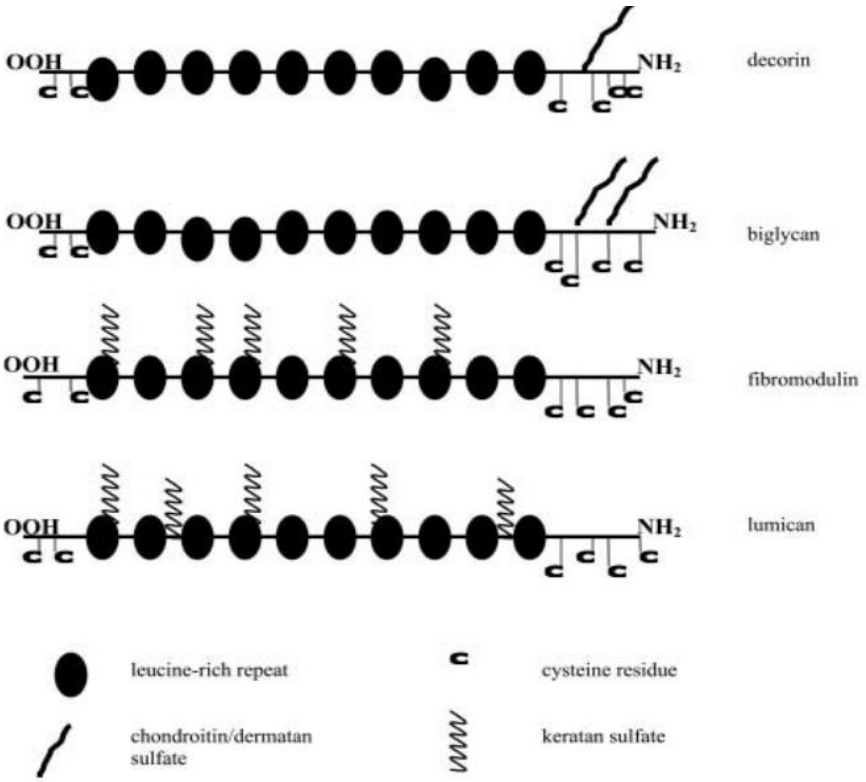

Figure 4: Schematic image illustrating the different small-leucine rich proteoglycans (SLRPs) present in tendon. Modified from Yoon and Halper, (2005).

Table 1: Resume of the properties of the most abundant proteoglycans within tendon. Adapted from (Yoon and Halper, 2005)

Name	Class	Core Protein size (kDa)	Structure and function in tendon
Decorin	SLRP	36	One GAG chain; Binds to fibrillar collagen; regulates collagen fibril structure and cell proliferation
Biglycan	SLRP	38	Binds to fibrillar collagen; predominant in cartilage
Fibromodulin	SLRP	42	Binds to type I collagen; helps formation of mature large collagen fibrils; modulation of tendons strength.
Lumican	SLRP	38	Binds to type I collagen; modulation of tendon strength.
Aggregan	Modular	220	Provides resilience; mainly present in the compressed regions

1.3.5. Elastin & Elastic Fibre Function

Elastic fibres are major components of the ECM in many dynamically loaded tissues, particularly those requiring fatigue resistance (Braverman & Fonferko 1982, Pierce & Hocott 1960) and those undergoing large strains. They are composed of elastin and fibrillin microfibrils (Kielty et al., 2002), and are normally categorized in terms of the amount of elastin present in their structure. Mature elastic fibres contain a dense elastin core accounting for approximately 90% of the entire fibre, whereas elaunin fibres contain an intermediate amount of elastin. Elastic fibres which are composed entirely of microfibrils are called oxytalan fibres (Montes, 1996). The low modulus of elasticity and high resilience of elastin, allows elastic fibres to complement the collagen fibrillary tensile strength (Kielty et al., 2002). These particular properties are extremely important to the function of certain tissues such as blood vessels, lungs and skin as they undergo high deformations and efficient recoil. Elastin is an elastomeric protein, and one of the major structural proteins which provides extensibility and flexibility to the ECM. It is an important load-bearing protein in the bodies of vertebrates. Elastin is used specifically in tissues requiring high fatigue resistance or energy storage, as a result of its highly elastic mechanical behaviour and resilience (Greenwald 2007, Oxlund et al., 1988, Lee et al., 2001).

Studies of elastin have generally focused on the cardiovascular system, where is thought elastin mechanical properties predominantly account for tissue stiffness at low strains. In an unloaded artery, both collagen and elastin appear undulated and wavy. As pressure increases and the artery reaches physiological loads between 50-150 kPa, elastin is straightened and loaded, but less than 10% of the collagen fibres are straight and load bearing (Clark & Glagov 1985). As the pressure increases above physiological loads, the collagen fibres become straighter and load bearing also (Wolinsky & Glagov 1964, Carta et al., 2009) (Figure 5). Similarly, in the skin, while collagen is the main source for the mechanical strength and stiffness, elastin is thought to be responsible for the initial extensibility of the tissue (Oxlund et al., 1988). Elastin contributes to the compliance of a tissue by maintaining collagen in a crimped configuration, acting as a shock absorber when the force is applied (Oxlund et al., 1988).

Studies of elastin in tendon are limited in number, and draw no firm conclusions. There remains debate concerning its abundance, or even presence, and no role for elastin in tendon has been identified (Shepherd & Screen 2013, Riley 2008).

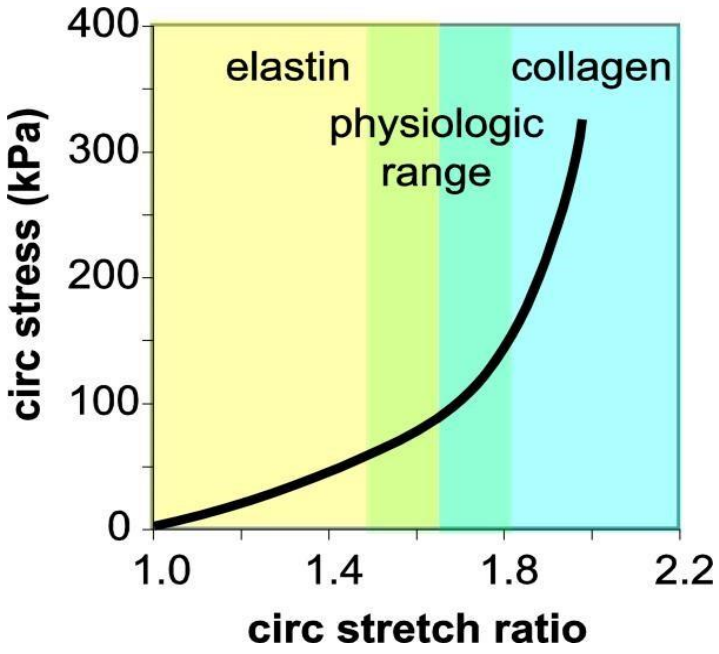

Figure 5: Representative circumferential stress-stretch relationship for the mouse ascending aorta. At low pressure, the low stiffness behaviour of the aorta is dominated by elastin and at high pressure, dominated by collagen. The range of physiological blood pressures are indicated on the graph. Image from Carta et al., (2009).

1.3.6. Elastin Biosynthesis and Biochemical Characterisation

Elastin, was initially characterised as an amorphous polymer. However, some recent studies have suggested that elastin contributes to a vast range of biologic properties (Blanchevoye *et al.*, 2013). Its presence in the extracellular matrix has important implications at the cellular and tissue level.

The elastin gene is localized in chromosome 7 in humans (Fazio et al., 1991) and expressed by various cell types during pre- and neo-natal phases of development (Davidsons et al., 1982). Tropoelastin, the product of the elastin gene, is a protein of approximately 800 residues and its full sequence is already known for the human, cow, chick, rat, mouse and sheep species (Bressan et al., 1987, Indik et al., 1987, Mauch et al., 1994, Raju & Anwar 1987, Wydner et al., 1994). The elastin gene is normally

composed of 34 exons (human) and 36 exons (bovine) and one intron (exon ratio of 20:1), some of which code for lysine-containing segments (cross-linking domains), others for hydrophobic sequences (Indik et al., 1987, Fazio et al., 1991) (Figure 6).

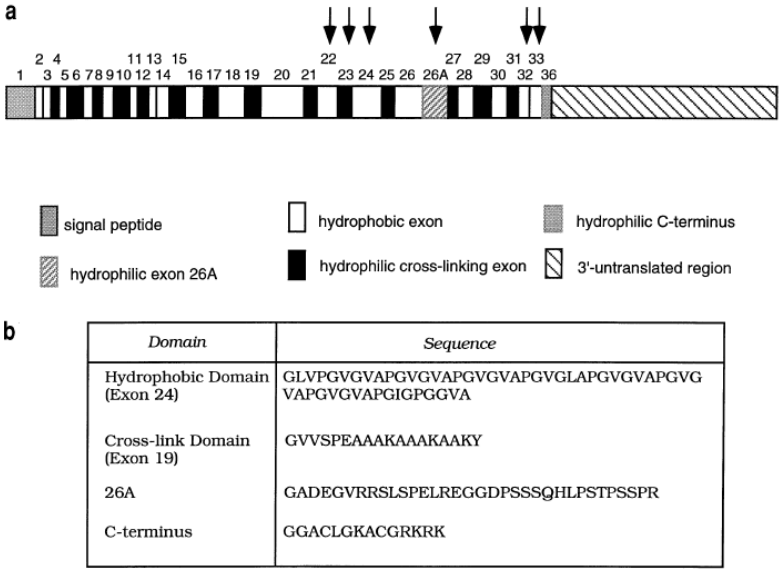

Domain	*Sequence*
Hydrophobic Domain (Exon 24)	GLVPGVGVAPGVGVAPGVGVAPGVGLAPGVGVAPGVG VAPGVGVAPGIGPGGVA
Cross-link Domain (Exon 19)	GVVSPEAAAKAAAKAAKY
26A	GADEGVRRSLSPELREGGDPSSSQHLPSTPSSPR
C-terminus	GGACLGKACGRKRK

Figure 6: Structure of human tropoelastin. (a) cDNA structure; (b) typical amino acid selected sequences Exons subjected to alternate splicing are marked with an arrow. Adapted from Vrhovski & Weiss (1998).

Tropoelastin is the soluble, monomeric form of elastin secreted by cells, which is present in solution in both globular and extended forms (Toonkool et al., 2006). Its hydrophobic domains are dominated by the following aliphatic residues: proline (P), alanine (A), valine (V), leucine (L), isoleucine (I) and glycine (G), which are very repetitive and usually described as di-, tri-,tetra-, hexa- and nona-peptides (Foster *et al.*, 1973). The tropoelastin crosslinking domains are either alanine-rich (termed KA) or proline-rich (termed KP) regions, comprising either two or three lysyl residues (Foster et al., 1974, Keeley et al., 2002). Thus, the tropoelastin structure consists of alternating hydrophobic and cross-linking domains.

1.3.7. Elastogenesis

The process responsible for the formation of functional elastin within the elastic fibre is known as elastogenesis. The deposition of elastic fibres is highly regulated during development and it is considered a very complex process. Elastogenesis starts inside the cell (Figure 7) when the tropoelastin molecule is synthesised. After that, tropoelastin binds to a receptor complex consisting of at least three proteins: a peripheral 67 kDa elastin-binding component in concert with 61 kDa and 55 kDa membrane-binding proteins. The 67 kDa domain is identical to β-galactosidase and has at least two binding sites: one for tropoelastin and another for lectin. The elastin-binding protein (EBP) binds the tropoelastin and acts as a chaperone, preventing premature intracellular aggregation of tropoelastin molecules (Hinek & Rabinovitch 1994). When the complex (tropoelastin-chaperone) is excreted into the extracellular region, the companion chaperone loses its affinity for tropoelastin when it interacts with galactosugars. Consequently, the tropoelastin is released locally and the chaperone is recycled (Hinek, 1997) (Figure 7).

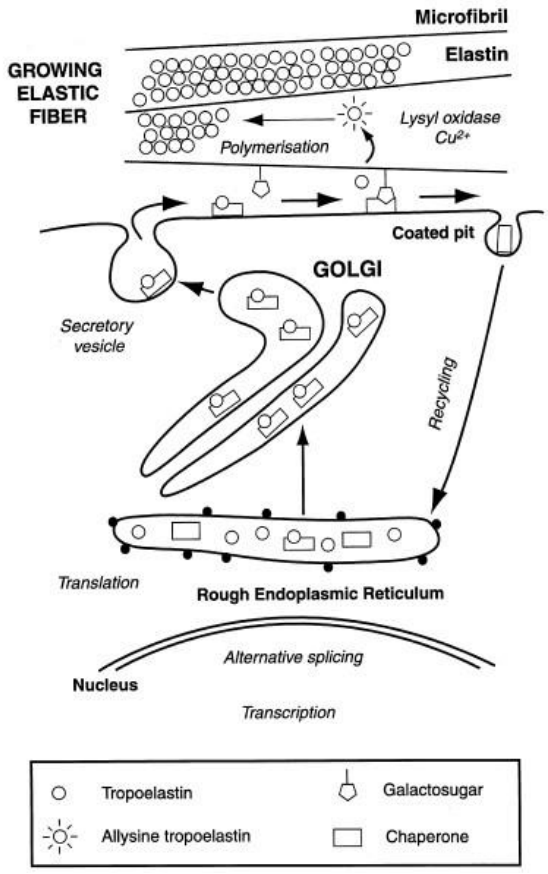

Figure 7: Schematic image of elastin deposition. Image adapted from Hinek, (1997).

There are three known fibrillin isoforms, which have different spatial and temporal expression patterns – fibrillin-1, -2 and -3 (Corson et al., 2004, Zhang et al., 1995). Fibrillin-1 (FBL-1) is the most abundant isoform in mature tissues, whilst fibrillin-2 (FBL-2) is usually expressed during early development stages (Ramirez & Pereira 1999). Both types of fibrillins are secreted as profibrilin dimers or trimers which then undergo N- and C- terminal processing to enable fibre assembly (Cain *et al.*, 2006). In Figure 8(a) it is possible to see the assembly of fibrillin into microfibrils and the association of microfibrils with tropoelastin to form elastic fibres. Initially, the profibrillin secreted is processed and assembled into pericellular microfibrils and microfibril bundles Figure 8a (i); the elastin globules are aligned correctly and promptly modified by lysyl oxidase. Then, the elastin is incorporated in the microfibril scaffold by irreversible polymerization Figure 8(ii); finally, in the core of the mature elastic fibre, it is visible, rope-like structures of highly cross-linked elastin (Ronchetti et al., 1998). In Figure 8b, Exon 21, for instance, encodes a cross-linking domain in which pairs of lysine residues (K) are separated by two or three alanine (A) residues. On the other hand, exon 24 encodes hydrophobic domains characterised by repeating PGVGVA motifs (Figure 8b) (Keeley et al., 2002). Tropoelastin is subjected to extensive alternative splicing (Indik *et al.*, 1987), and thus multiple tropoelastin isoforms are translated. Post-translational modifications of tropoelastin include the hydroxylation of some prolyl residues (Jacob & Hornebeck 1985).

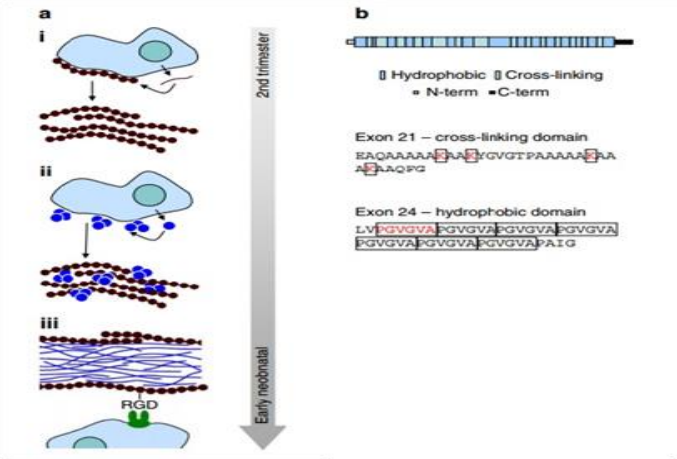

Figure 8: Schematic image of elastic fibre composition and assembly. Profibrillins are assembled into microfibrils (a_i) to form a microfibril scaffold for elastin deposition (a_{ii}) where elastin globules attach and crosslink, forming a rope-like structure (a_{iii}). Tropoelastin structure consists of an alternating hydrophobic and crosslinking domains (b).Adapted from Sherratt, (2009).

1.3.8. Elastin Crosslinking

Prior to elastic fibre formation, it is known that microfibrils act as a scaffold for the tropoelastin deposition. Indeed, after tropoelastin secretion into the extracellular space and subsequent assembly into microfibrils, the crosslinking occurs in the post-translational modification step. Crosslinking is initiated with the oxidative deamination of the ε-amino group of a κ residue to produce α-aminoadipic acid-δ-semialdehyde (allysine) by the enzyme lysyl oxidase (LOX) or LOX-like proteins. Intra- and intermolecular cross-links are then generated by non-enzymatic condensation of two allysine residues via aldol condensation which produces allysine aldol (AA), or by reaction of an allysine residue with the ε-amino group of another lysine residue via Schiff base reaction, which produces dehydrolysinonorleucine (Δ-LNL). The reducible crosslink has been suggested to further condense to form the stable and non-reductible trifunctional cross-links merodesmosine and cyclopentenosine, the tetrafunctional cross-links desmosine (DES) and isodesmosine (IDES), as well as pentafunctional cross-links such as allodesmosine and pentasine (Akagawa & Suyama 2000, Vrhovski & Weiss 1998, Bedell-Hogan et al., 1993, Reiser et al., 1992) (Figure 9).

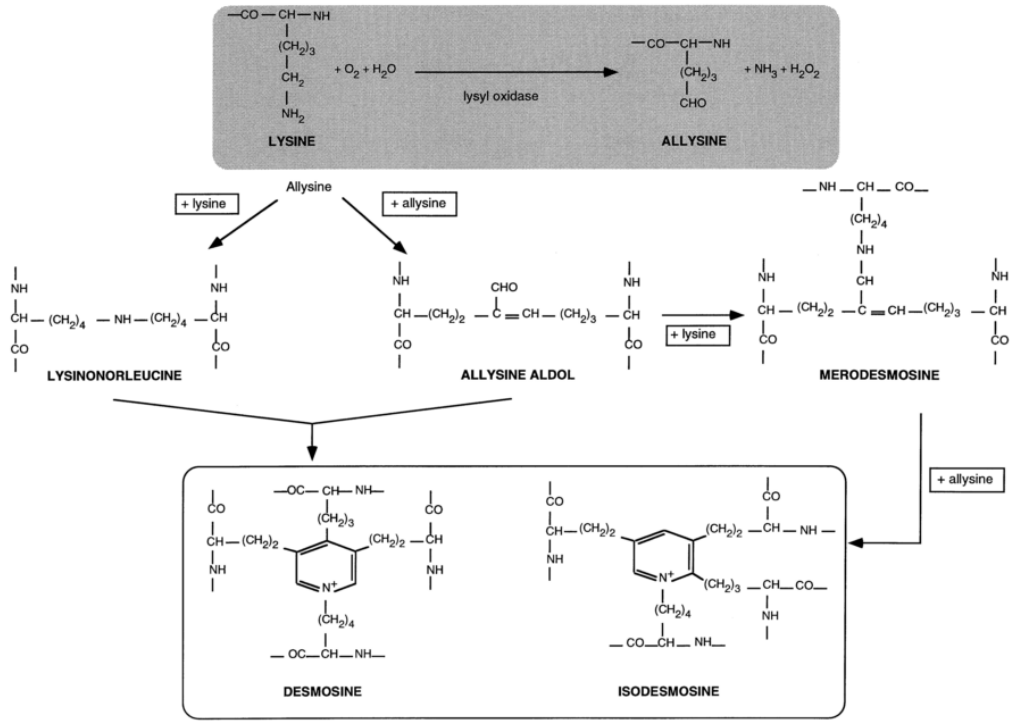

Figure 9: Structure and formation pathways of elastin crosslinks. Adapted from Vrhovski & Weiss (1998).

1.3.9. Elastic Fibre Longevity and Degradation

Usually, intracellular proteins have a short life-time. Intracellular enzymes, for instance, have a life-span measured in hours. However, many other ECM proteins can last several years. Some aspartic acid racemization studies suggested that collagen types I and II have life-times in human skin, articular cartilage and intervertebral disc of 15, 95 and 117 years, respectively (Sivan et al., 2008, Verzijl et al., 2000). However, elastic fibres and their molecular components usually last even longer. Elastin deposition starts in utero and reaches a maximum during early post-natal development (Berry et al., 1972). It is thought that fibrillin microfibrils are responsible for managing the elastogenic process, with FBN-2 expression preceding both tropoelastin and FBN-1 synthesis in most mammalian tissues (Ramirez & Pereira 1999), as FBN-2 is required for the deposition of tropoelastin (Tsuruga et al., 2007). Tropoelastin expression is down-regulated in humans within a few months of birth (Ramirez & Pereira 1999), whereas FBN-1 and FBN-2 are continually expressed. This suggests that the elastic fibres formed during early development stages remain in the tissues for the life-time of the organism. In vivo, elastic fibres present a remarkable longevity, when compared to other ECM and intracellular proteins. However, like any material, it gradually accumulates damage (Sherratt, 2009). Some human skin studies indicated that elastin, undergoes age-related damage, as it functions without replacement (Ritz-Timme et al., 2003).

Given this lack of replacement and gradual accumulation of damage, elastin functional efficacy decays in ageing organisms. ECM proteins that exhibit low turnover, are prone to degradation by enzymatic, chemical and biophysical mechanisms. Metalloproteinases (MMPs) are zinc-dependent endopeptidases responsible for remodelling and homeostasis of the ECM and also cell signalling regulation. To date, eight MMPs are thought to be able to degrade elastic fibres in vitro: MMP-2, -7, -9, -10, -12 and -14 can all degrade insoluble elastin, giving rise to soluble fragments (Chakraborti *et al.,* 2003), whilst fibrillin microfibrils are degraded by MMP-2, -3, -9, -12 and -13 (Tsuruga et al., 2007). In addition to MMP action, some studies have indicated that elastin is susceptible to reactive oxygen species (ROS) degradation, which can reduce the cross-linking, characteristic of aged elastic fibres (Umeda et al., 2001, Cantor et al., 2006). However, in contrast to this, the structural and functional changes of ECM proteins with age are commonly compromised by the

accumulation of pathological cross-links (Sherratt, 2009). Elastin cross-linking, which occur via the lysyl oxidase mediated deamination of lysine, leads to the formation of tetravalent desmosines and isodesmosines (Kielty et al., 2002). These cross-links, due to uncontrolled accumulation of glucose with ageing, experience several sequential modifications (formation of advanced glycan end products) which consequently cause an increase in tissue stiffness (Sims *et al.*, 1996). Additionally, elastic fibre structure in ageing tissues may also be affected by calcification, fixation of lipids and mechanical fatigue (Robert et al., 2008).

O'Rourke & Hashimoto (2007) suggested that mechanical fatigue is one of the crucial factors that cause elastic fibre failure. This study suggested that the microfibril/elastin interface within the elastic fibre structure was the most vulnerable region and, therefore the most affected.

1.4. Tendon Mechanics

Tendon is comprised of a well-ordered arrangement of load bearing collagen fibres, resulting in a material with highly anisotropic mechanical properties. These mechanical properties are crucial for function, ensuring tendons are stiff along their long axis and able to withstand large uniaxial loads. The aligned collagen fibres are surrounded by a proteoglycan rich matrix, resulting in a structure with good flexibility which is resistant to damage. Tendon is very often compared to a rope: while very strong under forces applied along the long axis, it cannot withstand longitudinal compression (Thorpe et al., 2015a).

To investigate the mechanical properties of tendon in vitro, uniaxial tensile mechanical tests are commonly performed at a constant strain rate, where tendon samples are simply gripped and stretched to failure. The force and extension throughout the test are recorded and typical force-extension curves are plotted (Figure 10). From these, considering the dimensions of the tendon, strain-stress curves are derived. In a typical strain-stress curve, four different regions can be identified: toe region, heel region, linear region and failure region (Figure 10). The toe region corresponds to the low stiffness behaviour of tendon and results from the straightening of collagen crimp and alignment of fibres. The heel region results from reordering of collagen molecules and some direct loading of different collagen parts. From this point, the application of further load will lead to the linear region, where collagen

fibres are directly loaded. It is still unclear what governs tendon extension in this region, but it is believe that it is a combination of extension and sliding of the collagen units. Although it has been hypothesised that proteoglycans play a role in managing this sliding behaviour and improving the resistance of tensile loading (Cheng & Screen 2007, Screen et al., 2004, Khodabakhshi et al., 2013), this has not been proved yet. Recent studies comparing fascicles from the SDFT and CDET, have shown that the extension mechanisms of fascicles from functionally distinct tendons are different, with CDET fascicle extension enabled by fibre sliding, whilst in SDFT fascicles extension occurs mainly through rotation and collagen extension, suggesting a helical substructure within energy storing tendon fascicles (Thorpe et al., 2013b).

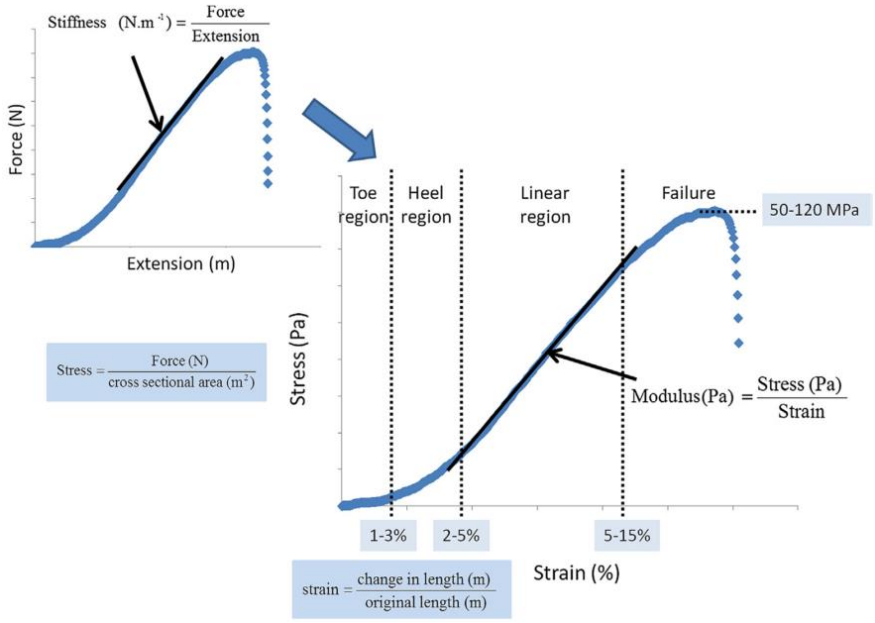

Figure 10: Schematic of a typical force-extension (inset-top left) and derived stress-strain curves for tendon. Different regions of the curve and typical stress – strain values are shown. Image taken from Thorpe et al., (2015a).

Related to this, Thorpe et al., (2012) have shown that, under physiological loads, the leading extension mechanism in energy storing tendons is sliding at the fascicle level, which would also prevent excess collagen loading. The matrix between fascicles, the interfascicular matrix (IFM), has been shown to be load bearing and elastic in nature, allowing the fascicles to slide when loaded and slide back following unloading (Thorpe et al., 2012, Thorpe et al., 2015b). It was additionally demonstrated

that a loss of these specialisations with ageing leads to reduced tendon resistance and fatigue damage (Thorpe et al., 2013a, Thorpe et al., 2014). A significant decrease in the capacity of sliding between SDFT fascicles with ageing, suggests an increase in the IFM stiffness, which results in tendon fascicles being loaded earlier. This means that in aged SDFTs the fascicles may be damaged during normal loading situations more easily. Unfortunately, it has not been possible to find in the literature an explanation for the changes in IFM stiffness with ageing, and one of the main reasons is because very little is known about the composition of the IFM.

It has been suggested that this loose connective tissue is comprised of type III collagen and PGs, and is synthesized and maintained by a small population of fibroblasts (Kannus 2000, Fallon et al., 2002). However, little is known about the structure and function of the IFM. Initially it was assumed that its function was just to bind the fascicles together. However some authors have suggested that IFM may have an important role in tendon function, contributing to tendon mechanical properties (Hirokawa & Hasezaki 2010). Our recent research has focused around understanding how energy storing tendons can behave more elastically and stretch further than positional tendons.

Thorpe et al (2012) have reported that the differences in SDFT and CDET mechanical behaviour are not due to the mechanical properties of the constituent tendon fascicles, but due to the differences in the amount of sliding between them. Data indicated that this fascicle sliding capacity in ES tendons is greater compared to positional tendons, under physiological loads (Thorpe et al., 2012). These differences in tendon mechanical properties are likely regulated by differences in tendon structure and composition. Various studies have found that the mature SDFT has a higher GAG and water content than the CDET, also that the SDFT has higher levels of cellularity compared to the CDET (Batson et al., 2003, Birch et al., 2008a). Some authors have mentioned the importance of proteins, such as lubricin and elastin in the management of IFM mechanical properties. Lubricin, which is localised in the IFM (Funakoshi et al., 2010), may allow greater sliding between fascicles (Kohrs et al., 2011). On the other hand, elastin seems to be important not only in fascicle sliding but also in the fascicle recoil. Although the location and distribution of elastin within tendons are not known exactly, some canine ligament and bovine tendon studies have reported that elastin seems to be localised between fascicles and around tenocytes (Smith et al., 2011, Grant et al., 2013). It was recently discovered that the matrix between fascicles

is load bearing and elastic in nature, allowing the fascicles to slide when loaded and slide back following unloading (Thorpe et al., 2012, Thorpe et al., 2015c). It was also suggested that a loss of these specialisations with ageing leads to reduced tendon resistance to fatigue damage (Thorpe et al., 2013a, Thorpe et al., 2014). Taking these results together, it was suggested that, in ES tendons, the IFM directly influences the mechanical properties of the whole tendon, whilst the IFM plays a less important role in the CDET (Thorpe et al., 2013c). This may also explain how the energy storing tendons are able to support much larger strains and greater extension than positional tendons (Thorpe et al., 2012, Thorpe et al., 2013a).

Unravelling these mechanism has exciting implications for treating tendon injuries and targeting prevention approaches to stop age related loss of tendon elasticity. Recent data suggest that changes to the interfascicular matrix (IFM) with age are the primary cause for tendon overload damage (Thorpe et al., 2013a). However, very little is known about the IFM. Recent published data from our group demonstrate the presence of high levels of proteoglycans in the IFM, and also elastin bridging across the IFM, linking fascicles, mainly in the energy storing SDFT (Thorpe et al., 2016a).

1.5. Elastic Fibre Localisation and Distribution in Tendon

Initially, it was thought that elastin was present in only 10% of all tendons however, later studies showed that elastic fibres can also be found in many tendons of most animal species, such as in the Achilles tendons of young and old rabbits, and in other rat tendons (Kannus, 2000). More recently, Grant et al., (2013) published some work on elastin localisation and organisation in bovine flexor tendons. Their results indicated that elastic fibres are densely distributed around tenocytes and between fascicles and longitudinally oriented along the tendon (Grant et al., 2013). Some transverse sections of tendon clearly showed the interaction between elastic fibres and cells and also a mesh-like elastic fibre structure was found in the interfascicular region (Grant et al., 2013) (Figure 11). Also, studies of the cruciate ligaments clearly showed the presence of elastic fibres on the surface of the collagen bundles, and very often in the interfascicular region where they showed a looser organisation (Smith et al., 2011). Later, C. Thorpe et al., (2016a) investigated the localisation and organisation of elastin

in both the energy storing SDFT and positional CDET and reported that, in energy storing tendons, elastin was significantly more abundant in the interfascicular matrix, compared to the fascicular matrix. These results confirm previously published work and open the debate on whether elastin plays an important role in tendon or not, and if it is tendon type specific.

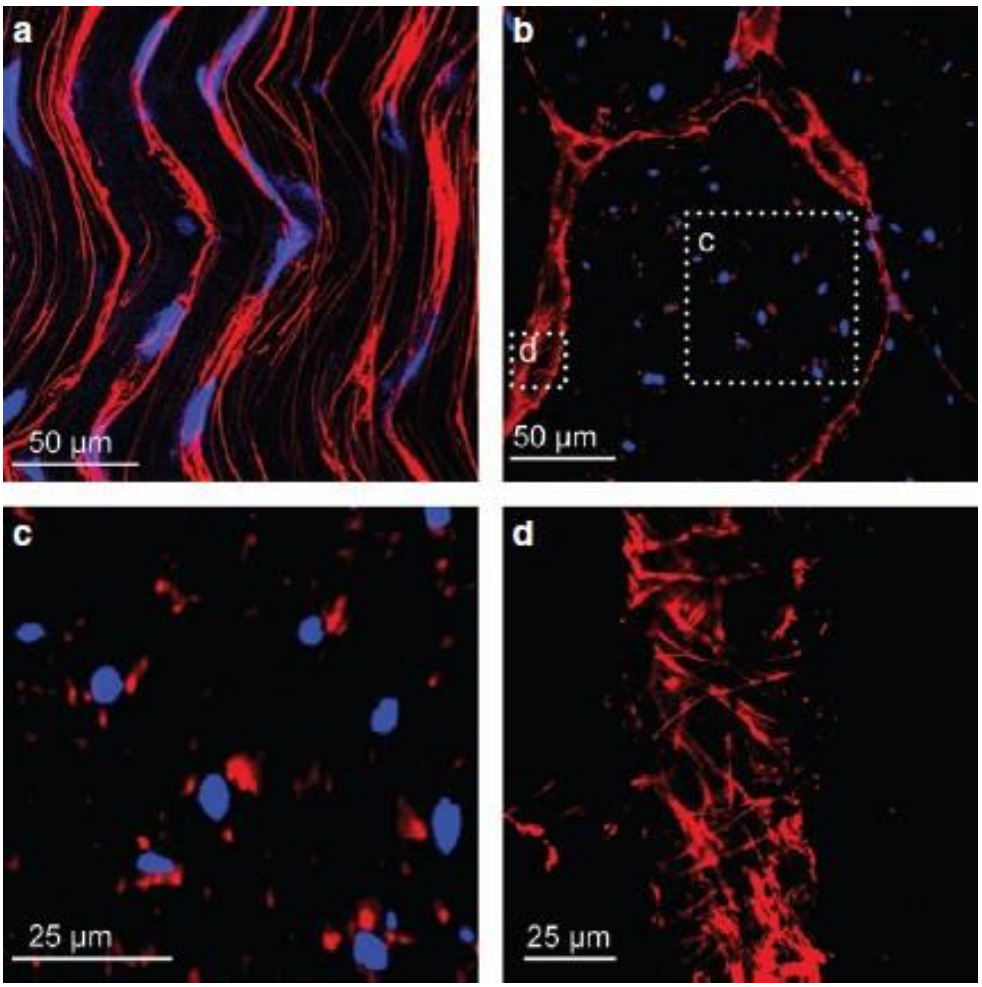

Figure 11: Image showing organisation of the elastin fibres in bovine flexor tendon. (a) Longitudinal 3D reconstruction from a 20µm z-stack showing various fibres (red ab3090 – FBN-1) localized around tenocytes (blue DAPI – cell nuclei). (b) Transverse sections showing a dense distribution of elastic fibres around cells and between fascicles. (c) High magnification transverse image highlighting the interaction of elastic fibres (red ab3090 – FBN-1) and cells (blue DAPI – cell nuclei). (d) 3D reconstruction of the mesh-like elastic fibre structure within the interfascicular matrix. Image taken from Grant et al., (2013).

1.6. Possible Role for Elastin in Tendon

Elastic fibres, whose role in tendon in not yet well understood, seem to have a sparse distribution within tendon (Kannus, 2000), however, very few studies have really focussed on understanding overall elastin localisation, organisation or function in tendon (Caldini et al., 1990, Parry & Craig 1978, Screen et al., 2015, Grant et al., 2013, Thorpe et al., 2016a).

Elastin is a major component of tissues in vertebrates which require rapid extension and complete recovery, such as the nuchal ligament (Davidsons *et al.*, 1982), aorta (Greenwald, 2002), lung (Pierce & Hocott, 1960) and skin (Oxlund et al., 1988). In tendon, on the other hand, elastin is a minor component, which does not mean that there is no role for elastin. In fact, previous studies suggested that elastin plays a very important role in sustaining the elasticity and tensile strength of these tissues (Ritz-Timme et al., 2003). Elastic fibres seem to function to help collagen recover its wavy configuration after muscle contraction and tendon stretch (Kannus, 2000).

More recently, it has been suggested that elastin is mainly localised to the interfascicular matrix and also around tenocytes (Grant et al., 2013). This close interaction between elastic fibres and cells sugests that elastic fibres play an important role in cell function. Indeed, the results from this study imply that the presence of elastic fibres around tenocytes may affect significantly the cell-level strains and consequently, their mechanobiological response to load. Additionally, it is thought that cells are well attached to fibres, being used as markers of how fibres are moving (Screen et al., 2005). During tendon deformation, groups of cells along one fibre move relative to those on adjacent fibres, so the elastic fibres may be present to help cells, and collagen fibres to return to their initial configuration. Additionally, the dense distribution of the elastic fibres between fascicles is likely to provide the IFM with elastic recoil capacity and stress protection, once it experiences large shearing forces during loading. Finally, in equine studies, elastin has been reported to be localised to the interfascicular matrix, mainly in energy storing tendons (Thorpe et al., 2016a). Previous work from the same group, indicated that the interfascicular matrix in energy storing tendons is specialised, as it has to extend more, be more elastic and compliant compared to other tendon types (Thorpe et al., 2013a). Hence, this suggests that elastin plays a role in overall tendon mechanics, allowing a greater interfascicular stretch and recoil that is required of an energy-storing tendon.

1.7. Project Aims and Objectives

1.7.1. Global Hypothesis

This thesis aims to test the global hypothesis that the IFM in energy storing tendons is specialised for function, and that elastin is the primary protein of importance for facilitating the high strain and rapid recoil behaviour of energy storing tendons.

1.7.2. Aims and Objectives

This hypothesis will be investigated through a series of hypotheses, and associated objectives, using in each case the equine superficial digital flexor tendon (SDFT) and common digital extensor tendon (CDET) as models of an energy storing and positional tendons, respectively.

Hypothesis 1

Elastin is more prevalent in energy storing tendons than positional tendons and is localised to the IFM in both tendon types.

Objective 1.1. Develop methods to determine elastin content in whole energy storing and positional tendons, and in different regions of the tendon (fascicles and IFM).
Objective 1.2. Develop methods to visualise elastin in tendon and its regional localisation.
Objective 1.3. Develop approaches to semi-quantify elastin visualised in the different regions of the tendon;

Hypothesis 2

Elastin becomes increasingly disorganised and fragmented with ageing, particularly in energy storing tendons.

Objective 2.1. Develop methods to assess elastin fragmentation with ageing in both positional and energy storing tendons.
Objective 2.2. Develop methods to quantify elastin organisation and fragmentation with ageing in both tendon types.

Hypothesis 3

IFM mechanical properties are directly influenced by elastin content, particularly in energy storing tendons.

Objective 3.1: Develop methods to remove elastin, and investigate mechanical properties of fascicles and IFM before and after elastin digestion.

Hypothesis 4

IFM fatigue resistance is directly correlated to elastin content.

Objective 4.1. Develop methods to determine fatigue properties of fascicles and IFM, before and after elastin digestion.

Hypothesis 5

Elastin functions to transfer stress between fascicles providing an extensible interface with high recoil ability in the energy storing tendons.

Objective 5.1. Develop methods to investigate the recoil ability of the IFM in energy storing tendons, before and after elastin digestion.

Hypothesis 6

Tendon mechanical properties are directly influenced by elastin content & elasticity of the IFM, particularly in energy storing tendons.

Objective 6.1. Develop methods to remove elastin, and investigate mechanical properties of tendon longitudinal sections, before and after elastin

Chapter 2 - Sample Acquisition and Preparation

2.1. Tendon Dissection

In order to perform all of the technical development and experimental work described in the next two chapters, the forelimbs of euthanised horses, aged 3-7 years (young group) and 15-19 years (old group), were gathered from a commercial equine abattoir and prepared in the same manner, described once in this chapter.

SDFTs and CDETs (Figure 12a_1 and a_2, respectively) were dissected free from the right and left limbs to the level of the metacarpophalangeal joint (Figure 12B). Tendons included in this study had no signs of previous injury at post-mortem examination. Tendons were secured to a dissecting board and all the connective tissue surrounding the tendon (sheath) was removed and stored in 1.5ml screw cap tubes for future analysis. Forceps were used to pull way the sheath from the surface of the tendon, which was then cut with a scalpel. Once all sheath was removed, tendons were divided into equal sized longitudinal sections, using a scalpel (Figure 12C). Each SDFT was divided into four longitudinal sections, while CDETs into two longitudinal sections (approximately 200 x 8mm each). Two of the longitudinal sections were assigned to immunohistochemical/biochemical analysis (Figure 12D) and the remaining to mechanical testing (Figure 12E).

2.2. Samples for Mechanical Testing

Longitudinal sections designated for mechanical testing were individually wrapped in tissue paper, previously impregnated with phosphate-buffered saline (PBS, Sigma, Poole, UK), and then in tin foil. These sections were then stored at -80ºC, with previous unpublished data from our group showing that tendon mechanical properties, specifically in similar size samples, are not affected by one freeze-thaw cycle.

When required, the frozen tendon sections were removed from the freezer and allowed to thaw for about 30 minutes at room temperature prior to use. During this period, sections were kept hydrated by spaying several times with PBS. According to the type of test to be performed, these longitudinal sections were used whole, or further dissected into smaller samples: fascicles and/or IFM samples (Figure 12E). These smaller samples would be used not only in mechanical testing, but also in a variety of other tests, mainly in the validation step.

2.2.1. Fascicle Dissection

Using a scalpel and size eleven blades, fascicles, proximally 40 mm in length and 0.2-0.4 mm in diameter, were dissected from the mid-metacarpal region of the tendon section, by cutting longitudinally through the tendon (Figure 12e_1). During the dissection, fascicle hydration was maintained by storing the fascicles on a Petri dish covered with tissue paper dampened with PBS.

2.2.2. IFM Samples Dissection

Groups of two intact fascicles (bounded by the IFM), were dissected from the mid-metacarpal region of the tendon section. Using a custom-made dissection rig, IFM samples (approx. 40mm in length) were secured under a stereomicroscope fitted with an analyser and rotatable polarized lens (Leica), which enables a better visualization of the two individual collagen fascicles (Figure 12e_2). After focusing the image, the opposing end of each fascicle was cut transversely with a scalpel, leaving 10mm of undamaged matrix in the middle (Figure 12e_2). The areas of the cuts were identified with a pen mark for easier recognition during later mechanical testing. After removing the fascicle pairs from the dissection rig, samples were placed on a Petri dish covered with tissue paper dampened with PBS (Figure 12e_3), similarly to the procedure adopted for the fascicles. The dissection process was completed quickly, to prevent samples from drying out.

2.3. Samples for Immunohistochemical and Biochemical Analyses

Sections assigned for immunohistochemical and biochemical analyses were dissected into small squared samples, approximately 5x5x5 mm in dimension (Figure 12D). Only samples isolated from the mid-metacarpal region of the sections were used. Samples intended for immunohistochemical analysis (Figure 12d_1) (minimum two samples per tendon type), were immediately embedded in optimal cutting temperature compound and snap frozen in hexane cooled on dry ice. From these, four longitudinal and four transverse cryosections, 5 and 10µm thick (2 slides each thickness), were then

cut from each sample and placed on poly-lysine slides, which were stored at -80ºC until required. Samples intended for biochemical analysis (Figure 12d_2) (minimum 4 samples per tendon type), were stored at -20 ºC in 1.5ml screw cap tubes for future analysis. During dissection, samples were kept hydrated by spraying several times with PBS. A list of materials used, with respective information regarding suppliers, catalogue and batch numbers, can be found in Appendix A.

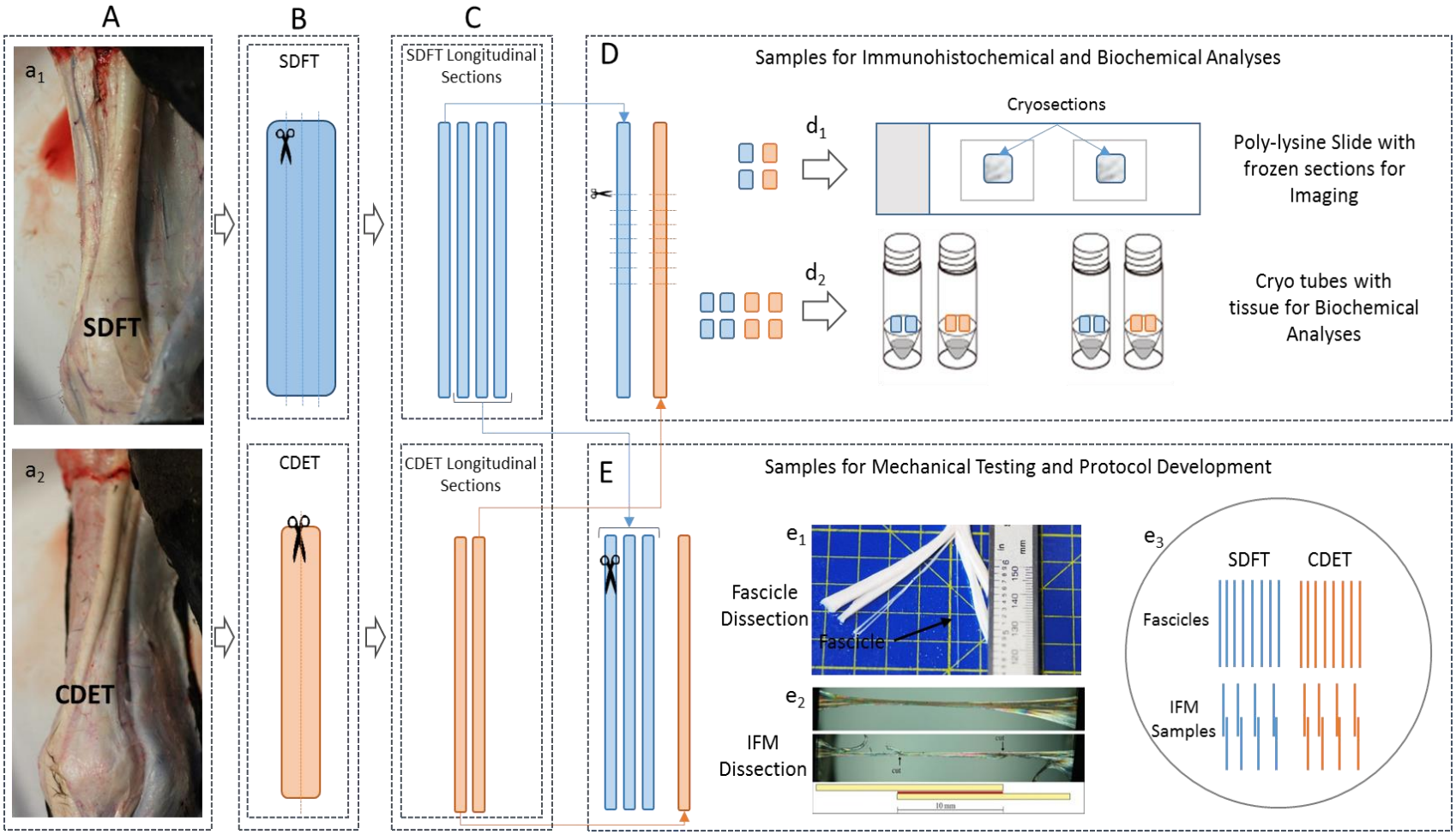

Figure 12: Schematic showing the main steps for tendon samples' preparation. IFM dissection image (d_2) adapted from Thorpe et al., (2015c).

Chapter 3 - Elastin Localisation and Organisation in Tendon

3.1. Introduction

The interfascicular matrix composition is still poorly defined. Previous studies have shown that the IFM has a distinct composition and greater cell density compared to fascicles (Thorpe et al., 2016c). Fascicles consist of highly aligned collagen fibres interspersed with sparsely distributed elongated cells, whilst the IFM is more disorganised in appearance, with a greater number of more rounded cells, more collagen type III and proteoglycans, but a lower collagen type I content (Thorpe et al., 2016c, Kannus 2000, Fallon et al., 2002). Additionally, recent work suggests a greater rate of matrix turnover within the IFM, which may act to maintain healthy tendon structure (Thorpe et al., 2016c).

Several recent studies have reported that the IFM is also rich in elastin (Grant et al., 2013, Thorpe et al., 2016a, Smith et al., 2011), where it may influence IFM and consequently whole tendon mechanics. Overall elastin content in tendon is low and it is sparsely distributed within fascicles (Kannus, 2000). However, its localisation to the IFM (Grant et al., 2013), suggests it may be particularly important for IFM function. However, there are no studies reporting relative elastin content and organisation between tendons regions, or changes with ageing in tendons with different functions.

3.2. Aims and Hypotheses

This chapter aims to quantify the total amount of elastin in different tendon types and age groups, and investigate elastin organisation and fragmentation in both fascicular matrix (FM) and IFM and how this changes with ageing. It hypothesises that elastin is more prevalent in energy storing than positional tendons, and is mainly localised to the IFM. It also hypothesises that elastin content decreases with ageing, especially in energy storing tendons, and lastly, that elastin becomes disorganised and fragmented with ageing, especially in energy storing tendons.

3.3. Quantitative Assessment of Elastin Content in Tendon

3.3.1. Development of FM and IFM Microdissection Protocol

In previous publications, researchers have reported the usage of manual microdissection as a successful method to provide very small amounts of tissue, dissected in situ, for biochemical analysis (Hunt & Finkelstein 2004, Thorpe et al., 2016c). Based on this knowledge, a manual microdissection technique was developed to isolate small amounts of FM and IFM from tendon sections, in order to determine the amount of elastin and other important ECM components such as collagen, sGAG and DNA in each region of the tendon. Samples of tendon sheath and whole tendon (IFM+FM) were also investigated. For a better understanding, Figure 13 shows the overall tendon structure, highlighting the tissue dissected and used for this specific analysis.

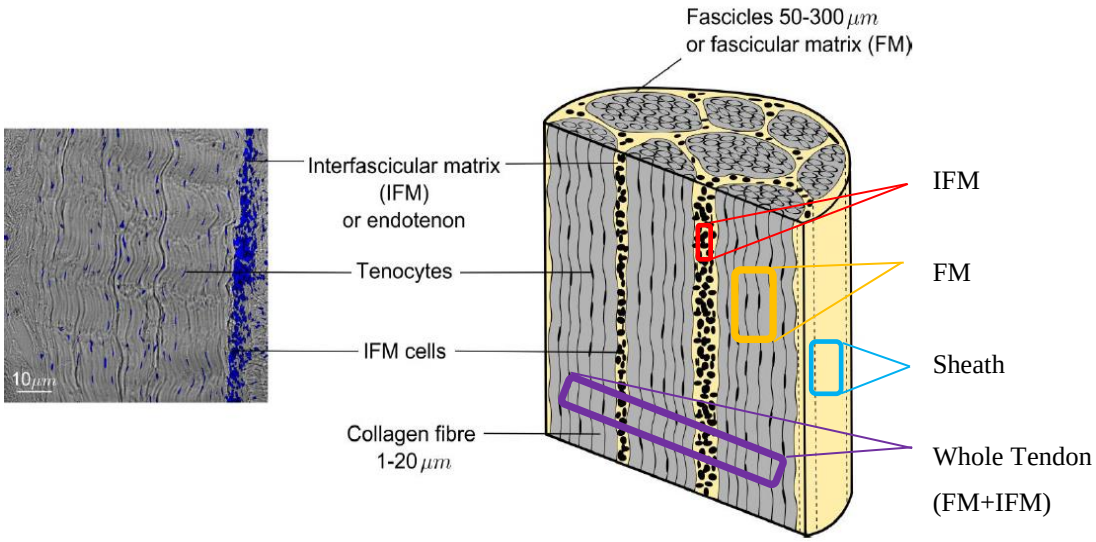

Figure 13: Schematic showing the overall tendon structure. The type of tendon tissue dissected is listed on the right hand side of the image: IFM, FM, Sheath and Whole Tendon. Adapted from Spiesz et al., (2015).

Tendon longitudinal sections, prepared as described in previous chapter, were used. Once defrosted, one end of the tendon section was secured to a dissecting board using a large spring clip. Thin longitudinal tendon sections were dissected from the middle of the tendon section (approximately 1-2mm thick), well away from the surface

and any remaining sheath (Figure 14a), then a single thin section placed under a stereomicroscope (Leica) (Figure 14b). The section was positioned on top of a layer of rubber with a cork board underneath (Figure 14b) and secured to both layers by a metal pin, enabling better visualisation of the fascicles and interconnecting IFM (Figure 14c).

Using microdissection tools, small amounts of FM and IFM were carefully dissected from the thin section and stored in 1.5ml screw cap tubes. After FM and IFM dissection, small transverse sections of this test piece (Figure 14c) were dissected from above the microdissection region. Sufficient tissue from each region was dissected to fill three tubes, each holding approximately 20mg (wet weight) of sample: one tube was assigned for general assays and two for an elastin assay.

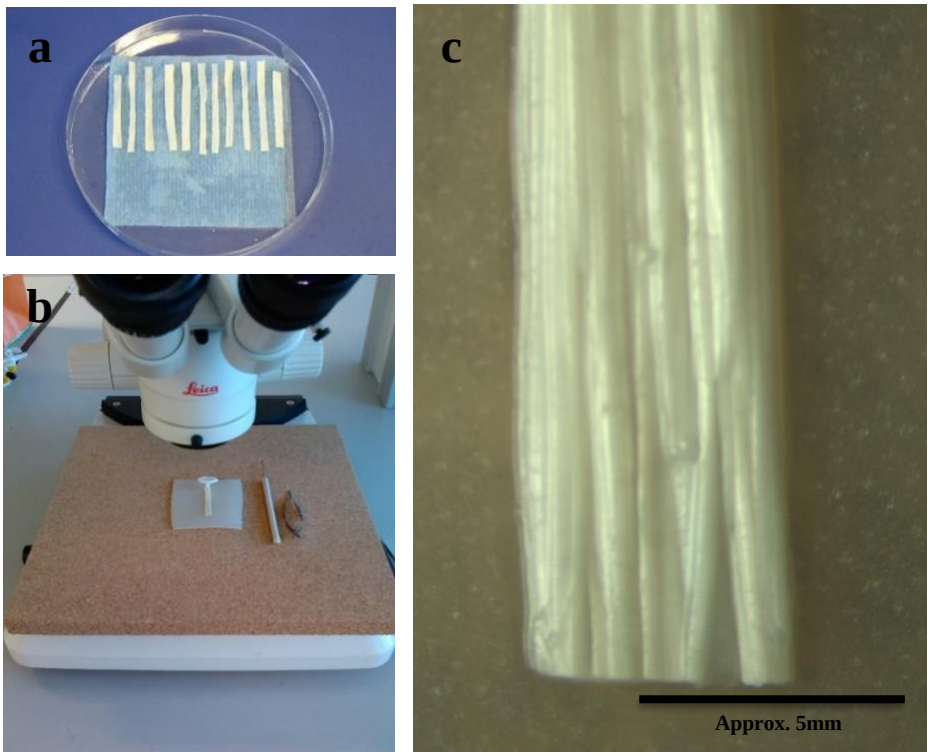

Figure 14: Image showing the initial steps of microdissection. (a) Thin sections were dissected from the tendons, stored in a petri dish and kept hydrated with PBS; (b) the thin sections were positioned under a stereomicroscope (Leica) and secured with a metal pin; (c) it was then possible to visualise fascicular and interfascicular matrix for microdissection.

3.3.2. Sample Preparation for Biochemical Analyses

After dissection, FM, IFM, Whole Tendon and Sheath samples were weighed using a high precision digital microgram scale with a resolution of 0.001 milligrams, and then freeze-dried for 24 hours. The lyophilised samples were reweighed, and water content calculated and expressed as a percentage of the wet weight. The samples were stored at -20°C until required for analysis.

3.3.3. Papain Digestion

In order to determine the amount of DNA, GAG and Collagen in each type of tendon tissue, papain (P3125, Sigma, UK), also known as papaya proteinase I, was used to digest the tissue (Thorpe et al., 2010b). Activated papain enzyme digestion solution (APEDS) was prepared with 4 units papain/ml papain buffer extract (100mM sodium phosphate buffer and 5mM Na_2EDTA (in ultra-pure water), pH 6.5) and 10mM L-cysteine hydrochloride)). For every 10mg (dry weight) of tissue, 1ml of APEDS was added. Tube samples were secured in a rotator placed inside the oven and digested for 18 hours at 60°C.

3.3.4. Assessment of Tendon Matrix Composition - DNA

After papain digestion, the DNA concentration of each sample was measured using a fluorometric assay adapted from that of Kim et al. (1988) using the bisbenzimidazole dye Hoechst 33258, which binds in the groove of the DNA double helix.

Aliquots of papain digested tissue (100µl) were diluted to 500µl with papain buffer extract (PBE), and 100µl of diluted sample pipetted into the appropriate wells of a 96 well plate. 100µl of dye (1µg/ml Hoechst 33258 in 10 mM Tris-HCL, 1mM $EDTA.Na_2$, 0.1 mM NaCl, pH 7.4) was added to each well. Fluorescence was measured using a fluorometer (FLUOstar OPTIMA); excitation wavelength: 360 nm, emission wavelength: 460 nm) in the presence and absence of dye to account for background tissue fluorescence. DNA concentration was calculated by comparison to a standard curve constructed using DNA standard stock (1mg/ml) which was diluted in PBE to concentrations from 0-20 µg/ml. The DNA concentration was expressed as µg/mg dry weight tendon tissue.

3.3.5. Assessment of Tendon Matrix Composition - GAGs

Sulphated glycosaminoglycan (GAG) content was measured using the dimethylmethylene blue assay, which is able to quantify total sulphated glycosaminoglycans. The dimethylmethylene blue dye (DMMB) binds sulphated glycosaminoglycans (GAGs) and forms a complex that absorbs light at 525 nm (Farndale et al 1986).

Aliquots of papain digested tissue (60 µl) were diluted to 180 µl with PBE, 40µl of diluted samples pipetted into the appropriate wells of a 96 well plate, and 250µl of DMMB reagent (1L deionised water, 16mg DMMB, 5 ml ethanol, 5g HCO2Na, pH 3.0) added to each well. Absorbance was measured using a spectrophotometer (SPECTROstar Nano) at 595 nm and the GAG concentration calculated by comparison to a standard curve constructed with a stock solution (1mg/ml) of bovine trachea chondroitin sulphate which was diluted in PBE to give concentrations from 0-60 µg/ml. GAG concentration was expressed as µg/mg dry weight tendon tissue.

3.3.6. Assessment of Tendon Matrix Composition - Collagen

Collagen content was calculated by measuring the concentration of the amino acid hydroxyproline, which is assumed to make up 14% of collagen dry weight (Birch et al., 1998), and correspond to a hydroxyproline : collagen ratio of 1:7.69. Hydroxyproline content was calculated using a method adapted from Bergman and Loxley (1963) and Bannister and Burns (1970), where hydroxyproline is oxidised by chloramine T and coupled with dimethylbenzaldeyde (DMBA) which results in a coloured product which can be visualised using a spectrophotometer at 550 nm (Bergman & Loxley 1963, Bannister & Burns 1970, Birch et al. 1998)

Aliquots of papain digested tissue (100µl) were hydrolysed overnight in HCl (37%) at 110°C, dried for 48 hours at 50°C and re-suspended in 200µl of ultra-pure water. Aliquots of the hydrolysed samples (100µl) were diluted to 10ml with PBE, and 60µl of the diluted samples pipetted into the appropriate wells of a 96 well plate. 20 µl of assay buffer (1.5ml 1-propanol, 1 ml ultra-pure water and 5 ml citrate stock buffer (100ml ultra-pure water plus 5.04 g citric acid monohydrate, 11.98g sodium acetate trihydrate, 7.22g anhydrous sodium acetate, 3.4g sodium hydroxide and 1.26ml acetic acid (99.7%), pH 6.1)) and 40 µl of chloramine T reagent (141 mg Chloramine T, 0.5ml ultra-pure water, 0.5ml 1-propanol and 4 ml citrate stock buffer) were added to

each well. Samples were left to stand for 20 min to allow hydroxyproline oxidation to complete. The colour reagent (6ml 1-propanol plus 3ml 70% perchloric acid and 4.5g 4-(Dimethylamino) benzaldehyde) was finally added (80µl) and all reagents mixed until the solution became clear. The plate was then covered with SealPlate, wrapped in tinfoil and incubated at 60°C for 20 min. After a 25 minutes cooling period, the absorbance was measured on a spectrophotometer (SPECTROstar Nano) at 570 nm. Hydroxyproline concentration was calculated by comparison to a standard curve, prepared using a 50µg /ml hydroxyproline solution in PBE, from which standards from 0-450 ng/well were prepared. Collagen content determined from hydroxyproline content, and expressed as a percentage of dry weight tendon tissue.

3.3.7. Assessment of Tendon Matrix Composition –Elastin

In order to determine the total amount of elastin in tendon, the FASTIN elastin assay was used. Previous studies have used this colorimetric assay mainly to determine the amount of elastin in urine, but only very few have examined tissue (Grant et al., 2015, Nimeskern et al., 2016). Thus, a protocol was developed combining the manufacturer's instructions and similar studies (Grant et al., 2015, Nimeskern et al., 2016, Smith et al., 2014). There were a few steps that required optimisation: sample preparation, amount of tissue used for quantification and number of extractions performed.

3.3.7.1. Fastin Elastin Assay Protocol

To measure elastin content, the Fastin Elastin Assay (FASTIN Elastin Assay Kit, Biocolor, UK) was adopted. Before the assay could be performed, all test samples required the conversion of the native hydrophobic elastin into a water soluble derivate: α-elastin. The number of extractions needed to guarantee the complete solubilisation of the tendon elastin was not known. Previous studies in ligament indicated that, at least 6 extractions would be necessary to solubilise all elastin (Smith et al., 2014), whereas studies in rat tail fascicle indicated that 2 extractions would be sufficient to extract all tissue elastin (Grant et al., 2015). To be confident all elastin would be removed, six extractions were carried out in this initial experiment. A test sample without tissue was also included to serve as a sample blank. To complete one extraction, samples were heated to 100°C in 750µl of 0.25M oxalic acid. After each

one-hour extraction period, the tubes were allowed to cool for about 10 min and then centrifuged at 10000rpm for 10 min. The supernatant was pipetted off, into a 1.5ml Eppendorf, and tubes weighed before and after the liquid removal, to determine how much supernatant was pipetted off. To begin the next extraction, a further 750µl of 0.25M oxalic acid was added to the residual tissue and the procedure repeated.

The elastin in the extractions, was in the form of α-elastin, which has a molecular weight from 60-84 kDa, and, could therefore be directly assayed using the procedure described for soluble elastin (Fastin Elastin Assay Kit, Biocolour, UK). α-elastin standards, with concentrations from 0-70 µg/ml, were prepared in duplicate using a 1mg/ml α-elastin standard solution (Biocolour, UK), and to all test samples, the sample blank and the standards, an equal volume of Elastin Precipitating Reagent was added (see Table 2 as an example for standards preparation).

Table 2: Standards preparation protocols for the Tendon Elastin assay

Standard ID	Vol 0.25M Oxalic Acid	Vol 1mg/ml α-elastin standard solution	Vol Elastin Precipitating Reagent
STD 0	100 µl	0 µl	100 µl
STD1	0 µl	5 µl	5 µl
STD2	0 µl	10 µl	10 µl
STD3	0 µl	30 µl	30 µl
STD4	0 µl	70 µl	70 µl

Tubes were briefly vortex to mix contents and left for 15 minutes to complete the precipitation of α-elastin. Then, tubes were centrifuge at 9500 rpm for 10 min and the liquid drained into a beaker. After removing the majority of the liquid by inverting the tubes, the remaining liquid was removed from each tube using thin strips of filter paper. 1 ml of Dye Reagent was added to each tube, briefly vortexed and placed on a mechanical shaker for 90 min to allow reaction between the α-elastin and the dye (Figure 15a). Once again, tubes were then centrifuge at 9500 rpm for 10 minutes, and all liquid removed from tubes to remove unbound dye (Figure 15b and c). The elastin-dye complex could be observed as a reddish-brown deposit in the bottom and inside lower wall of the tubes (Figure 15d). Finally, 250µl of Dissociation Reagent was added to each tube, and tubes vortexed twice at 10 minutes intervals, to ensure that all bound dye had passed into solution. 200µl from each tube were transferred to the appropriate

well of a 96 well flat bottom microwell plate, placed into a Spectrophotometer (SPECTROstar Nano) and absorbance was measured at 513 nm. Elastin concentration was calculated by comparison to a standard curve generated by the α-elastin standards, and expressed as a percentage of dry weight of tendon tissue.

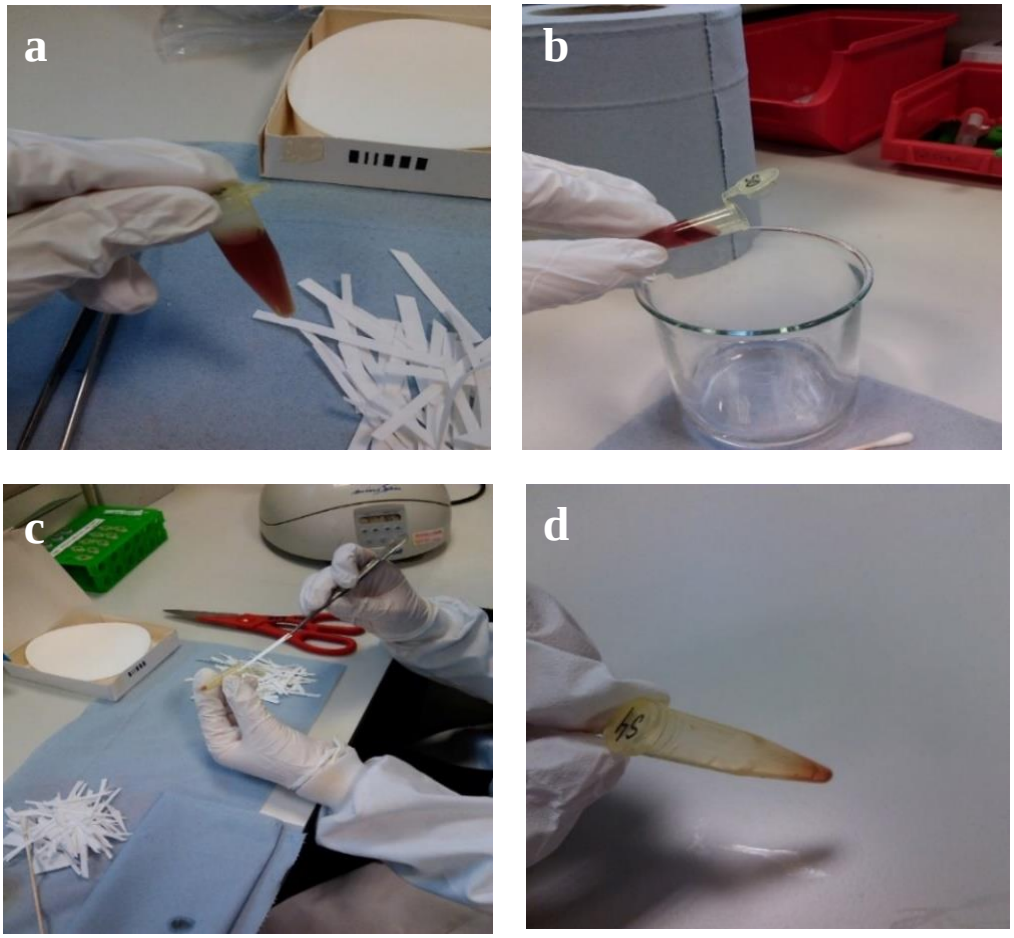

Figure 15: Pictures showing some of the Fastin Elastin Assay (Biocolor) protocol steps. After the addition of the dye reagent to all tubes (a); tubes were drained of unbound dye by inverting the tube (b); with any remaining liquid removed from each tube using thin strips of filter paper (c). The elastin-dye complex could be observed as a reddish-brown deposit in the bottom and inside lower wall of the tubes (d).

3.3.8. Statistical Analysis

All statistical analyses in this chapter were carried out using the software Minitab 17 for Windows. Data were tested for normality using the Anderson – Darling test. If normally distributed, a two-way ANOVA (grouping information using the Tukey Method and 95% confidence) was used to evaluate differences between treatments and age groups. Treatment and horse age were used as factors for the ANOVA. The number of each individual donor was also included in the analysis of variance (nested with the horse age) to ensure each fascicle from the same tendon was not considered an independent biological repeat, but instead a "technical repeat". Data that did not follow a normal distribution was first transformed using a Box Cox transformation, and if still not normally distributed, a nonparametric test: The Mann–Whitney was used. The statistical test used for each parameter is indicated in the captions of the graphs. All the results were considered statistically significant for $p<0.05$.

3.3.9. Tendon Matrix Composition - Results and Discussion

Preliminary data comparing the concentrations of each matrix component in each tendon region are summarised in Table 3. At a whole tendon level, results demonstrated significantly less GAG in the CDET than SDFT and also an increase in GAG with age in SDFT tendons. There were also significantly more cells in the SDFT than in the CDET, and water content was significantly higher in the young SDFT, but this increase was lost with ageing.

These data generally confirm previous studies (Batson et al., 2003, Birch et al., 1998), and it has been previously hypothesised that differences in tendon matrix composition affect the material and mechanical properties of the tissue. For example, a higher water content is hypothesised to be associated with a less stiff material (Birch 2007), whilst glycosaminoglycans are thought to be responsible for organising collagen fibrils, particularly during development (Scott, 1995), and the increased GAGs in energy storing tendons might be a result of the need for more tightly organised collagen in these tendons.

Whilst whole tendon data were readily compared to previous studies, compositional data from different regions of tendon was inconclusive and of concern, and regional specific data, relating to the fascicular matrix, interfascicular matrix and sheath, were not statistically analysed due to their incoherence (Table 3). Specifically, the content of GAG, DNA and collagen in the whole tendon was notably lower than the sum of these components across the constituent FM + IFM regions, whilst elastin content in old SDFT samples was higher in the IFM in isolation than across whole samples. Whilst this indication of high elastin levels in the IFM supports the hypothesis, the substantial variability in regional data, particularly from the IFM is of major concern. Variation was too large to suggest simple analytical variance, indicating a loss of sample during the preparation or technical issues around accurately weighing and analysing small quantities.

Table 3: SDFT and CDET tendon matrix components concentration from the equine forelimb. Tendons were separated into two groups based on age – Young (3-7 years old) and old horses (15-19 years old). Data from Old CDET are not displayed, as these experiments were not performed. Data are displayed as Mean ± SEM owing to poor confidence in the microdissection technique. Significant differences between groups are only provided for whole tendon samples, and are flagged with: *p<0.05; **p<0.01 and ***p<0.001 and between age groups with: [a] p<0.05; [b] p<0.01 and [c] p<0.001 (all normally distributed data – ANOVA)

		Young SDFT (Mean ± SEM)	Young CDET (Mean ± SEM)	Old SDFT (Mean ± SEM)
Water Content (%)	FM	69.96 ± 1.38	59.67 ± 1.21	56.40 ± 1.51
	IFM	78.49 ± 10.42	72.46 ± 2.53	71.07 ± 0.73
	Whole (IFM+FM)	73.62 ± 2.00***	62.87 ± 0.55	66.78 ± 1.24[a]
	Sheath	83.38 ± 1.52	85.29 ± 0.87	84.51 ± 1.25
GAG (µg/mg)	FM	7.85 ± 0.23	3.58 ± 0.14	9.34 ± 0.41
	IFM	7.25 ± 0.48	3.69 ± 0.73	9.89 ± 1.19
	Whole (IFM+FM)	9.95 ± 0.76*	4.10 ± 0.10	11.28 ± 0.64
	Sheath	9.74 ± 0.23	13.78 ± 1.98	11.73 ± 0.68
DNA (µg/mg)	FM	1.80 ± 0.16	1.05 ± 0.13	1.97 ± 0.62
	IFM	1.94 ± 0.54	2.34 ± 0.89	3.49 ± 1.25
	Whole (IFM+FM)	3.11 ± 0.29*	1.67 ± 0.13	3.17 ± 0.73
	Sheath	9.74 ± 0.45	10.56 ± 0.46	10.35 ± 0.56
Collagen (%)	FM	73.62 ± 2.39	79.42 ± 2.06	68.93 ± 5.34
	IFM	65.08 ± 2.04	68.54 ± 2.03	55.05 ± 11.78
	Whole (IFM+FM)	81.60 ± 3.89	86.71 ± 1.09	93.66 ± 4.01
	Sheath	80.03 ± 1.52	73.58 ± 4.39	88.42 ± 6.67
Elastin (%)	FM	1.37 ± 0.07		2.10 ± 0.25
	IFM	2.05 ± 0.04		3.17 ± 0.18
	Whole (IFM+FM)	1.45 ± 0.11		1.55 ± 0.07
	Sheath			

Results may indicate that there is an additional tendon region for which tissue is lost during preparation, leading to inconsistent comparisons of regional composition. Sheath tissue was included in the analysis to review this, however it did not help interpret the data, and with the previous samples dissected specifically from the core it seems highly unlikely. Further, nothing was removed during dissecting and all tissue was transferred to one of the regional analysis tubes (FM or IFM). It is therefore hypothesised that difficulties arise from the microdissection technique itself.

The microdissection technique has proved time consuming and difficult to standardise, with low quantities of IFM available, which are difficult to dissect and weigh, particularly guaranteeing complete separation of fascicular matrix and IFM. Thus, it was decided that microdissection was not a viable technique for the quantitative analysis of elastin in tendon, and additional approaches were explored:

1) The Fastin elastin assay was further optimised to quantify the amount of elastin in the whole tendon tissue;
2) Other methods, such as multiphoton and immunohistochemistry, were used to semi-quantify the amount of elastin in different regions of the tendon.

3.3.10. Development of Fastin Elastin Assay Protocol

In the preliminary attempt at using the Fastin elastin assay (section: 3.3.7.1), six extractions were completed, which is timely and costly. Further, a large amount of elastin was collected from samples, with final quantities surpassing the amounts in the standard curve. Preliminary results showed that above 100µg/ml, the standard curve generated by the α-elastin standards was no longer linear. A series of preliminary experiments established that reducing by half the amount of tissue used (from 20mg to 10mg wet weight), only 2 extractions would be needed to extract all tissue elastin. Additionally, to facilitate tissue hydrolysis in 0.25M oxalic acid, and to help homogenise the tissue, whole tendon samples were powdered before the freeze drying step. The finalised Fastin elastin assay protocol for the whole tendon elastin quantification is described in Appendix B1.

3.3.11. Whole Tendon Elastin Quantification- Results

Utilising the newly optimised protocol for the Fastin elastin assay (Appendix B1), tendon elastin content was determined. Results showed that elastin content in the whole tendon tissue was significantly greater in the energy storing SDFT ($3.02\% \pm 0.60$) than in the positional CDET ($1.72\% \pm 0.18$, $p < 0.001$) (Figure 16). With age, the amount of elastin decreased in the SDFT ($2.17\% \pm 0.27$, $p < 0.01$) whereas no age related changes were seen in the positional CDET (Figure 16). These results support the hypothesis that elastin is more prevalent in energy storing tendons and decreases in amount with ageing.

The optimisation of the Fastin elastin assay protocol, based on preliminary results discussed in section 3.3.9, allowed a greater elastin extraction from the whole tendon samples using less tissue and less extractions.

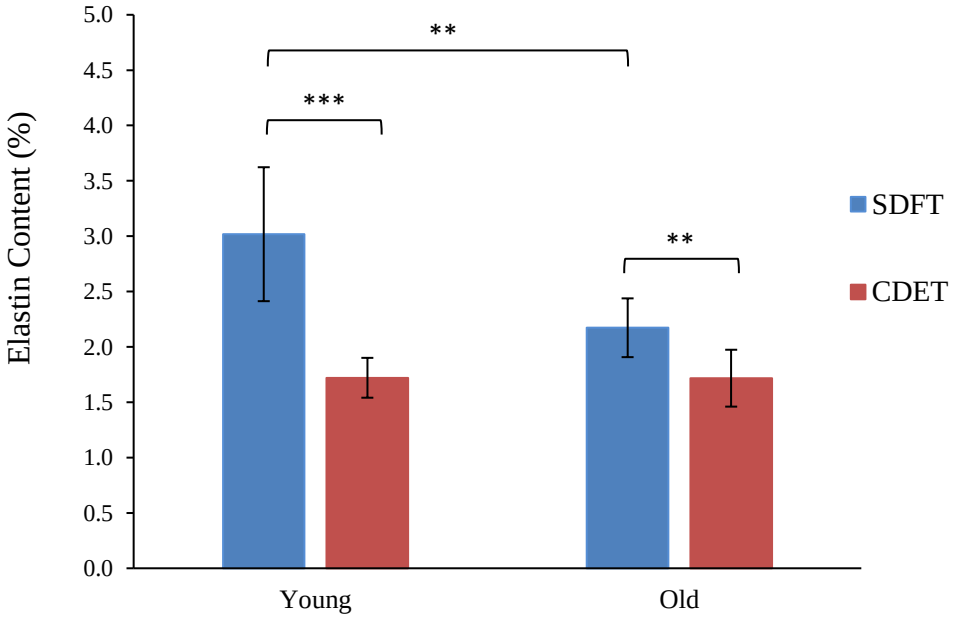

Figure 16: Elastin content expressed as a percentage of dry weight of tendon tissue from 14 horses aged 3 to 7 years (defined as young group, n=7) and 15 to 19 years (old group, n=7). Significant differences between tendon types and age groups are identified by: ** $p<0.01$ and *** $p<0.001$ (normally distributed data – ANOVA). Data are displayed as mean ± standard deviation.

3.4. Assessment of Elastin Localisation in Tendon

Previous data indicating elastin localisation to the IFM (Grant et al., 2015, Thorpe et al., 2016a), suggest it may be particularly important for IFM function, although a quantitative assessment of elastin localisation has yet to be carried out. Further, there are no studies reporting elastin organisation or changes with ageing in tendons with different functions. Therefore, in this study, multiphoton microscopy and immunohistochemistry techniques were used to assess elastin localisation and organisation in both tendon types and age groups, hypothesising that elastin is mainly localised to the IFM in both tendon types.

3.4.1. Sample Preparation for Multiphoton Microscopy

For the validation of the elastin visualisation using multiphoton microscopy, different types of samples were used. The table below summarises all different tissues used and how they were prepared.

Table 4: Summary of sample acquisition and preparation for multiphoton microscopy.

Tissue Type	Animal	Preparation	Mounting Medium
Fascicles and IFM samples	Equine	SDFT and CDET Longitudinal sections were removed from freezer and allowed to thaw; fascicles and IFM samples were dissected as described previously (Thorpe *et al.*, 2012)	Mowiol or PBS
Tendon Cryosections	Equine	Cryosections were removed from the freezer and allowed to thaw for one minute.	Mowiol or PBS
Aortic Tissue (Positive Control)	Porcine	Aorta tissue was collected from the abattoir and small thin pieces of the media layer manually dissected (5x5x0.5mm)	PBS

Samples were mounted with either PBS or Mowiol as described in Table 4. Mowiol 4-88 (Polysciences, Inc., TA) is a commonly used mounting medium in immunofluorescence, as well as many other molecular biology techniques. It is a solution of polyvinyl alcohol and it hardens with time, having the same refractive index as immersion oil. Mowiol was prepared in the laboratory following the procedure described in Appendix B2.

One drop of mounting medium was added to a poly-lysine slide. Individual samples were placed flat on top of each slide and approximately 15-20µl of extra medium was added to the sample. A coverslip was placed on top of the sample and slides incubated in the dark overnight to harden. Samples mounted in PBS, were sealed with nail polish, and kept in the fridge until required.

3.4.2. Multiphoton Microscopy Protocol

Samples were imaged using two-photon confocal microscopy to collect second harmonic generation (SHG) illumination. An inverted Leica laser scanning confocal TCS SP2 microscope with a tunable Ti:Sapphire femto-second multiphoton laser (Spectra-Physics), was used to obtain images. Samples were illuminated at 820 nm and the resulting signal was collected in the backward scattering direction (epi), after filtration through a SP700 dichroic. The photo-multiplier tube (PMT) was set to collect two-photon fluorescence at 500-650nm for elastin and 390-410nm for collagen. A x20 and x63 (Oil-immersion) objective were used. Images were acquired with a frame average of 2 and a line average of 16 at intervals of 1 µm in the z-direction, each with a field of view equal to 238.1 x 238.1 µm containing 1024x1024 pixels. Collagen and elastin were assigned green and red, respectively.

3.4.3. Multiphoton Microscopy – Preliminary Results and Discussion

	Green Channel Collagen	Red Channel Elastin	Merged Channels
IFM Sample 20x in Mowiol	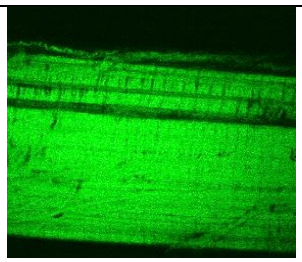	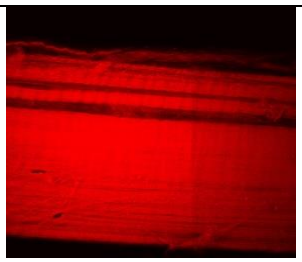	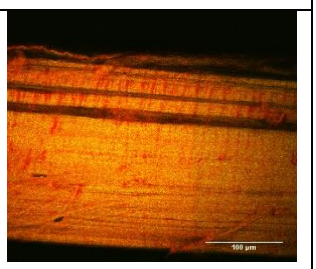
IFM Sample 20x in PBS	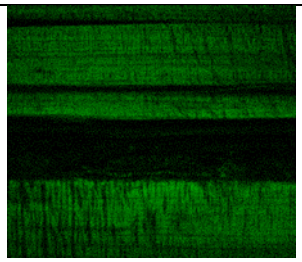	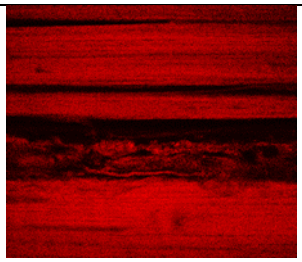	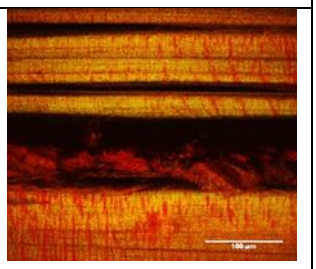
SDFT Cryo-section 20x in Mowiol	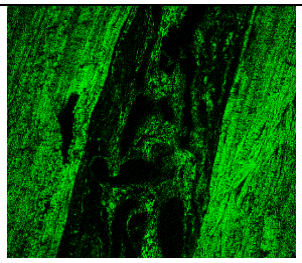	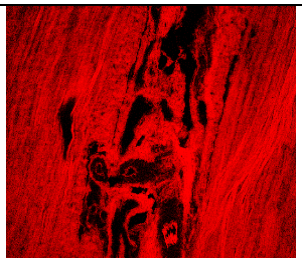	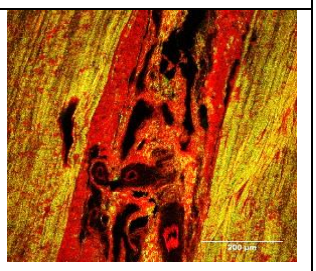
SDFT Cryo-section 20x in PBS	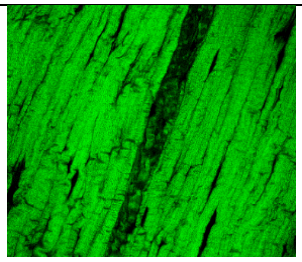	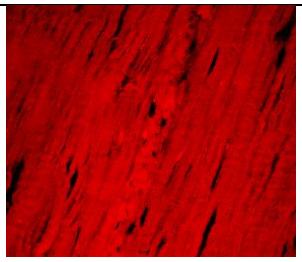	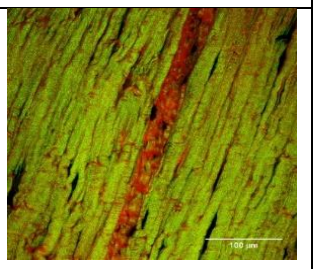
Aorta 63x in PBS	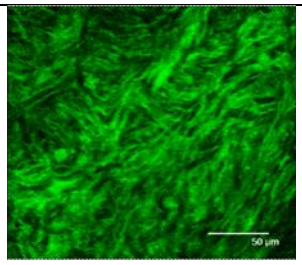	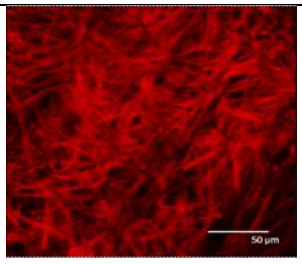	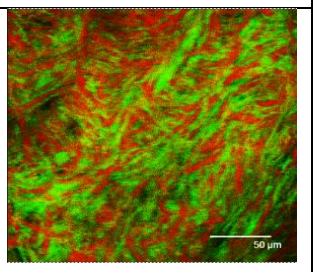

Figure 17: Representative two-photon confocal images taken from a range of tendon and aorta samples.

Results from the multiphoton imaging were not satisfactory. Images from tendon samples showed substantial background, making it impossible to see elastin fibres (Figure 17). Also, there was no clear difference in image quality between samples mounted PBS or Mowiol, as all images showed substantial background (Figure 17).

Samples of porcine aorta tissue were included in this study to validate the elastin imaging. In this case, using the same imaging protocol, images showed significantly less background and it was possible to distinguish elastin fibres from collagen fibres, most evident when both channels are merged, where it was possible to see that collagen and elastin co-localise (Figure 17).

As an attempt to overcome the intense background fluorescence, IFM samples were mounted with Vectashield, following a similar procedure to the one used when mounted with Mowiol. Vectashield is a hard set antifade mounting medium, commonly used in fluorescence microscopy (Chen *et al.*, 2011). Samples were imaged using the same multiphoton protocol described in section 3.4.2. Representative images are showed below (Figure 18).

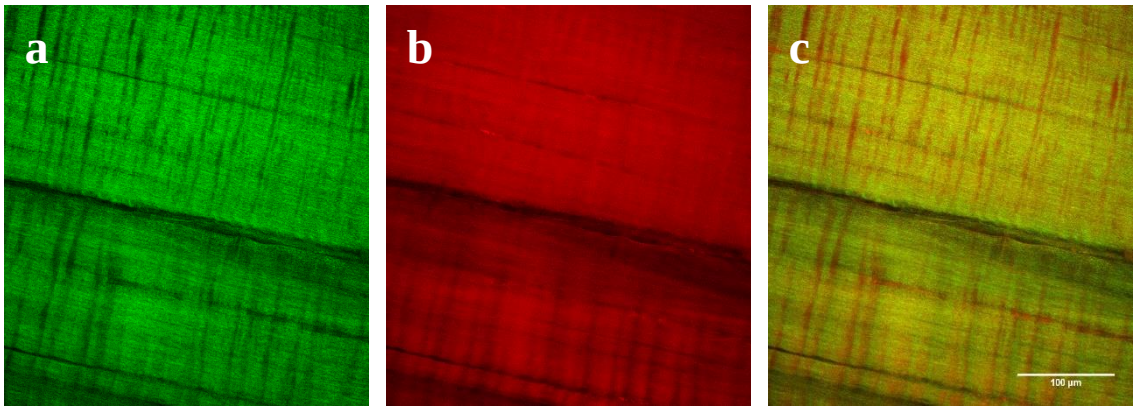

Figure 18: Representative two-photon confocal images showing a single IFM sample from a SDFT mounted with Vectashield. Collagen (a) elastin (b) and both channel's (c) images have the same magnification. A 20x objective was used. Scale bar 100µm.

Images of IFM samples mounted with Vectashield showed no visible reduction of the background with no clear visualisation of elastin fibres. The high levels of background fluorescence are likely related to the extremely high collagen content in tendon, compounded by its dense, highly organised orientation. Multiphoton imaging is commonly preferred, as it allows elastin and collagen visualisation without having

to use immunohistochemical techniques, which are timely and costly. However, autofluorescence in the large, dense tendons offers insufficient image clarity to continue its use. Thus, immunohistochemistry techniques were used as an alternative approach to determine elastin localisation in tendon.

3.4.4. Elastin Immunostaining Development

For elastin immunostaining validation, previously prepared longitudinal and transverse cryosections (Chapter 2), were allowed to thaw for 1 minute, before fixing with ice-cold methanol (−20 °C) for 20 minutes. Slides were rinsed 3 times in phosphate-buffered saline (PBS), treated with hyaluronidase (Sigma, H3884) (4800 units/ml in PBS containing protease inhibitor cocktail (complete mini, Roche)) to increase tissue permeability (Csóka et al., 1997), and incubated over night at room temperature. Cryosections that had not been treated with hyaluronidase were also included in this study. Cryosections were washed 3 times in PBS and incubated in blocking buffer (10% goat serum in PBS) for 1 hour at room temperature. They were then drained and incubated in the primary antibody. Two primary elastin antibodies were tested: ab9519 (Abcam Cambridge, UK) and E4013 (Sigma, UK). No previous equine studies with these antibodies were identified, but they were validated showing positive elastin staining in canine ligament tissue (Smith et al., 2011). Both antibodies were diluted in 5% goat serum in PBS (1:100 and 1:500 dilutions, respectively) and applied to different sections (approximately 100ul of antibody per section) before incubation overnight at 4 °C. After overnight incubation, sections were washed in PBS and incubated with Alexa Fluor 555 Goat anti-Mouse IgG Secondary Antibody diluted in 5% goat serum (1:500 dilution) for 1 h at room temperature (protected from light). Finally, sections were washed and mounted with ProLong Gold Antifade reagent with 4′, 6-diamidino-2- phenylindole (DAPI), and allowed to cure overnight, at 4 °C in the dark, before being sealed with nail polish and imaged. Imaging was performed on a confocal microscope (Leica TCS SP2) using × 40 (oil) objective. Table 5 summarises the first set of test combinations for this validation.

Table 5: Summary of the first validation tests. Elastin staining was compared between two different antibodies and also with or without hyaluronidase treatment.

Cryosections Used for validation	Hyaluronidase Treatment	Primary Antibody	Secondary Antibody	Comments
Young SDFT **(transverse section 10µm thick)**	Yes	Ab9519 (1:100)	Alexa Fluor 555 Goat anti-Mouse IgG (1:500)	Figure 19a
Young SDFT **(transverse section 10µm thick)**	No	Ab9519 (1:100)		Figure 19b
Young SDFT **(longitudinal section 10µm thick)**	Yes	Ab9519 (1:100)		Figure 19c
Young SDFT **(longitudinal section 10µm thick)**	Yes	E4013 (1:500)		Figure 19d

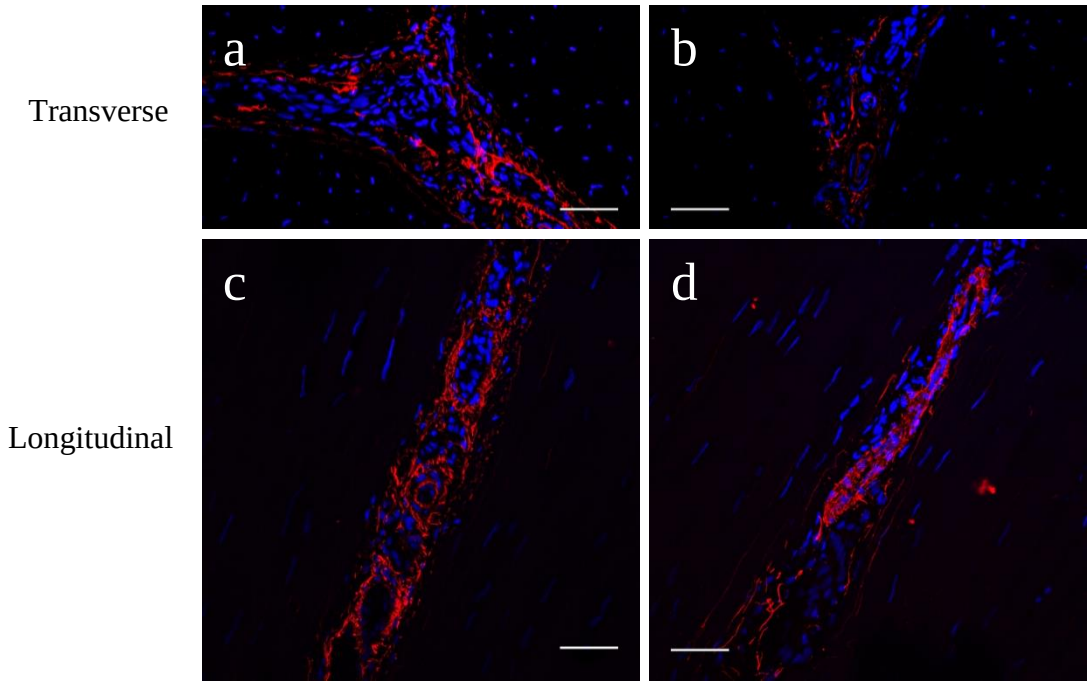

Figure 19: Representative confocal images investigating elastin staining (red) and cell nuclei (blue) in young SDFT cryosections. The respective details of the different conditions tested are summarised in Table 5 (above). Images a and b contain 1024*508 pixels and c and d 1024*1024. Scale bar: 50µm.

Both antibodies worked in equine tendon samples, but confocal images from samples treated with hyaluronidase (Figure 19a) looked slightly clearer compared to images from non-treated samples (Figure 19b). Thus, hyaluronidase treatments were performed in all samples and the Ab9519 antibody (Abcam, Cambridge, UK) was chosen for further staining of elastin fibres in this study.

Although both primary and secondary antibodies appear to work, it was necessary to test them for non-specific staining. Thus, negative controls were performed on longitudinal cryosections from young SDFTs and CDETs (10µm thick).

Negative controls were performed by either omitting the primary antibody from the blocking buffer or by using an isotype control (mouse IgG1 (M5284; 1:100 dilution)) instead of the primary antibody (Table 6, Figure 20c, d). These methods serve to test both primary and secondary antibodies for non-specific staining. Samples were stained as described in section 3.4.5 and imaged using confocal microscopy (Leica TCS SP2) and a × 40 (oil) objective. Representative images showing the outcome of these tests are also shown in Figure 20.

Table 6: Summary of the negative controls performed on both SDFT and CDET cryosections.

Test	Samples	Treatments	Primary Antibody Used	Secondary Antibody Used	Comments
Negative Control by primary antibody omission	Young CDET (longitudinal sections)	Hyaluronidase (Sigma, H3884)	Ab9519 (1:100)	Alexa Fluor 555 Goat anti-Mouse IgG (1:500)	Figure 20a
	Young CDET (longitudinal sections)	Hyaluronidase (Sigma, H3884)	No Primary Antibody	Alexa Fluor 555 Goat anti-Mouse IgG (1:500)	Figure 20b
Isotype Control	Young SDFT (longitudinal sections)	Hyaluronidase (Sigma, H3884)	Mouse IgG1 M5284 (1:100)	Alexa Fluor 555 Goat anti-Mouse IgG (1:500)	Figure 20c
	Young CDET (longitudinal sections)	Hyaluronidase (Sigma, H3884)	Mouse IgG1 M5284 (1:100)	Alexa Fluor 555 Goat anti-Mouse IgG (1:500)	Figure 20d

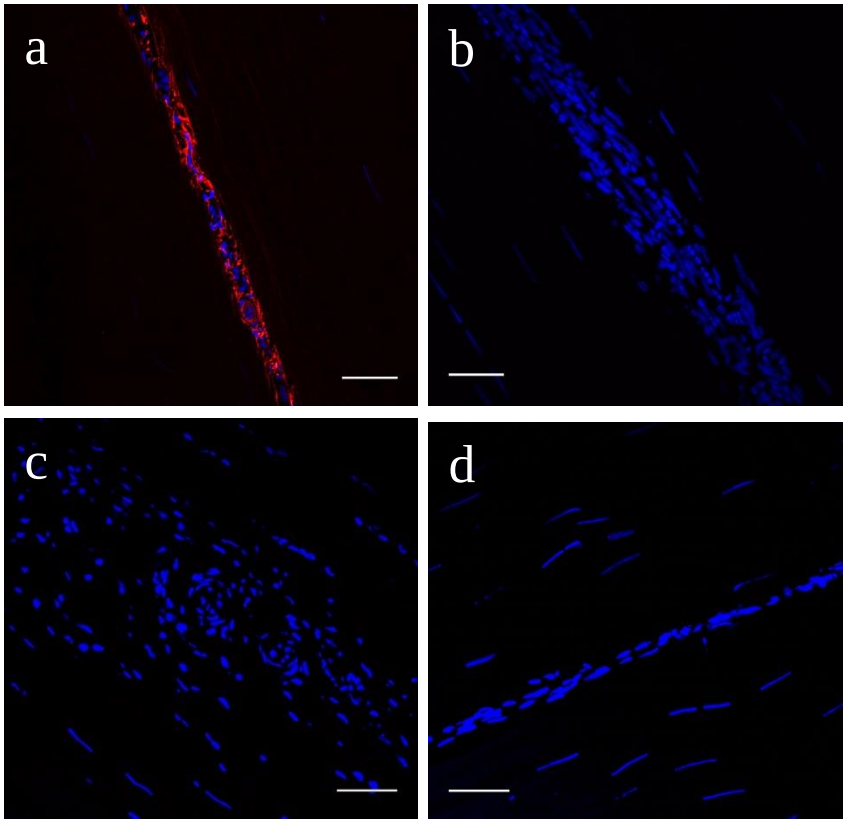

Figure 20: Representative images for cryosections, where staining shows elastin (red) and cell nuclei (blue). The respective details of the different conditions tested are summarised in Table 6 (above). No elastin staining was observed in any control images. Scale bar= 50μm.

While elastin staining was visible in Figure 20a, where the primary antibody was included, no staining was observed in Figure 20b, where the primary antibody was omitted form the blocking buffer. This suggests that neither the primary nor secondary antibodies show non-specific staining. Additionally, by replacing the primary antibody with the isotype control in both SDFT (Figure 20c) and CDET (Figure 20d) sections, no elastin staining was observed, which suggests that the primary antibody is not binding any non-specific antigens that could be present in the tissue. Taken together, data provide confidence that neither the primary nor the secondary antibodies show non-specific staining. The finalised elastin immunostaining protocol for young and old SDFT and CDET cryosections is described in Appendix B3.

A positive control for elastin immunostaining was also investigated, with samples from the equine palmar common digital vein. Small samples of the equine palmar vein were harvested from the forelimbs of one young (6 years) and one old (18 years) horses, within 24 hours of death. Two small samples, approximately 20mm in length and 4mm in diameter, were dissected from each limb and rinsed in PBS (Figure 21a). These samples were cut in smaller pieces and immediately embedded in optimal cutting temperature compound (Figure 21b) and snap frozen in hexane cooled on dry ice. Four longitudinal and four transverse cryosections, 10µm thick, were cut from each sample and placed on poly-lysine slides, which were stored at -80 °C until required for immunostaining.

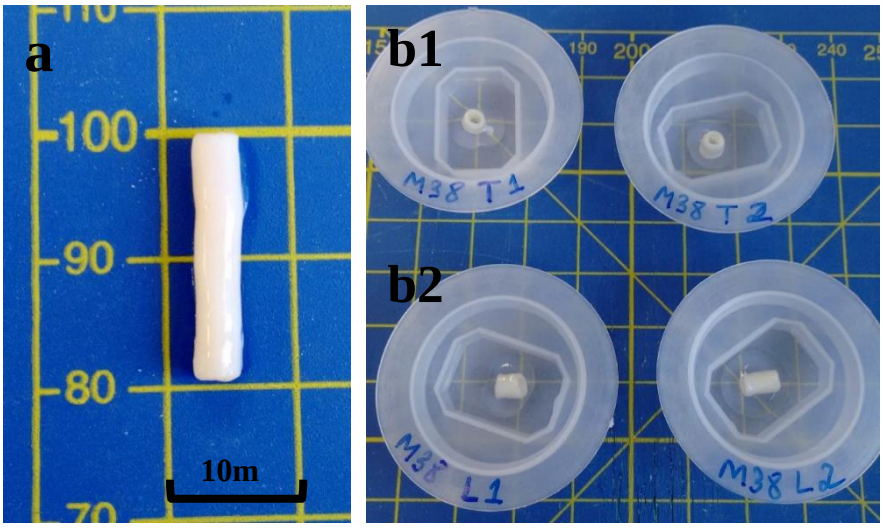

Figure 21: Representative images showing part of the equine palmar common digital vein (a). Samples were cut in smaller pieces and placed in plastic cryomolds (b). Transverse (b1) and longitudinal (b2) cryosections, 10µm thick, were cut from each sample.

Longitudinal and transverse cryosections of equine palmar common digital vein were used as positive controls. Poly-lysine slides were removed from the freezer and allow to thaw for 1minute. Cryosections were stained for elastin (Ab9519) and cell nuclei using the same protocol described before (section 3.4.4), however, instead of methanol, 4% paraformaldehyde was used to fix the sections. Sections were imaged using confocal microscopy (Leica TCS SP2) and a × 40 (oil) objective. To confirm the absence of non-specific staining, no primary antibody was included in the blocking buffer for one of the cryosections (Figure 22b). Representative images are shown below.

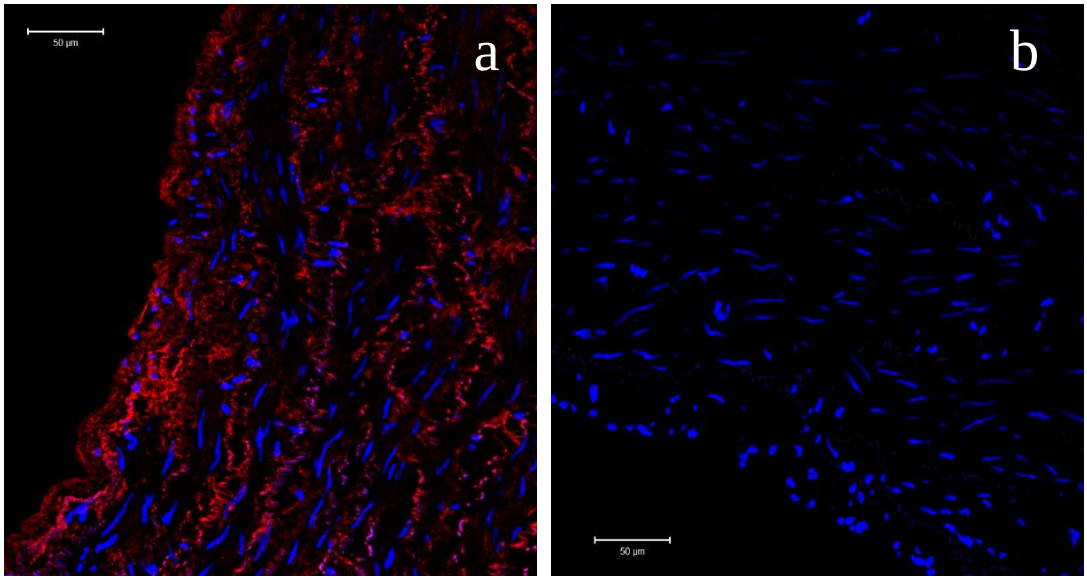

Figure 22: Representative confocal images of the positive control performed on a transverse section of the equine palmar common digital vein showing the organisation of elastin (red) and cell nuclei (blue). Transverse cryosections that included the primary antibody (a) illustrates the elastin organisation and localisation. Similar cryosections where the primary antibody was omitted from the blocking buffer (b) showed no elastin staining. Scale bar: 50µm.

Confocal images of the equine palmar common digital vein immunostained for elastin and cell nuclei showed a typical elastin distribution and localisation as commonly seen in these tissues (Figure 22a) (Zócalo *et al.*, 2013), providing further confidence that the elastin antibody used in this study (Ab9519) works for equine tissue.

3.4.5. Elastin Localisation in Tendon – Results and Discussion

In order to investigate elastin organisation and localisation in young and old SDFTs and CDETs, cryosections from horses aged 3 to 7 years (defined as young group, n=3) and 15 to 17 years (old group, n=3) were prepared. Elastin and cell nuclei were stained, following protocols outlined in Appendix B3. For each section, at least 2 regions were imaged in an area where both fascicular and interfascicular regions could be visualised. Images were captured at a resolution of 1024 × 1024 pixels.

Immunostaining images showed that elastin is mainly localised to the IFM in both tendon types. Barely any elastin fibres were seen in the fascicular matrix. Images suggested that there is more elastin in the SDFT IFM (Figure 23a) compared to the CDET IFM (Figure 23b). With ageing, no changes in elastin staining were seen in the CDET (Figure 23d), whereas elastin staining appeared to decrease in the SDFT (Figure 23c).

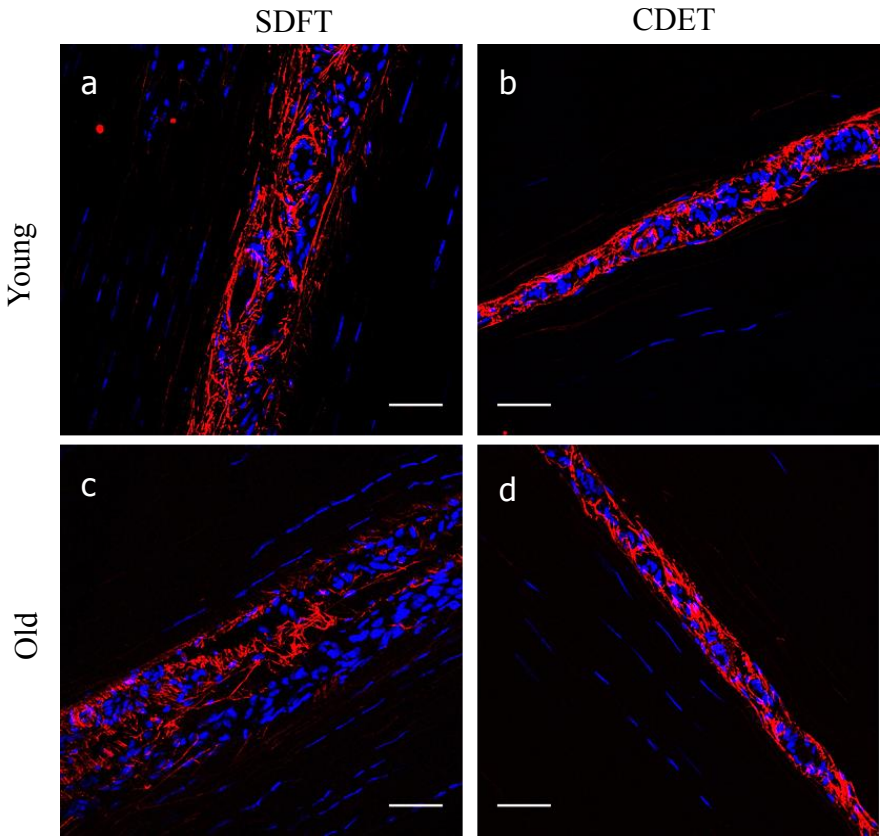

Figure 23: Representative confocal images showing elastin (red) organisation in young and old SDFT and CDET. Longitudinal sections from young SDFT (a), young CDET (b), old SDFT (c) and old CDET (d) were immunostained for elastin (red). Cell nuclei were also stained (blue). Scale bar: 50µm.

A closer look at these images also shown that elastin seems to be localised around circular/oval structures that resemble blood vessels, particularly in the IFM of the energy storing SDFT. This raised some concerns whether the elastin seen in the IFM was mainly associated with blood vessels present in the tissue. Previous studies have shown that tendon blood vessels tend to be present between fascicles, providing the source of tendon vascularization. Thus, it was decided to investigate this further.

Additional cryosections from young and old SDFTs and CDETs (n=2) were immunostained simultaneously for both elastin (ab9519, Abcam Cambridge, UK) and the endothelial cell marker CD31 (rabbit polyclonal, ab28364, Abcam Cambridge, UK; 1:25 dilution). Alexa Fluor 555 Goat anti-Mouse IgG and Alexa Fluor 488 Goat anti-Rabbit IgG were used as secondary antibodies for elastin and CD31, respectively. Longitudinal and transverse cryosections of the equine palmar common digital vein from young and old horses (n=2) were also used to serve as positive controls. Sections were stained for elastin, CD31 and DAPI. Sections were immunostained following the protocol described in section 3.4.4., except 4% paraformaldehyde was used to fix the sections instead of methanol, as preliminary results indicated a better image quality for endothelial cell markers when fixed in PFA.

The equine palmar common digital vein positive control confirmed that the CD31 stained worked in equine tissue (Figure 24). Images taken of transverse sections of the equine vein clearly showed typical elastin organisation in blood vessels with endothelial cells in small vessels embedded in the media and adventitia of the vein (Figure 24).

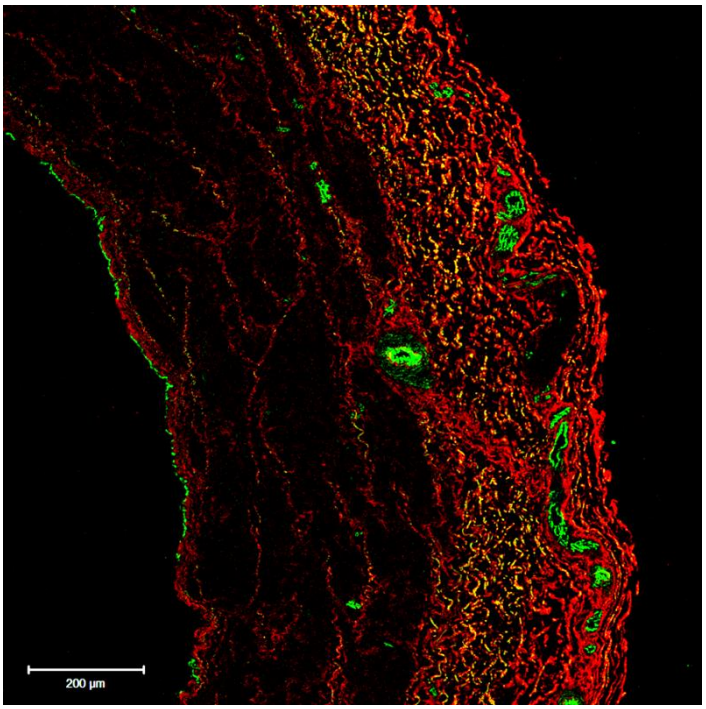

Figure 24: Representative image of the CD31 positive control performed on a transverse section of the equine palmar common digital vein showing the organisation of elastin (red) and CD31 (green). Scale bar= 200µm. Endothelial cells in small vessels embedded in the media and adventitia of the vein are clearly seen.

CD31 staining was also seen in all tendon samples. However, staining consistently detected only very low levels of CD31, which were always localised exclusively to the IFM region (Figure 25), indicating that the majority of elastin within tendon is not associated with the presence of blood vessels.

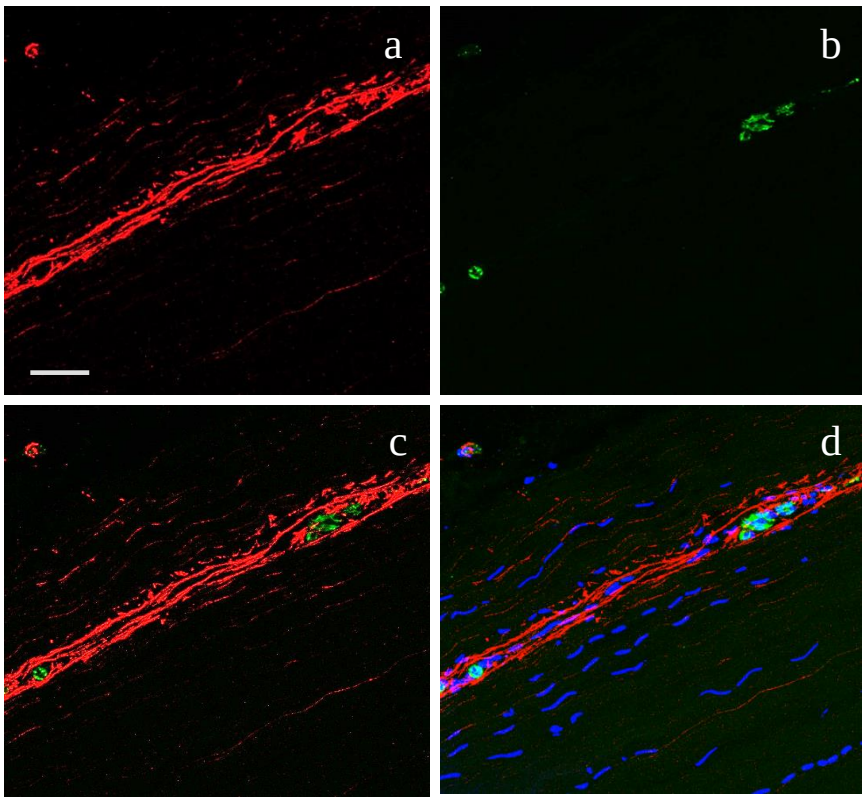

Figure 25: Representative images of a single longitudinal section of the SDFT showing elastin (red) (a) and CD31 (green) (b) staining as isolated channels. The combined elastin and CD31 staining can be seen in image c. Sections were also stained with DAPI (blue) and this channel of information is additionally shown in (d). Scale bar= 50μm.

Taken together, results from the immunostaining suggested that there is more elastin in the IFM of energy storing tendons then in the positional tendons correlating positively with previous quantitative analysis that elastin is more prevalent in energy storing tendons (section 3.3.11). Still to be determined is the amount of elastin in each region of the tendon. Since microdissection was not a viable technique for the regional quantitative analysis of elastin in tendon, a semi-quantitative approach was developed to determine the amount of elastin in each tendon structure (FM and IFM from the immunohistochemistry) and investigate how it varies with ageing.

3.5. Semi-quantification of Regional Elastin in Tendon

3.5.1. Elastin Semi-Quantification Methodology

Semi-quantitative analysis of the elastin immunostained confocal images was performed using ImageJ software. The first step was to establish an unbiased method to identify both fascicular matrix (FM) and interfascicular matrix (IFM) areas, based on their appearance under bright-field microscopy and UV fluorescence. Cell morphology and density, alongside collagen organisation and density were adopted as determining factors to distinguish the two regions (Figure 26). Whilst in the FM, cells are elongated, aligned with the collagen fibres and sparsely distributed, in the IFM, cells are round, high in number and randomly distributed.

The IFM region was manually drawn only using the bright field images merged with the blue channel (cell nuclei), so that the elastin fibres localisation would not influence the delimitation of the IFM area. Once the region of interest (ROI) was delimited, both blue and red (elastin) channels were merged and the amount of elastin in each region determined in a semi-quantitative manner by calculating the percentage area stained positive for elastin.

Although images were taken on different days, the same thresholding was applied to all images, prior to analysis, so that the staining intensity would be as consistent as possible. As an additional measure, the ratio of IFM : FM area was also determined for each image, enabling a comparison of the area occupied by IFM between tendon types and determination of how it changes with age.

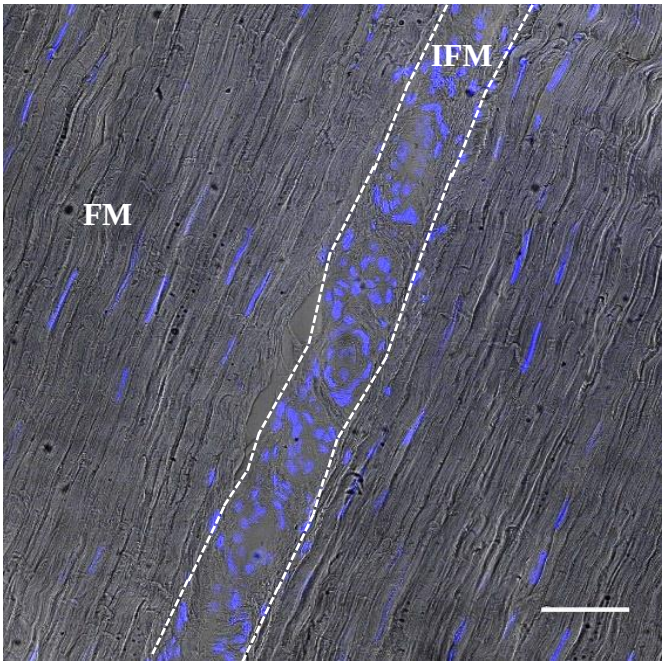

Figure 26: Representative image of a longitudinal section of the SDFT showing tendon structure and cell morphology used to identify the IFM, which is enclosed by white dashed lines. Note the greater cell density, and more rounded morphology of cells, in the IFM compared to those in the FM. Scale bar= 50μm.

3.5.2. Elastin Semi-Quantification in Tendon – Results and Discussion

Results revealed that most of the elastin (>90%) was localised to the IFM in both SDFTs and CDETs (Figure 23, Figure 27). The IFM in the SDFTs showed greater immunostaining for elastin (area fraction: 15.5% ± 4.2) compared to the IFM in the CDETs (7.6% ± 3.7, $p<0.001$) (Figure 27a). Likewise, the fascicular matrix in the SDFTs showed a larger percentage of elastin staining (0.24% ± 0.12) than the CDET FM (0.03% ± 0.02, $p<0.001$) (Figure 27b), although values were an order of magnitude less than measured in the IFM.

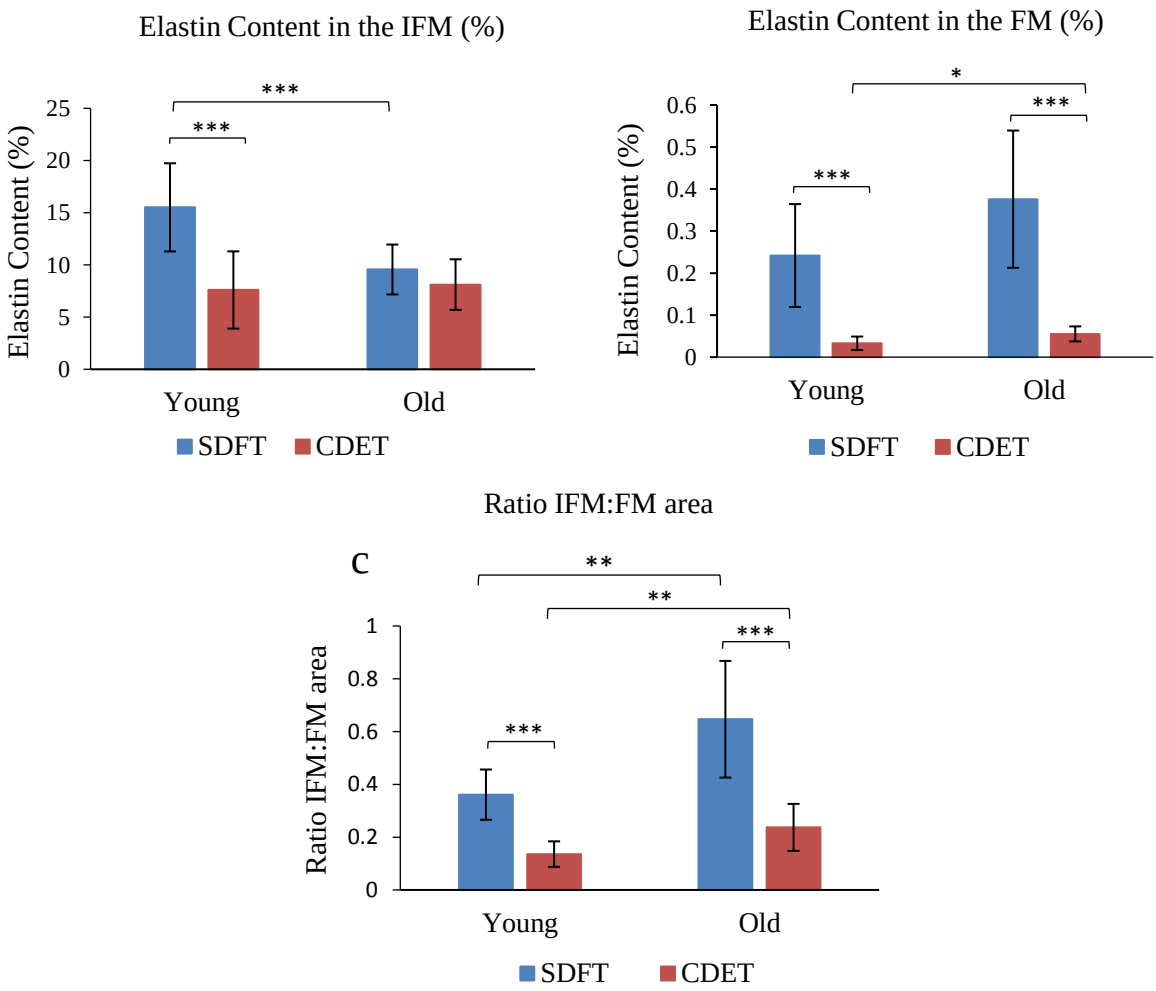

Figure 27: Percentage area of IFM (a) and FM (b) showing positive immunostaining for elastin in young and old SDFTs and CDETs. Note the differences in scale between the IFM (a) and FM (b) regions. The ratio of IFM : FM area was also calculated for all samples, and is compared across tendon types and age groups (c). Significant differences between tendon types and age groups are identified by: * $p<0.05$, ** $p<0.01$ and *** $p<0.001$ (all normally distributed data – ANOVA). Data are displayed as mean ± standard deviation.

There was a decrease in the amount of elastin staining with age in the SDFT IFM (9.6% ± 2.4, $p<0.001$), whilst no age-related changes were seen in the CDET IFM (Figure 27a). In the fascicular matrix, there was a minor increase ($p=0.038$) with ageing in the percentage of elastin in the positional CDET and no age-related changes in the SDFT (Figure 27b).

Concerning the amount of IFM in each tendon type, there was a significantly greater IFM : FM area ratio in the energy storing SDFT (0.36 ± 0.10) compared to the positional CDET (0.14 ± 0.05, $p<0.001$), and this ratio increased with age in both tendon types ($p<0.01$) (Figure 27c).

These results support the hypothesis that elastin is localised to the IFM in both tendons types, with a higher prevalence in the IFM of energy storing tendons compare to positional tendons. Semi-quantitative analysis focusing on percentage area stained positive for elastin does not take into account overlapping fibres and so, an intensity measurement may assist in more fully characterising elastin prevalence. However, these results correlate well with the elastin localisation data, previously shown in this thesis (section 3.3.5). These results have now been published, reporting for the first time, on elastin localisation and semi quantification in different tendon types and how it changes with age (Godinho et al., 2017).

3.6. Assessment of Elastin Organisation in Tendon

3.6.1. Image Scoring Methodology

Semi-quantitative methods to assess elastin organisation in the immunostained images were also explored. Image scoring is one of the most traditional methods to assess organisation of different structures from microscopy images. Hence, this technique was first used to investigate elastin organisation in tendon. Confocal images were scored semi-quantitatively for elastin organisation by four independent scorers, blinded to tendon type and age. The observers were asked to score overall elastin organisation, and elastin fibre alignment parallel and perpendicular to the IFM. For each image, overall elastin organisation within the IFM was scored on a scale from 1 to 5, where 1 denoted highly disorganised elastin fibres and 5 denoted highly organised elastin fibres. A representative image of a longitudinal section from a young SDFT was chosen and presented to all independent scorers. Scorers were provided context, in that a highly organised elastin structure (5) would mean they could identify one or more clear directions with which nearly all fibres were aligned, whilst highly disorganised elastin fibres (1) would equate to no clear directionality to any fibres.

Looking more specifically at the orientation of elastin in the IFM, overall direction of elastin alignment (parallel or perpendicular to the IFM) was also scored on a scale from 1-5, where 1 was used to denote parallel to the IFM and the tendon long axis and 5 to denote high alignment in that direction.

This type of assessment is limited, as it is affected by the subjective interpretation of the observers. Considering that observers will occasionally agree or disagree simply by chance, it is crucial to measure the agreement between them. The kappa statistic (or kappa coefficient) is the most commonly used statistic for this purpose (Viera & Garrett, 2005). A kappa of 1 indicates perfect agreement, whereas a kappa of 0 indicates agreement correspondent to chance. Thus, inter observer agreement was assessed by using an online software tool (http://dfreelon.org/utils/recalfront/recal3/) which determines the average pairwise Cohen's Kappa statistic (Viera & Garrett, 2005).

3.6.2. Image Scoring – Results & Discussion

Scorers reported that in both young and old tendons, SDFT elastin fibres showed significantly greater alignment perpendicular to the IFM (Figure 28c), whilst a significantly greater proportion of CDET elastin fibres were aligned parallel to the IFM (Figure 28b). Additionally, there was a significant reduction in the overall elastin organisation with ageing in SDFTs, which was not evident in CDETs (Figure 28a).

Data shown in Figure 28 report a mean ± standard deviation of sample variability, adopting a mean of each observers score for each individual sample. Observer variability was further investigated with the analysis of the Cohen's Kappa. The average pairwise Cohen's Kappa for the overall elastin organisation, fibre alignment parallel to the IFM and perpendicular to the IFM were: 0.45, 0.48 and 0.39 respectively, where 0.21–0.40 is considered fair agreement, 0.41–0.60 moderate agreement, 0.61–0.80 substantial and 0.81–1 almost perfect agreement between assessors (Viera & Garrett, 2005).

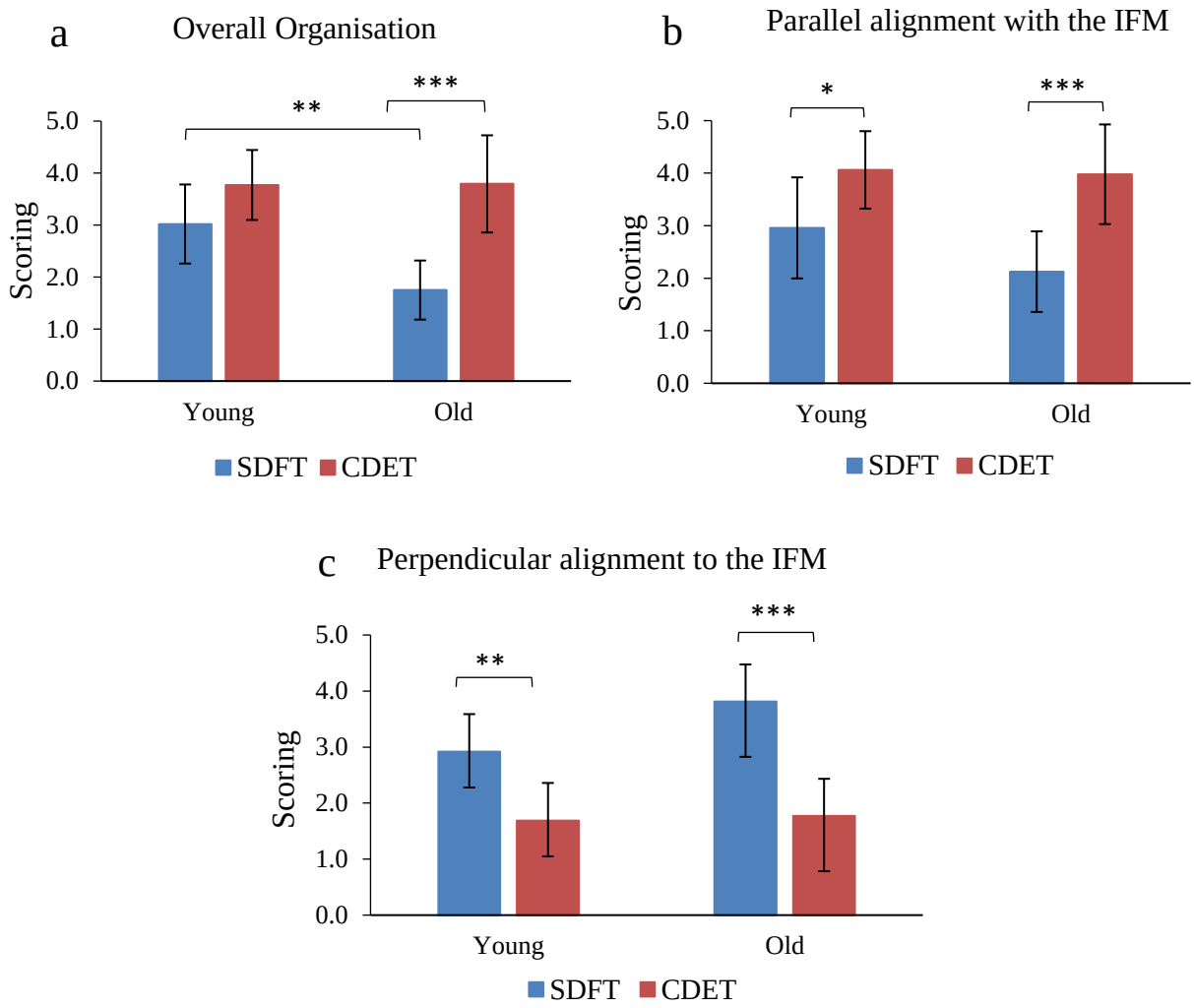

Figure 28: Image scoring for overall elastin organisation (a), alignment of elastin parallel with the IFM (b) and alignment of elastin perpendicular to the IFM (c). Overall elastin organisation within the IFM was scored on a scale from 1 to 5, where 1 denoted highly disorganised elastin and 5 denoted highly organised elastin. A scale of 1-5 was also used for elastin alignment parallel or perpendicular to the IFM, where 1 denotes poor alignment in the direction of interest and 5 denotes high alignment in that direction. Significant differences between tendon types and age groups are identified by: *$p<0.05$, **$p<0.01$ and ***$p<0.001$ (all normally distributed data – ANOVA). Data are displayed as mean ± standard deviation of sample variability, adopting a mean each observer score for each individual sample.

3.6.3. Fast Fourier Transform - Method Development

These data provide a first report of elastin organisation in tendon and how it is affected by ageing. However, as previously mentioned, blind scoring is very dependent on the user, and although the inter observer agreement was reasonable, there is still a high subjectivity implicit. Thus, using a more objective technique to investigate elastin organisation would improve the robustness of the analysis.

The confocal images of elastin organisation were also analysed using a Fast Fourier Transform (FFT), which allows the extraction of quantitative data regarding elastin fibre orientation and alignment (Liu, 1991). First, the orientation of the tendon long axis was defined from the ordered structure of fascicular matrix. Four lines were drawn connecting the rows of tenocytes within the tendon fascicle, and from these, the average fascicle orientation was established, and adopted as the tendon long axis (Figure 29a). The directionality plugin was run in Fiji/ImageJ (Schindelin et al., 2013) which, having performed a FFT on the original image, determines the preferred orientation of structures present in the input image relative to the defined long axis. The plugin assumes any line of 2 or more pixels in length to be a fibre. This plugin computes a frequency distribution histogram, from the transformed image, indicating the number of structures in a given direction (Figure 29b). Briefly, it divides the image into small squares and computes their Fourier power spectra. Later, these spectra are analysed in polar coordinates and the power is measured for each angle (Liu, 1991). Data were reported in bins of 2 degrees over an angular range of 180 degrees (-90 to +90 degrees), with zero degrees denoting alignment with the tendon long axis. The circular standard deviation was calculated for each image, using CircStat (MATLAB) which returns the circular standard deviation of a vector of circular data. The mean and standard deviation of the circular standard deviation were determined for each tendon type and age group. To facilitate data visualisation, values were grouped together to generate 9 bins (20 degrees each).

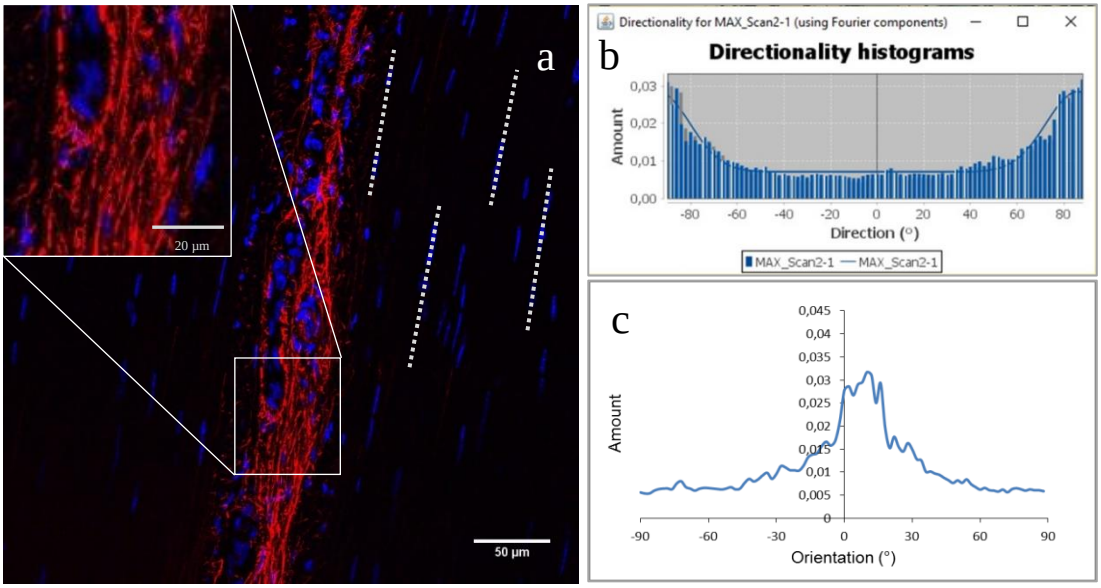

Figure 29: Pictorial representation of the methods used to determine the distribution of elastin fibre alignment within histological sections. The orientation of the tendon long axis was first established. Four lines were drawn connecting rows of tenocytes within the tendon fascicle and, from these, an average orientation was calculated and adopted as the tendon long axis (a). The orientation of elastin fibres within the IFM (seen more clearly in the inset) was then determined relative to the tendon long axis. The image J Directionality plugin was then run, to give frequency distribution histograms, indicating the number of fibres in any given direction, initially relative to the image x axis, reporting the data in bins of 2 degrees over an angular range of 180 degrees (-90 to +90 degrees, where 0 is aligned with the x axis) (b). Taking the calculation of tendon long axis, described in part a, fibre angles were corrected, such that 0 degrees would correspond to the direction of the tendon long axis, and the frequency distribution redrawn (c).

3.6.4. Elastin Organisation in Tendon – Results & Discussion

Analyses of the frequency distribution of elastin fibre orientation in each image showed no significant differences in the circular standard deviation between tendon types in young samples, and no age related changes in CDETs (Table 7 and Figure 30a and b). On the other hand, old SDFTs have a higher circular standard deviation compared to young SDFTs (Table 7, Figure 30a), indicating that elastin fibres in energy storing tendons become more disorganised with age. Also, old SDFTs showed a higher circular standard deviation compared to old CDETs (Table 7), suggesting that the age related loss of elastin organisation is specific to the SDFT.

Table 7: Circular standard deviation values, denoting the variability in elastin organisation in young and old SDFTs and CDETs. A larger number denotes more randomly distributed fibres. Significant differences between age groups are flagged with: *$p<0.05$, whilst significant differences between tendon types are denoted by: [a] $p<0.001$ (normally distributed data – ANOVA). Data are displayed as Mean ± Standard Deviation.

Circular Standard Deviation	**Young**	**Old**
SDFT	42.81 ± 2.86*	46.10 ± 3.38
CDET	40.37 ± 4.02	37.32 ± 5.52[a]

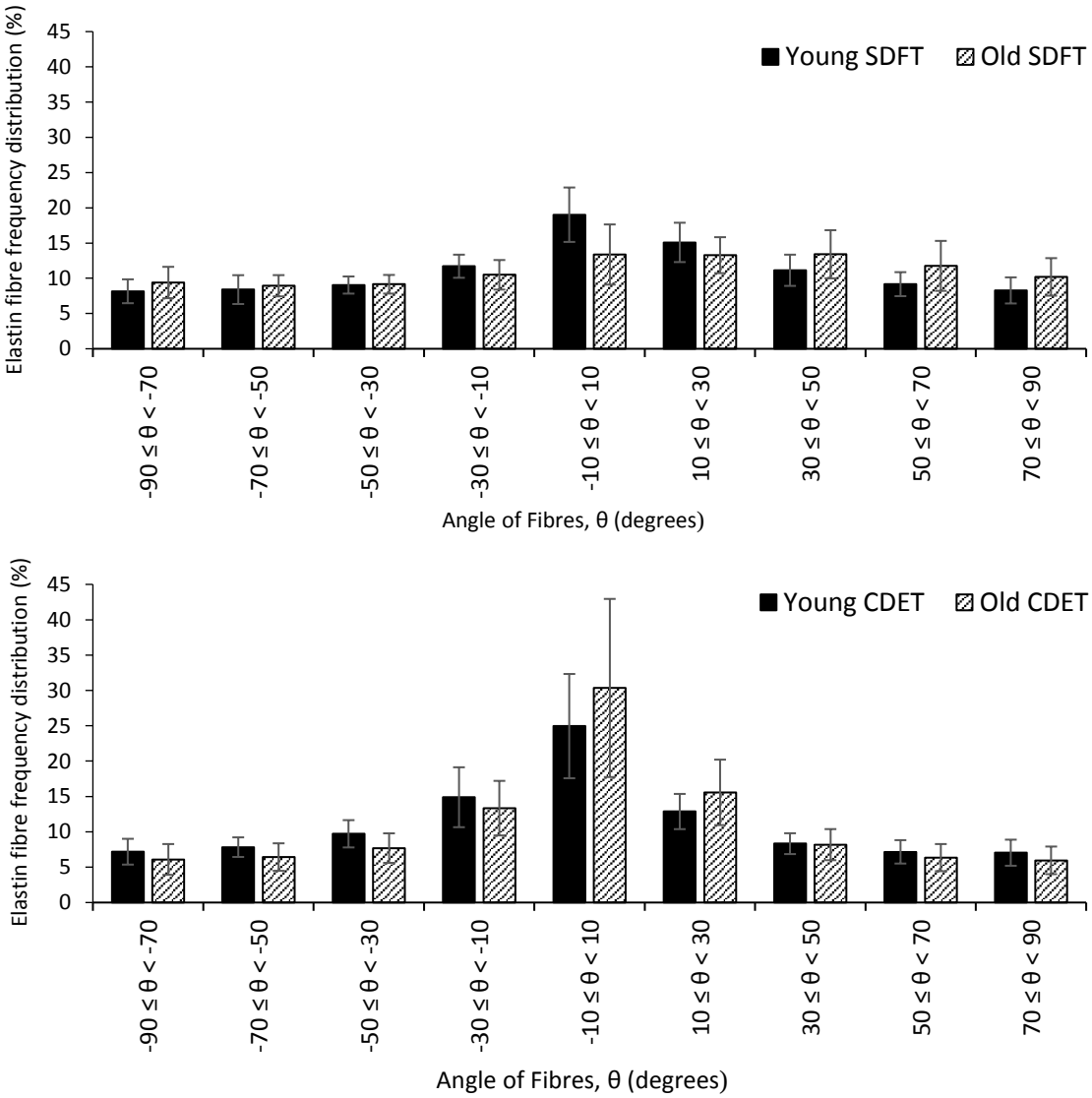

Figure 30: Frequency distribution of elastin fibre alignment, comparing young and old SDFT samples (a) (n=3), and young and old CDET samples (b) (n=3), with data combined from 48 images from three tendons from each group. Angles (θ) are given relative to the long axis of the tendon (denoted as 0 degrees). Data are displayed as mean ± standard deviation.

These results support the initial hypothesis that elastin becomes disorganised with ageing, mainly in energy storing tendon.

Previous studies have suggested that, with ageing, elastin undergoes damage which accumulates over time (Robert et al., 2008) and report an increase in elastin fragmentation with ageing, mainly in cardiovascular tissue (Sherratt, 2009, Greenwald, 2007). Taken together, the loss in elastin organisation in energy storing tendons, might be related to elastin fragmentation.

3.7. Assessment of Elastin Fragmentation in Tendon

3.7.1. Desmosine Quantification – Method Development

To explore elastin fragmentation with ageing in both tendon types, the presence of desmosine, a crosslink unique to mature elastin, was investigated as a marker of elastin fragmentation (Luisetti et al., 2008, Sherratt 2009, Lee et al., 2001, Heinz et al., 2011).

Tendon samples were separated into soluble and insoluble fractions using guanidine hydrochloride extraction and the amount of desmosine in each fraction was determined. Whilst the desmosine in the insoluble fraction represents the functional elastin crosslinked within the tendon matrix, the desmosine in the soluble fraction represents the crosslinked mature elastin which has been partially degraded.

3.7.1.1. Protein Extraction

Approximately 70mg wet weight of tendon, from 6 young and 6 old SDFT and CDET explants, previously prepared as described in Chapter 2, was used for desmosine analysis. Preliminary results showed that this amount of tissue was enough to perform the whole experiment. Tissue was powdered and freeze dried overnight, resulting in approximately 20mg of lyophilised powdered tissue.

Soluble proteins were extracted by incubating overnight with agitation at 4°C in guanidine hydrochloride (GuHCl; 600µl of 4M guanidine hydrochloride, 50mM sodium acetate, pH 6.8 plus protease inhibitor cocktail) (Birch et al., 2008). The remaining pellet was centrifuged (15000g for 15 minutes) and the supernatant collected, after which the pellet was re-suspended in GuHCl and the extraction process repeated. A solution of 50 mM sodium acetate in 95% ethanol was added to the supernatant, at a ratio of 900 µl per 100 µl of supernatant. The soluble fraction was precipitated overnight at -20 °C, and the supernatant was removed following centrifugation (16000 g for 25 min). The pellet was washed three times (to remove all guanidine) with 95% ethanol in water, air dried and re-dissolved in 600 µl of 50 mM sodium acetate. The insoluble fraction was washed six times with water and freeze dried for 24h. Samples were weighed to determine how much soluble protein was extracted. Samples were then assayed for desmosine content as described below.

3.7.1.2. Desmosine Quantification

A solid–phase competition Enzyme-linked Immunosorbent assay (ELISA) (B.I.T.S.® Desmosine ELISA Kit (Mologic Ltd, UK) was adopted to quantify levels of the crosslink desmosine as a marker of elastin degradation (Luisetti *et al.*, 2008). This kit has been optimised in terms of assay range, specificity and interference to measure desmosine excreted into human urine as a free form, when elastin is degraded (Watanabe et al., 1989, Gunja-Smith 1985). Although desmosine in humans is identical to desmosine in different animal species, using this kit to measure desmosine in tendon tissue still represents a big challenge and requires validation of the its performance.

First, total elastin content was measured in a small amount of both the soluble and insoluble fractions of each sample, using the FASTIN elastin assay, as developed previously (finalised protocol in Appendix B1). Approximately 300µl of the re-dissolved soluble fraction (in 50mM sodium acetate) was measured and directly assayed. No dilutions or extractions were required. Regarding the insoluble fraction, approximately 2x2mg dry weight tissue was weighed and extracted twice in 0.25M oxalic acid. The resultant supernatant was assayed and the amount of elastin determined.

Then, the remaining soluble and insoluble fractions of each sample were hydrolysed with 6M HCl (5mg/ml) for 48h at 110°C. Once cooled, samples were neutralised by adding an equivalent amount of 6M NaOH to every sample. pH paper was used to confirm that samples had a pH of approximately 7, as it had been established that if samples were too basic or acidic, the ELISA would not work. It should be noted that, as part of the validation process, direct removal of the HCl was attempted through lyophilisation, however poor mixing of proteins prevented use of this approach and necessitated the use of NaOH as neutralising agent

Soluble and insoluble fractions were diluted prior to assay: 1:3 and 1:10, respectively to bring them within the range of the standard curve. Previous tests were performed to determine the range of standards and the sample dilution factors. The ELISA protocol was performed according to the manufacturer's instructions (Mologic LTD, UK). Both standards and test samples were assayed in duplicate. Desmosine content was determined by comparison to a standard curve and expressed as ng desmosine per mg of elastin content.

3.7.2. Desmosine Quantification – Results and Discussion

Results showed that in the insoluble fraction, the amount of desmosine was significantly greater in the CDET (5720.8 ng DES/mg elastin ± 1516.8) compared to the SDFT (1776.1 ng DES/mg elastin ± 888.6, $p<0.01$) (Figure 31a). However, no tendon type differences were seen in the soluble fraction (Figure 31b). Similarly, in the old group, the amount of desmosine was significantly greater in the CDET (6758.5 ng DES/mg elastin ± 1875.4) compared to SDFT (2871.8 ng DES/mg elastin ± 1418.9, $p<0.01$) (Figure 31a) with no tendon type differences identified in the soluble fraction (Figure 31b). No age-related differences in desmosine content were seen, either in the soluble or insoluble fractions.

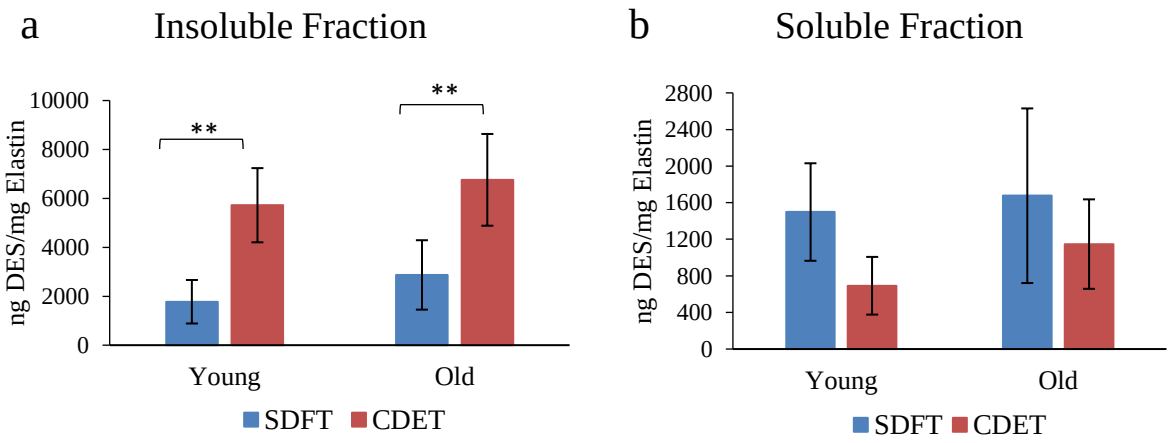

Figure 31: Desmosine content expressed as ng desmosine per mg of elastin in both insoluble (a) and soluble (b) fractions of SDFTs and CDETs from horses separated into 2 groups based on age (n=6/age group). Note the differences in scale in the y axis between a and b. Significant differences between tendon types and age groups are identified by: ** $p<0.01$ (all normally distributed data – ANOVA). Data are displayed as mean ± standard deviation.

3.8. Discussion

The majority of these results have been published in S*cientific Reports* (Godinho et al., 2017). This is the first study to quantify elastin content in two functionally distinct tendons, additionally reporting changes with ageing. The organisation and distribution of elastin fibres were also investigated, using several techniques to characterise their alignment, organisation and fragmentation in both young and old SDFTs and CDETs. The results broadly support the hypotheses, showing a greater amount of elastin in the energy storing SDFT, mainly localised to the IFM. With ageing, there was a decrease in elastin content and organisation in the energy storing SDFT, although no fragmentation was identified.

Most of the elastin (>90%) was localised to the IFM in both tendon types, with greater elastin staining observed in the SDFT IFM compared to the CDET IFM. These findings support previous studies that have shown the IFM is comparatively rich in elastin, both in tendon (Grant et al., 2013) and ligament (Smith et al., 2011). Further, the data confirm recently published work suggesting a greater abundance of elastic fibres in the IFM of the energy storing SDFT, relative to the CDET IFM (Thorpe et al., 2016a). Previous studies have shown that the IFM in the SDFT is more extensible and less viscoelastic compared to CDET IFM (Thorpe et al., 2012, Thorpe et al., 2015b). Therefore, these data suggest that the presence of elastin may provide the IFM with its elastic recoil ability, necessary for the efficient energy storing and return that is required in energy storing tendons (Thorpe et al., 2015b).

It is important to highlight that this study is focused on equine tendon, and specifically on elastin as a component of the IFM. It is possible that energy storing tendons from other species utilise different mechanisms to facilitate extension, or that IFM components other than elastin confer the specialised mechanical properties of the IFM. However, the role of the SDFT, as an extreme energy storing tendon (Alexander, 1991), makes it a useful tendon to investigate, as we would expect specialisations to be more pronounced. Also, as we are investigating structural differences associated with fatigue resistance, an initial focus on elastin seems appropriate.

It should be noted that some of the elastin seen in the IFM may be associated with blood vessels. Indeed, the positive staining for endothelial markers observed in all samples of both tendon types, confirms the presence of blood vessels in both the SDFT and CDET, and localisation of vessels to the IFM, agrees with previous data

identifying this region as the source of tendon vascularisation (Tempfer & Traweger 2015, Fenwick et al., 2002).The extent of CD31 staining is perhaps surprising, with every region of IFM in all samples staining positive, indicating that vascularisation of the IFM is extensive in all tendon types, not just the more highly loaded energy storing tendons. However, despite the prevalence of CD31 staining, a qualitative analysis of the IFM highlighted that the majority of elastin was not localised exclusively to the region of CD31 staining and vessels, suggesting a role for elastin as an integral component of the tendon matrix also. Applying a fast Fourier transform to the confocal images, yielded quantitative data about elastin alignment and orientation, and allowed comparison with a more traditional histological image scoring approach (Liu 1991, Berens 2009). In the young group, there were no significant differences in elastin organisation between tendon types, with both frequency distributions identifying a predominant fibre orientation parallel to the IFM. This seems at odds with the additional image analysis performed by the independent scorers, who reported that there were a greater number of elastin fibres aligned perpendicular to the IFM in the young SDFT than in the CDET. However, a closer comparison of the quantitative frequency distribution data does suggest that a greater proportion of fibres are fully aligned with the IFM in the CDET than the SDFT and fibres orientation is more evenly distributed in the SDFT. As fibres denoted "perpendicular" to the IFM by the scorers are unlikely to be at a precise angle of 90 degrees, it is likely the range of "perpendicular" fibres are seen across the bins at either end of the frequency distribution data, where greater values are seen for the SDFT compared to CDET. The presence of perpendicularly aligned elastin fibres in the SDFT IFM, suggests that, elastin orientation in the IFM may indeed play a crucial role in allowing fascicles to slide. We hypothesise that elastin fibres oriented in this perpendicular manner may serve as a "bridge" between adjacent fascicles, which would assist in returning fascicles to their initial location once external forces have been removed.

With ageing, circular standard deviation increased in the SDFT, resulting in a significant difference in elastin organisation between old SDFTs and CDETs. This suggests that elastin fibres in the IFM of CDETs tend to remain more closely aligned with the tendon long axis than those in the IFM of the SDFTs, which become more dispersed with age.

These data correlate well with image scoring, which indicated a significant decrease in the overall organisation of elastin in old SDFTs compared to young SDFTs.

Taken together, the results indicate that elastin becomes more disorganised with ageing in the energy storing SDFT. It was notable that, a significant increase in the IFM : FM area ratio in both tendon types was observed with ageing, suggesting that the IFM may be losing its structural integrity, possibly associated with changes in elastin organisation and decreased elastin content (Godinho et al., 2017). In contrast, previous studies have reported a significant reduction in SDFT IFM thickness with ageing, mainly in the distal region of the tendon (Ali et al., 2018). This might be explained by the different sectioning orientation these samples might undergo prior to further analysis. Often during sectioning, IFM region is damaged and the IFM tissue gets ripped apart, which may cause a misleading increase in thickness.

In this study, immunofluorescent methods were used to assess semi-quantitatively the amount of elastin in different tendon compartments. Attempts were made to establish the absolute amounts of elastin within the IFM and FM in both tendon types using a microdissection technique. However, this technique has proved time consuming and difficult to standardise. Laser capture microdissection was considered as an alternative approach to collect specific matrix regions. However, while the use of this technique allows isolation of different regions of tendon tissue with negligible contamination, it only allows the collection of very small amounts of tissue, such that biochemical assays would not be possible. Fortunately, biochemical assays are not the only available techniques that allow absolute quantification of the proteins in the laser captured tissue. Mass spectrometry is a well-established technique which also allows to determine the abundance of proteins in a sample. However, previous studies were unable to detect elastin in laser captured samples of FM and IFM, likely a technical issue because elastin is extremely insoluble and highly crosslinked, and therefore particularly difficult to identify using mass spectrometry (Thorpe et al., 2016c, Dakin et al., 2014). Future studies should focus on improving the methodology by implementing a few additional steps to the mass spectrometry analysis which have been suggested to help on the elastin detection (Heinz *et al.*, 2013).

As elastin is highly hydrophobic and crosslinked, it is also highly resistant to proteolytic degradation. However, under repetitive loading, it undergoes damage which accumulates over time (Robert, Robert and Fu, 2008). With ageing, elastin is also degraded through chemical mechanisms which affect its function (Robert, Robert and Fu, 2008). Studies have shown an increase in elastin fragmentation with ageing,

which links to changes in tissue elasticity in cardiovascular tissues and increased human mortality (Sherratt 2009, Greenwald 2007).

Indeed, previous studies have demonstrated that the IFM stiffens with age and becomes less fatigue resistant in energy storing tendons (Thorpe et al., 2013a, Thorpe et al., 2017). Elastin is a highly extensible, elastic and fatigue resistant protein, hence the overall reduction in IFM elastin seems likely associated with reduced IFM extensibility (Godinho et al., 2017). Further, the associated reduction in IFM fatigue resistance in ageing tendons has previously been linked to reduced IFM recoil after loading (Thorpe et al., 2013a, Thorpe et al., 2017, Thorpe et al., 2015c, Thorpe et al., 2016b), and current data indicates that this may stem for the loss of elastin organisation and reduction in elastin "bridges" between fascicles (Godinho et al., 2017) .

Taking these findings together, it was hypothesised that the reduction in elastin content and increasing elastin disorganisation seen with ageing may be due to elastin fragmentation (Godinho et al., 2017). Thus, in the current study, desmosine, an unique crosslink in mature elastin, was used as a marker of elastin fragmentation (Luisetti et al., 2008, Sherratt 2009, Lee et al., 2001, Heinz et al., 2011). The number of desmosine crosslinks was measured in the insoluble fraction (functional elastin crosslinked within the tendon matrix), and also in the soluble fraction (crosslinked mature elastin which has been partially degraded and therefore can be solubilised (Luisetti et al., 2008)). Data showed a 2-fold greater amount of desmosine per unit elastin content in the insoluble fraction of CDETs compared to SDFTs, however, no tendon type differences were seen in the soluble fraction.

These results were unexpected and do not support the hypothesis. This might be due to the fact that the method used cannot detect fragmentation if the fragments remain insoluble. Alternatively, this might indicate that CDETs are more densely crosslinked compared to SDFTs. Previous studies have shown that the cross-linked regions of elastin are more rigid than regions free of crosslinks, meaning more crosslinking would reduce the overall compliance of the surrounding structure (Anwar, 1990). This may explain why CDET IFM is less extensible than SDFT IFM. Similarly, in the old group, the CDET has a greater number of desmosine crosslinks in the insoluble fraction compared to SDFT. In the soluble fraction, once again, no significant changes were identified. However, it is important to highlight the greater variation in the SDFT data, mainly in the soluble fraction, compared to CDET. This could be due to variations in exercise history between horses, which may lead to

different levels of mechanical degradation within the tendon and different degrees of crosslink fragmentation. Unfortunately, it was not possible to collect an exercise history for the horses used in this study. It is also noteworthy that previous studies have demonstrated large variations in the mechanical properties of the IFM in the SDFT, particularly in the stiffness, failure properties (Thorpe et al., 2015c), and fatigue resistance (Thorpe et al., 2017, Thorpe et al., 2016b). These individual variations may result in the large variations in SDFT failure properties reported previously (Thorpe et al., 2013a, Batson et al., 2003) and also aid in explaining why some individuals are more at risk of tendon injury than others.

Chapter 4 - The Effect of Elastin Depletion on the Mechanical Properties of Tendon

4.1. Introduction

Previously published work has focused on understanding how energy storing tendons can behave more elastically and stretch further than positional tendons. Two key energy storing tendon specialisations have been discovered; individual fascicles are helically wound like springs for elasticity (Thorpe et al., 2013b), and the matrix between fascicles is load bearing and elastic in nature, allowing fascicles to slide when loaded and slide back when load is removed (Thorpe et al., 2012). It has also been demonstrated that a loss of these specialisations with ageing leads to reduced fatigue tendon resistance (Thorpe et al., 2013a, Thorpe et al., 2014). Unravelling these mechanisms has exciting implications for treating tendon injuries, not only providing the functional understanding from which to develop treatments, but also for targeting preventive approaches to stop age-related loss of tendon elasticity.

Published data suggested that changes to the interfascicular matrix (IFM) with ageing are a primary cause of tendon overload damage (Thorpe et al., 2013a). However, very little is known about the IFM and its overall contribution to tendon mechanics. Recent studies have shown high levels of proteoglycans in the IFM, and also elastin bridging across the IFM, linking fascicles (Thorpe et al., 2016a, Thorpe et al., 2016b).

In chapter 3, it was shown that overall elastin content in tendon is low, but mainly localised to the IFM of energy storing tendons (Kannus 2000, Grant et al., 2013, Godinho et al., 2017) suggesting that it may be of particular importance for IFM function, mainly in energy storing tendons. This chapter investigates the functional consequences of elastin in tendon in further detail, focusing on the energy storing SDFT.

4.2. Aims and Hypotheses

The interaction of structural molecules in the extracellular matrix (ECM) of tendon influences its mechanical properties and response to load. Understanding how individual molecules contribute to the overall mechanics of the tissue is very important to better understand and treat tendon injuries, which affect severely both humans and animals. However, defining the mechanical role of a minor component of the ECM such as elastin, where it makes up less than 5% of the tendon dry weight, is challenging. Common approaches are either the use of genetic knockout models, or direct enzymatic treatment, combined with mechanical testing (Grant et al., 2015, Beenakker et al., 2012).

It is hypothesised that IFM failure and fatigue properties will be detrimentally affected by a reduction in elastin content, whilst fascicle mechanical properties will not be affected. It was further hypothesised that SDFT IFM ability to recoil will be affected by elastin digestion. Lastly, it was hypothesised that tendon fatigue resistance is directly correlated to elastin content and elasticity of the IFM. These hypotheses were tested by performing elastase treatments to remove elastin from tendon sections, fascicles and IFM samples followed by analysis of the samples' failure and fatigue properties. A custom designed uniaxial rig was also used to investigate IFM recoil ability after cyclic loading.

4.3. Sample Preparation for Validation of Elastin Removal

Prior to any mechanical characterisation, it was necessary to optimise methods for removing elastin from tendon fascicles and IFM samples.

Fascicles and IFM samples are of similar size and considered together for validation purposes. To simplify the validation process and to ensure penetration of the enzyme throughout the tissue, groups of at least 2 fascicles, joined by the IFM, were prepared for validation, such that if the removal of elastin was successful across fascicles and IFM in these larger samples, no difficulties will be anticipated for single fascicles.

A SDFT quarter sections (n=1; 7 years old; Chapter 2) was removed from the freezer and allowed to thaw for 30min at room temperature, while being kept hydrated by spraying several times with PBS. Using a scalpel and size eleven blades, roughly 20-25 groups of 2 intact fascicles (bounded together by the IFM), were dissected, and stored in a petri dish with a layer of tissue impregnated with PBS and placed in the fridge until required. Samples served as their own controls by comparing analysis with and without treatment.

4.4. Elastase Treatment Validation – Method Development

To validate the elastase treatment, dose response experiments (enzyme concentration) were performed to determine the amount of elastase needed to digest the elastin in a pre-set incubation period of 16H. A 16H incubation period was set as a similar time period to other studies, and one which was compatible with the time available to do each experiment. Pairs of fascicles were divided into 3 groups: fresh, control and elastase. Samples in the "fresh" group remained stored in the petri dish in the fridge and were used within 16hours; samples in the "control" group were incubated in the buffer solution without elastase while samples in the "elastase" group were incubated in the buffer solution with elastase, both for 16 hours at room temperature. The purpose of having a "control" group in the validation is to help differentiate the influence of the incubation of the IFM samples from the action of the elastase in the specimens.

While some studies have shown that 1U/ml and 36 hours of incubation were enough to digest approximately 50% of elastin from rat tail fascicles (Grant et al., 2015), others showed that 3U/ml and 12 hours would be enough to digest similar

percentages of elastin from rat caudal and lumbar motion segments (Barbir et al., 2010) and human lumbar spines samples (Smith et al., 2008). Considering that both samples tested in these studies are of similar size to tendon IFM samples, it was decided to first test IFM samples treated under one of the following conditions: control (0 U/ml), 2 U/ml, 4U/ml or 6U/ml elastase (approx. 4 IFM samples/condition). IFM samples were incubated in the control buffer (5ml 1x PBS plus 0.1mg/ml soybean trypsin inhibitor (SBTI)) with the specified amount of elastase (trypsin-free porcine pancreatic elastase, EPC134, Elastin Products Co., Owensville, MO). Elastase concentration (U/ml) was determined based on manufacturer-stated activity of >9 U/mg of protein on the substrate Suc-Ala-Ala-Ala-pNA, and that 1U will hydrolyse 1 μmol of substrate/minute at pH 8.3 and 25°C. Soybean trypsin inhibitor was added to the control buffer as it has been suggested that it helps block proteolytic action against collagen, in case the elastase is contaminated with trypsin (Oxlund et al., 1988, Henninger et al., 2013). Previous studies have established that 0.1mg/ml SBTI is enough for disabling any trypsin activity in the elastase solution (Grant et al., 2015).

4.4.1. Immunostaining - Methodology for Measuring Elastin Depletion

Confocal microscopy was used to investigate changes to the tissue composition with the elastase treatment. After incubation, one sample of each group: fresh, control, elastase (2U/ml, 4U/ml and 6U/ml) was rinsed twice in PBS, to facilitate removal of digested elastin fragments trapped in the tissue macrostructure, and immunostained for elastin and cell nuclei. Samples were fixed in 4% PFA for 30 min at room temperature, and then washed 3x in PBS. Samples were incubated in 10% Goat Serum for 1H at room temperature and then incubated overnight in the elastin antibody (Ab9519; 1:100 dilution in 5% Goat Serum) at 4°C. They were then washed 3x in PBS and incubated in the secondary antibody (555 Goat anti Mouse IgG H+L, 1:500 in 5% Goat Serum) for 1H at room temperature (protected from light). After incubation, samples were washed 3x in PBS and incubated, for 5min, in DAPI staining (1:1000 in 5% goat serum). Preliminary results showed better cell nuclei staining if DAPI staining was carried out first, instead of combined Prolong Gold with DAPI staining step, as it seems to penetrate the tissue better. Tissue samples were finally washed twice in PBS, placed on poly-lysine slides and mounted with prolong Diamond antifade, and

coverslipped. Samples were stored in the fridge overnight to cure and imaged within 24 hours.

Samples were analysed under a laser scanning confocal microscope Zeiss ELYRA (Carl Zeiss AG, Oberkochen, Germany). A 63x oil objective was used for all imaging. Confocal z series were taken with a format of 225 x 225μm and a pixel size of 0.11 x 0.11μm and a z-step size of 0.25μm.

4.4.2. Immunostaining - Preliminary Results & Discussion

Samples from each treatment were imaged and while elastin was visible in both fresh and control samples, no elastin was seen in any of the samples incubated in the elastase solutions (2, 4 nor 6 U/ml). Thus, it was decided to prepare further samples and incubate them in solutions with a lower elastase concentration: 0U/ml 0.2U/ml and 2U/ml, while keeping the same incubation period (16H) and temperature (room temperature).

A longitudinal section of another young SDFT tendon (6 years old), previously prepared was used. IFM samples were dissected and incubated for 16H in one of the solutions as previously described: 0U/ml 0.2U/ml and 2U/ml. A few samples were kept aside for the fresh group and stored in a petri dish at 4°C until required. After incubation, samples were washed in 2x in PBS and divided into 2 groups – samples for biochemical analysis and samples for immunohistochemical analysis. Fresh samples were also equally divided. Samples for biochemical analysis were stored in cryotubes at -20°C until required, whereas samples for immunohistochemistry analysis were prepared as explained previously (4.4.1).

Immunohistochemistry images showed elastin fibres in the IFM region of both fresh (Figure 32a) and control (Figure 32b) samples. Very few elastin fibres where seen in the samples treated with 0.2U/ml elastase (Figure 32c), and no elastin fibres were seen in the 2U/ml elastase treated samples (Figure 32d).

These data confirmed the preliminary result that all elastin was removed with an elastase concentration equal or above 2U/ml. Thus, in order to further validate the elastin depletion and to investigate potential non-specific degradation of other structural ECM molecules, biochemical analyses were performed.

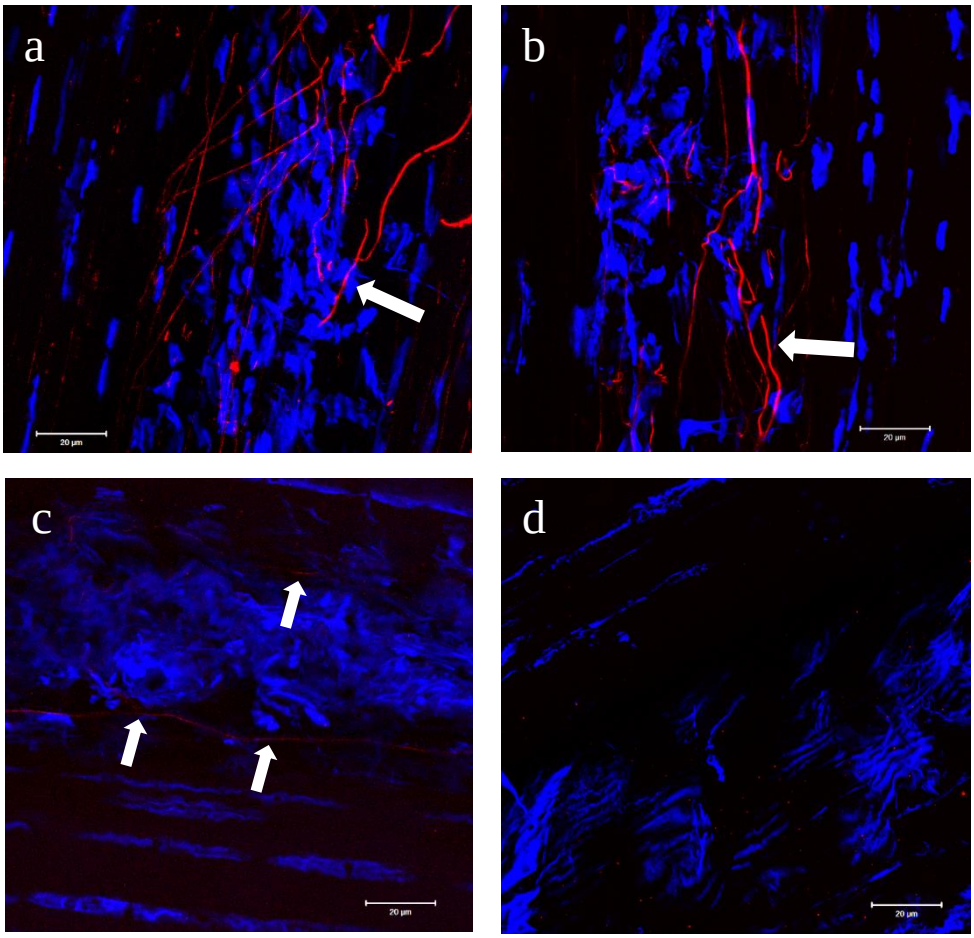

Figure 32: Representative confocal images showing IFM fresh samples (a) and after incubation in control buffer (b), 0.2U/ml elastase solution (c) and 2U/ml elastase solution (d) stained for elastin (ab9519 – red) and cell nuclei (DAPI-blue). The IFM region was imaged using a 63x oil objective lens. Scale bar: 20µm. Visible elastin fibres are noted with white arrows.

4.4.3. Biochemical Analysis – Methodology for Elastin Measuring Depletion

The Fastin elastin assay (Fastin Elastin Assay Kit, Biocolor, UK), hydroxyproline assay (Birch et al., 1998) and DMMB assay (Farndale et al., 1986) were used to quantify the amount of elastin, collagen type I and sulphated GAG in fresh, control, 0.2U/ml and 2U/ml elastase treatment groups. In each group, at least 4 samples were included (to ensure enough tissue to perform all three biochemical assays). All samples were powdered using a Micro dismembrator and then freeze dried. From each treatment group, approximately 2x3mg (dry weight) of the resulting tissue was measured, and stored in 2 different tubes for the Fastin Elastin assay. The remaining tissue (10-20mg dry weight) was solubilised in papain (section 3.3.3) in preparation for the hydroxyproline and DMMB assays. All assays were carried out following protocols described in section 3.3.2.

4.4.4. Statistical Analysis

All statistical analysis in this chapter were carried out using the software Minitab 17 for Windows. Data were tested for normality using the Anderson – Darling test. If normally distributed, a two-way ANOVA (grouping information using the Tukey Method and 95% confidence) was used to evaluate differences between treatments and age groups. Treatment and horse age were used as factors for the ANOVA. The number of each individual donor was also included in the analysis of variance (nested with the horse age) to ensure each fascicle from the same tendon was not considered an independent biological repeat, but instead a "technical repeat". Data that did not follow a normal distribution was first transformed using a Box Cox transformation, and if still not normally distributed, a nonparametric test: The Mann–Whitney was used. Details about the test used for statistical analysis in each instance is included in the captions of the graphs. All the results were considered statistically significant for $p<0.05$. Data in bar graphs are displayed as mean ± standard deviation. Box plots graphs show all data points (small circles). The bottom and top of the boxes represent the first and third quartiles, while the line inside the box represents the median. The ends of the whiskers correspond to the lowest/highest data point of the distribution.

4.4.5. Biochemical Analysis – Results

Results from the Fastin elastin assay showed a significant reduction of tissue elastin content when incubated in either 0.2U/ml or 2U/ml elastase (approximately 59% and 71% elastin reduction, respectively) compared to fresh samples (Figure 33). No significant differences were seen between fresh and control samples, suggesting that the elastin content of IFM samples was not affected by incubation itself, but only when elastase was present in the solution. Although the more concentrated enzyme treatment reduced the elastin content by approximately 11%, this difference was not statistically significant, suggesting that the 10 fold increase in elastase concentration does not proportionally result in a reduction of elastin (Figure 33).

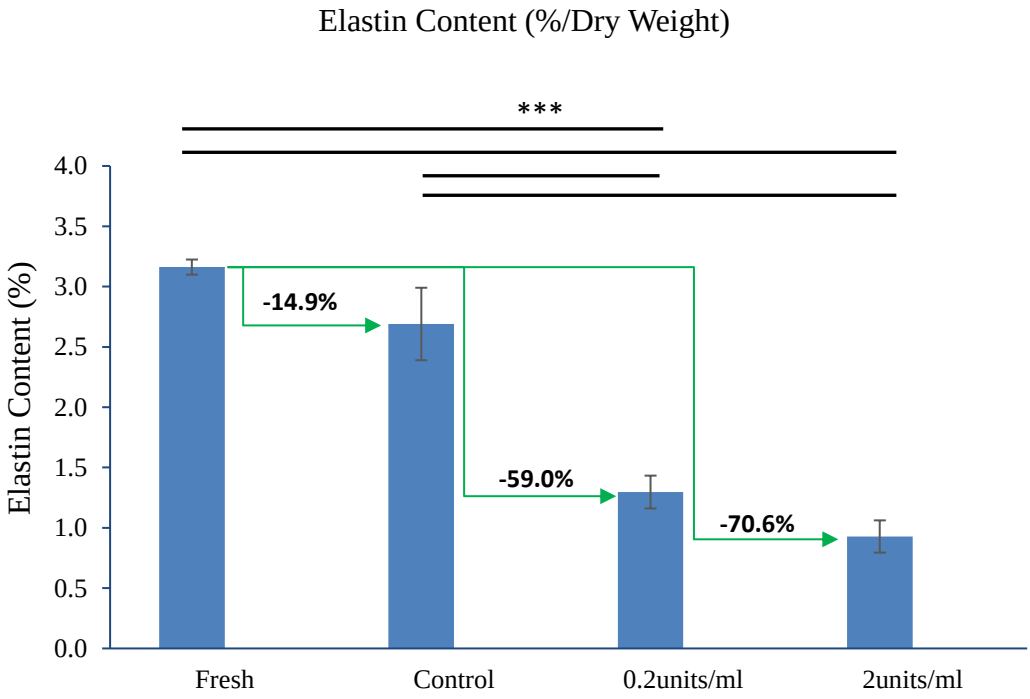

Figure 33: Elastin content, expressed as a percentage dry weight of tendon tissue, with the percentage of elastin reduction shown with the green arrows and associated numbers. Samples from 1 horse aged 6 years were used. Significant differences between treatments are identified by: *** $p<0.001$ (normally distributed data – ANOVA). Data are displayed as mean ± standard deviation.

Results from the DMMB assay showed no significant changes in GAG content between fresh and control samples. However, a significant GAG reduction was seen when samples were incubated in 0.2U/ml and 2U/ml elastase (approximately 74% and 80% GAG reduction, respectively) compared to fresh samples (Figure 34). These results suggest that GAG content is not affected by the incubation itself, but is affected by the presence of elastase. There were no significant differences in GAG content between samples incubated in 0.2U/ml and 2U/ml (Figure 34).

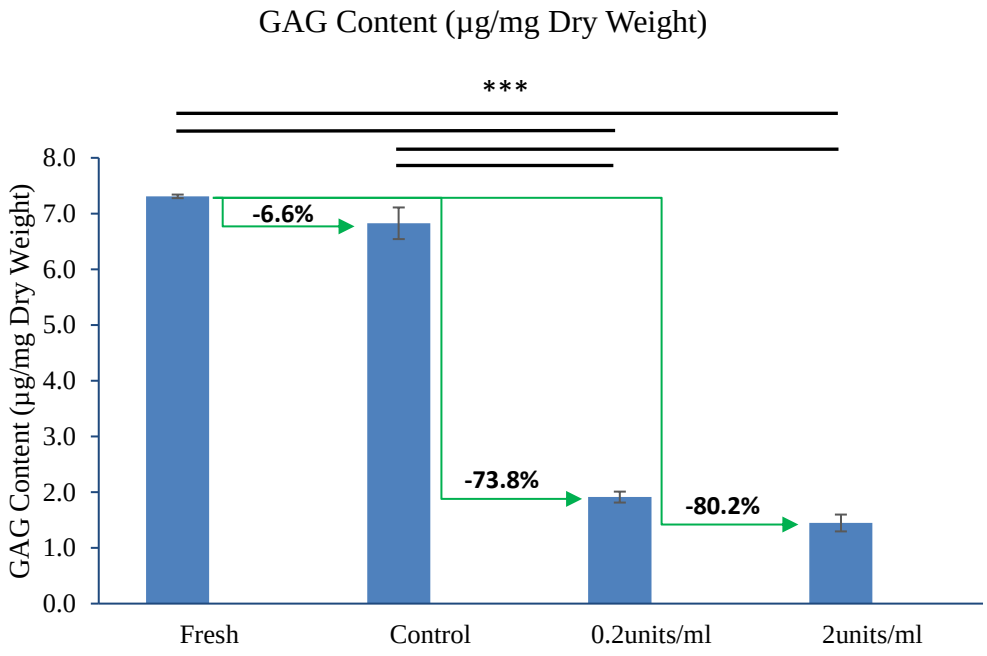

Figure 34: GAG content, expressed as µg/mg dry weight of tendon tissue, with the percentage of GAG reduction shown with the green arrows and associated numbers. Samples from 1 horse aged 6 years were used. Significant differences between treatments are identified by: *** $p<0.001$ (normally distributed data – ANOVA). Data are displayed as mean ± standard deviation.

Results from the hydroxyproline assay showed no significant changes in collagen content between any treatments (Figure 35), but a trend towards increased collagen content, particularly after elastase treatment.

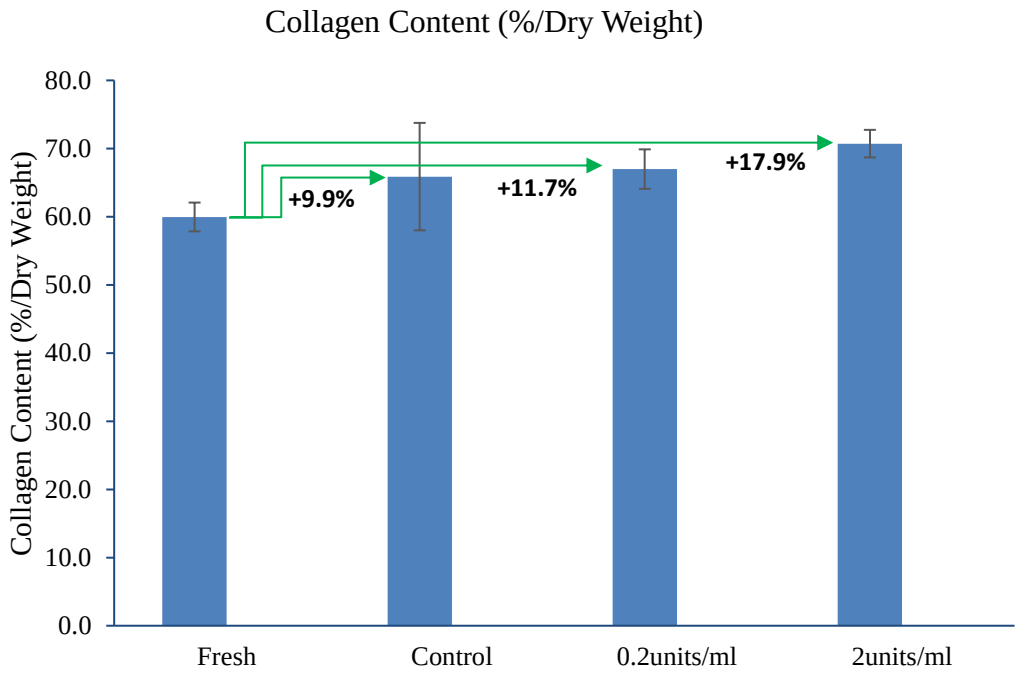

Figure 35: Collagen content, expressed as a percentage dry weight of tendon tissue, with the percentage of collagen increase shown with the green arrows and associated numbers. Samples from 1 horse aged 6 years were used. No significant differences (normally distributed data – ANOVA). Data are displayed as mean ± standard deviation.

4.4.6. Elastase Treatment Validation – Discussion

Results from the biochemical analysis showed an elastin reduction of over 70% when samples were incubated in a 2U/ml elastase solution. These results support previous studies, that have reported similar elastin reduction, when comparable treatments were performed (Grant et al., 2015, Smith et al., 2008). Immunohistochemistry data showed no elastin fibres when samples were subject to the same treatment (2U/ml elastase). The low amount of elastin measured by the Fastin elastin assay might be a result of elastin fragments trapped in the tissue, which were either too small to visualise with immunohistochemistry or digested in such a manner that the elastin antibody no longer recognised them.

Elastase treatment also resulted in a significant decrease in GAG content, particularly in a 2U/ml elastase solution (>80%). Previous studies have similarly reported significant reduction of GAG content (32-92%) in other tissues exposed to elastase treatments, likely occurring as GAG is less tightly bound within the ECM, and thus easily released by any disruption (Smith et al., 2008, Jacobs et al., 2012, Grant et al., 2015). Whilst the loss of GAG is of concern, several previous studies have investigated the effect of GAG digestion on tissue mechanics, as it has been suggested GAGs may have an important function as facilitators of load transfer between fibrils, and failed to show real changes in mechanics when GAGs are enzymatically removed from the tissues (Legerlotz et al., 2013, Lujan et al., 2009).

In contrast to GAGs, collagen content was not reduced by treatments, but there was a trend towards increased collagen content in samples exposed to elastase. These data are unsurprising when it is noted that data are presented as percentage of dry content, and elastin and GAG content were both drastically reduced.

There were no significant differences in elastin, GAG or collagen content in samples treated with 0.2U/ml and 2U/ml, suggesting a logarithmic effect and thus diminishing returns from increasing the enzyme concentration. Nonetheless, digestion of elastin was consistently elevated at 2U/ml relative to 0.2U/ml. The validation was performed in young samples, which have shown a higher amount of elastin (Chapter 3). As no differences in elastin crosslinking between young and old SDFT samples were identified in previous tests, elastin in young and old samples was expected to be digested similarly.

Taking these results together, it was decided to use 2U/ml elastase solution to remove elastin from the IFM and fascicle samples, and subsequently, assess changes in their mechanical properties.

4.5. Failure Properties of SDFT Fascicles and IFM Exposed to Elastase

4.5.1. Sample Preparation

SDFTs from 5 young (3 to 7 years – young group) and 5 old (15 to 19 years - old group) horses were used. Approximately 45 fascicles and 45 IFM samples were dissected from longitudinal tendon sections previously prepared, as described in Chapter 2. Fascicles and IFM samples were equally separated into 3 groups: Fresh, Control and Elastase (15 fascicles and 15 IFM samples/treatment/tendon used). After dissection, samples in the fresh group were tested within 16 hours and the remaining samples were incubated for 16 hours at room temperature in control buffer or control buffer + elastase.

4.5.2. Incubation Protocol

Fascicles and IFM samples in the Control group were placed in a petri dish and covered with 5 ml of 1x PBS plus 0.1mg/ml SBTI solution. Samples in the elastase group were also placed in a petri dish and 5 ml 2U/ml elastase (trypsin-free porcine pancreatic elastase, EPC134, Elastin Products Co., Owensville, MO) in 1x PBS plus 0.1mg/ml SBTI solution was added. Samples were incubated for 16H, at room temperature, with moderate agitation.

4.5.3. Fascicles and IFM Failure Properties – Protocol for Testing

After incubation, samples were removed from the solutions, rinsed twice in PBS and transferred to a new petri dish with tissue paper dampened with PBS. After incubation, fascicle diameter was measured using a non-contact laser micrometer (Thorpe et al., 2013a) (Figure 36). Assuming that fascicles have a circular shape, the smallest Cross Section Area (CSA) of fascicles was calculated using the formula below [1].

$$CSA = \pi r^2 \qquad [1]$$

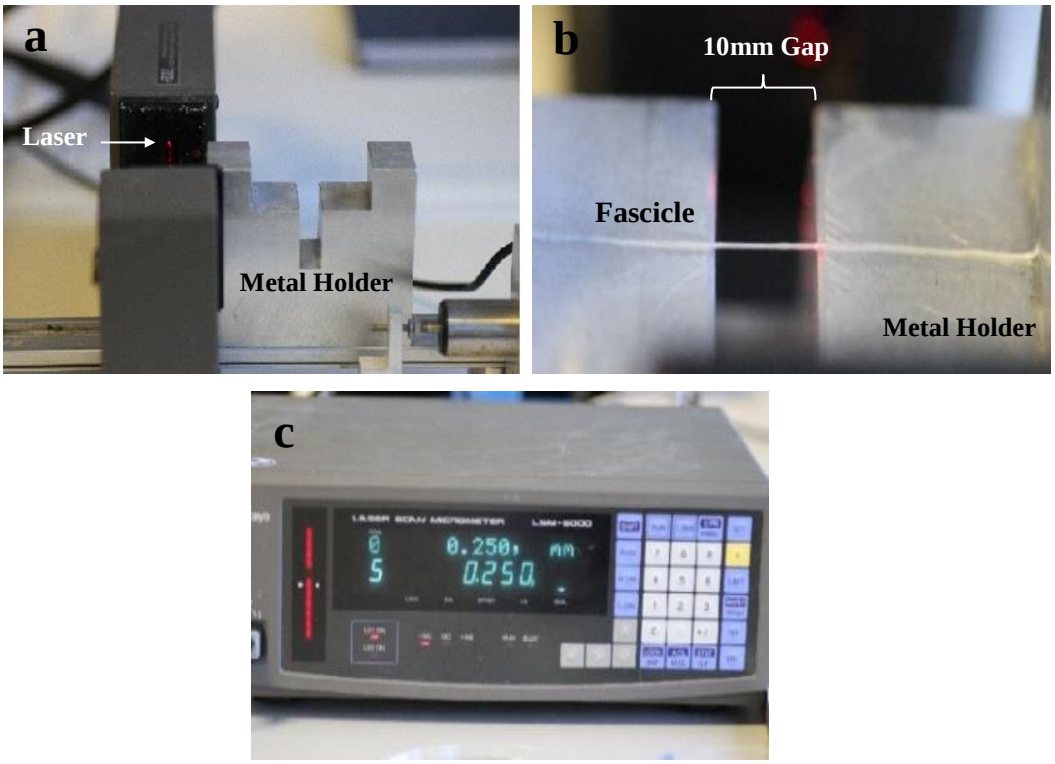

Figure 36: Images showing the procedure for measuring the diameter of fascicles using a non-contact laser micrometer (a). Fascicles are placed in a metal holder (b), which has a 10mm gap. The metal holder is manually moved so that the 10mm gap is exposed to the laser beam. The metal holder is moved so the length of the fascicle in the 10mm gap travels though the laser beam and the diameter of the fascicle continually recorded along the testing region (b). The smallest number was taken (c) and used as the final diameter of the fascicle, for calculating CSA.

The failure properties of fresh, control and elastase treated fascicles and IFM samples were investigated. For mechanically testing these samples, an electrodynamic testing machine (Instron ElectroPuls 1000) with a 250N load cell, was used (Figure 37a). Samples were gripped using pneumatic grips (gripping pressure of 4Bar) with a layer of rubber (0.3mm thick) and sandpaper (0.1mm thick) over each grip surface. The distance between the grips was set to 20mm. The test method was set using the Instron software for dynamic and fatigue testing (WaveMatrix™).

Fascicles were secured in the grips (Figure 37b) and pre-loaded to 0.1N, which represents a load of approximately 2% of fascicle typical failure load, to remove the slack. After the pre-load, the value of grip to grip distance was recorded as the correct value of gauge length. Then, fascicles were preconditioned with 10 loading cycles between 0 and 3% strain (approx. 25% of failure strain) using a sine wave at frequency of 1Hz. Immediately after preconditioning, fascicles were pulled to failure, at room temperature, at a strain rate of 5% per second. Samples was kept hydrated by spraying with PBS. For each test, the location of sample failure was also recorded (e.g. broke in the middle or in the grips; slipped in one or in both grips) and any fascicles that broke close to the grips or slipped were excluded from further analysis.

IFM samples were pre-loaded to the smallest positive load value that could be detected (approximately 0.02N; to remove slack). Once the intact end of each opposing fascicle was gripped (Figure 37c), the interfascicular matrix was pre-conditioned with 10 loading cycles between 0 and 0.5mm of extension (approx. 25% of failure extension) using a sine wave at frequency of 1Hz. Then, samples were pulled apart to failure at a speed of 1mm/s at room temperature (Figure 37d). Samples were kept hydrated by spraying with PBS. For each test, the location of sample failure was also recorded. In cases where fascicles broke rather than pulling apart, samples were left out of further analysis.

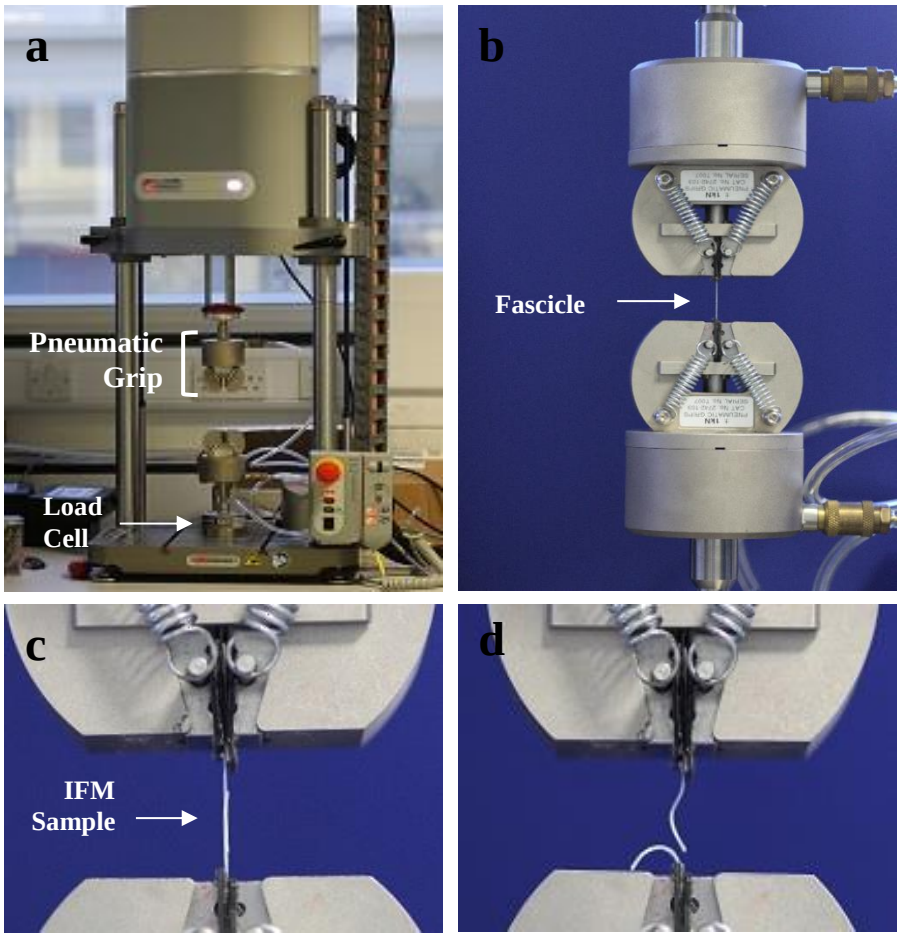

Figure 37: Images showing an electrodynamic testing machine - Instron ElectroPuls 1000 - with a 250N load cell (a). Fascicles (b) and an IFM samples (c) were secured in the pneumatic grips, prior to testing. Samples were pulled to failure at room temperature. Image showing an IFM sample where the opposing fascicles were totally pulled apart at the end of the test is also included (d).

4.5.4. Calculation of Fascicle and IFM Failure Properties

Force and displacement data for both fascicles and IFM failure tests were continuously recorded at 100 Hz during both preconditioning and pull to failure. Due to some unexpected noise from the machine, force data was smoothed, prior to any calculations, using a 9-point moving average filter (Legerlotz et al., 2010). Displacement at which the initial pre-load was reached was taken as the start point for the test to failure in both fascicles and IFM samples.

MATLAB was used to determine all mechanical test outputs from the data directly. Failure load was determined as the maximum load samples sustained prior to failure, and failure extension as the extension at the point of failure load. A continuous stiffness was calculated across every 9 data points of each force-extension curve. From these data, a maximum stiffness value was determined.

For each fascicle sample, engineering stress and strain were calculated using the CSA (calculated from the previously measured individual fascicle diameter) and effective gauge length, respectively. A continuous modulus was calculated across every 9 data points of each stress strain curve and smoothed using a 5-point moving average filter. From these data, a maximum modulus value was determined.

For all samples, hysteresis was also calculated as the percentage difference in the area under the loading and unloading curves comparing behaviour in the first and tenth preconditioning cycles.

After analysis, any fascicle or IFM sample in which failure properties or maximum modulus were more than 2.5 times above or below the standard deviation of the mean, were excluded.

4.5.5. Fascicle Failure Properties – Results

Fascicle failure and viscoelastic properties are shown in Figure 38- Figure 40. There were no significant differences between treatments in any of the failure nor viscoelastic properties. No significant differences with ageing were identified in any of the calculated parameters either. These results correlate well with previous studies, where no major ageing changes were identified in SDFT fascicles (Thorpe et al., 2015c), and also support the initial hypothesis that elastin, which comprises less than 1% of the total area occupied by the fascicular matrix, does not have an effect on the mechanical properties of fascicles when removed. It is important to note that engineering stress calculations were adopted, such that CSA was considered unchanged throughout the failure tests, as it is extremely hard to determine changes in CSA during these tests. Whilst a calculation of true stress would account for this, and larger stress would be expected during the latter stages of the test, the difficulties in accurately calculating values precludes its use. Further, the measurement of stress is commonly confounded in biological tissues, owing to the fibre composition and hydrated nature of the tissue. The large diameter changes seen during tests stem primarily from water movement and not changes to fibre volume, making a stress calculation potentially flawed. For these reasons, almost all tests utilise an engineering stress calculations, hence this parameter is important for comparing across studies. However, assuming that SDFT fascicles have a Poisson's ratio of approximately 1.3, it was calculated that during the latter stages of the fascicle failure tests, CSA would decrease approximately 26% (Thorpe, C., et al., 2013b).

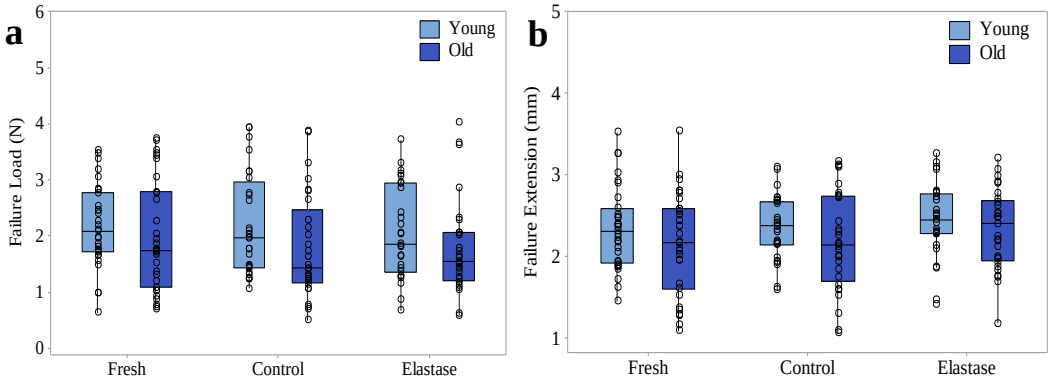

Figure 38: Failure Load (a) and Failure Extension (b) young and old SDFT fascicles subject to different treatments: Fresh, Control and Elastase (n=5/age group; total samples tested: 15/treatment/tendon). No significant differences were identified (all normally distributed data – ANOVA).

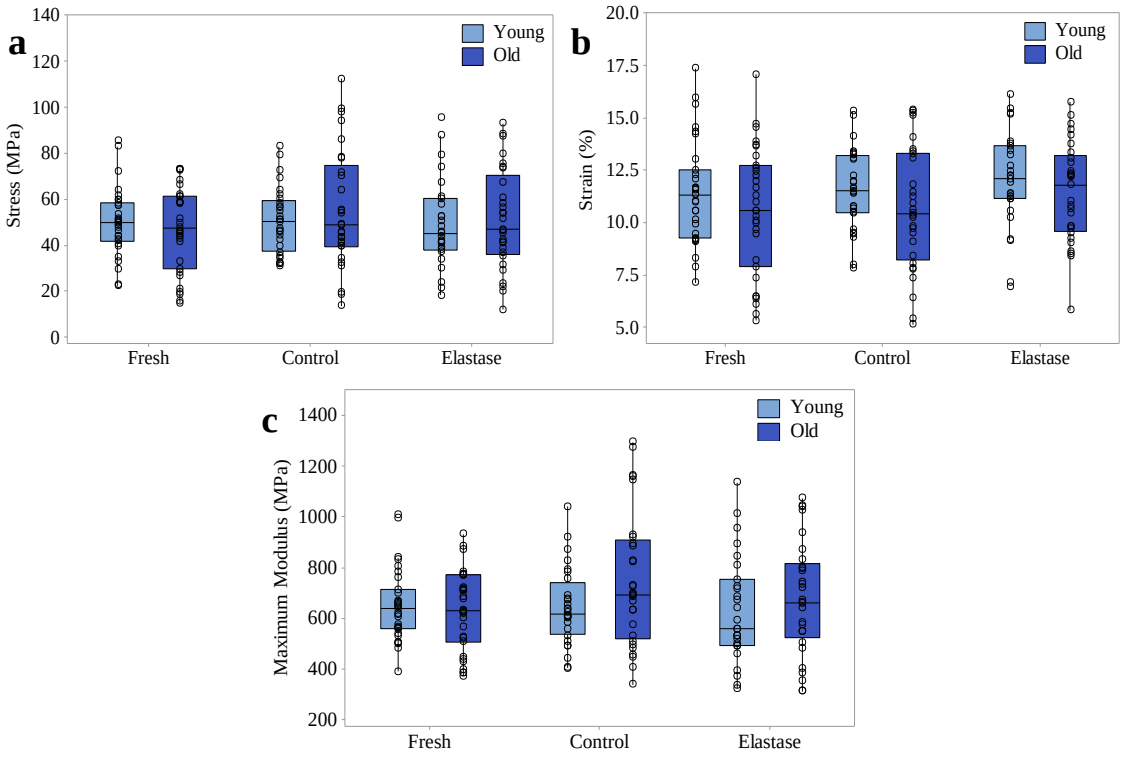

Figure 39: Stress (a), Strain (b) and maximum modulus (c) of young and old SDFT fascicles subject to different treatments: Fresh, Control and Elastase (n=5/age group; total samples tested: 15/treatment/tendon). No significant differences were identified (all normally distributed data – ANOVA).

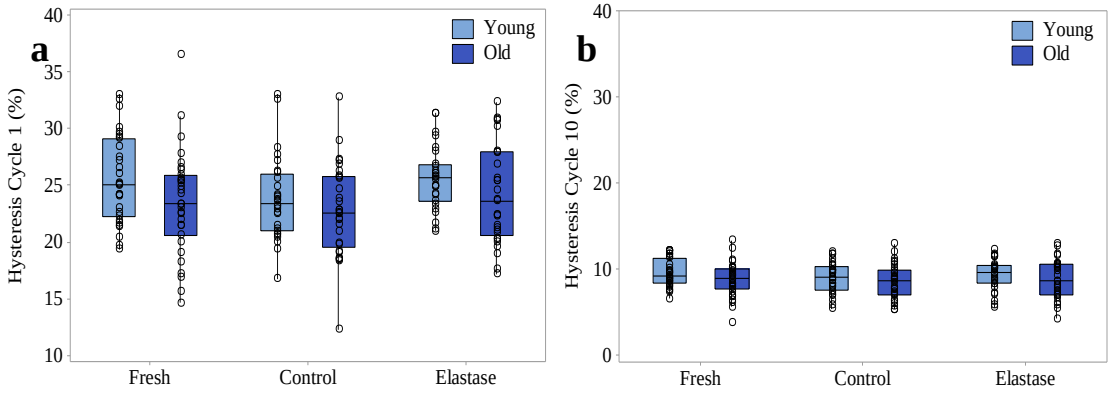

Figure 40: Hysteresis Cycle 1 (a) and Hysteresis Cycle 10 (b) of young and old SDFT fascicles subject to different treatments: Fresh, Control and Elastase (n=5/age group; total samples tested: 15/treatment/tendon). No significant differences were identified (all normally distributed data – ANOVA).

4.5.6. IFM Failure Properties – Results

IFM failure and viscoelastic properties are shown in Figure 41 and Figure 42, respectively.

Fresh IFM samples showed similar mechanical properties to previously published data, with a failure force of around 1.5N, two thirds that of fascicles (Thorpe et al., 2015c, Thorpe et al., 2013a). No significant differences between fresh and control samples were found in any of the parameters calculated, which indicates that any treatment related differences are due to the elastase treatment and not due to the incubation.

By contrast, the overall mechanical properties of IFM samples exposed to elastase were significantly affected. Results showed a significant reduction in the IFM failure load (Figure 41a) and maximum stiffness (Figure 41c) when elastin is removed, both in the young and old groups. Data also showed an overall increase in hysteresis in cycle 1 (Figure 42a) in young and old samples, and cycle 10 (Figure 42b) in young samples, between fresh/control and elastase treated samples.

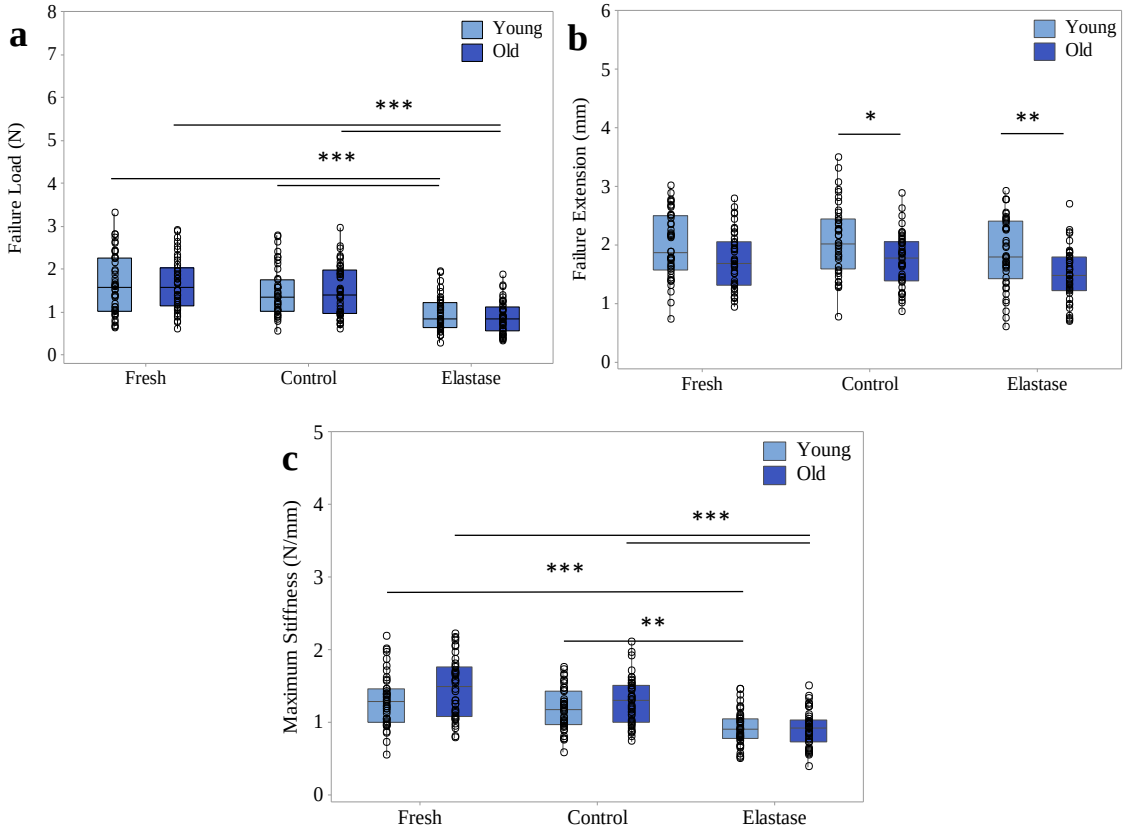

Figure 41: Failure Load (a), Failure Extension (b) and Maximum Stiffness (c) of young and old SDFT IFM samples subject to different treatments: Fresh, Control and Elastase (n=5/age group; total samples tested: 15/treatment/tendon). Significant differences are flagged with: *p<0.05; **p<0.01 and ***p<0.001 (all normally distributed data – ANOVA).

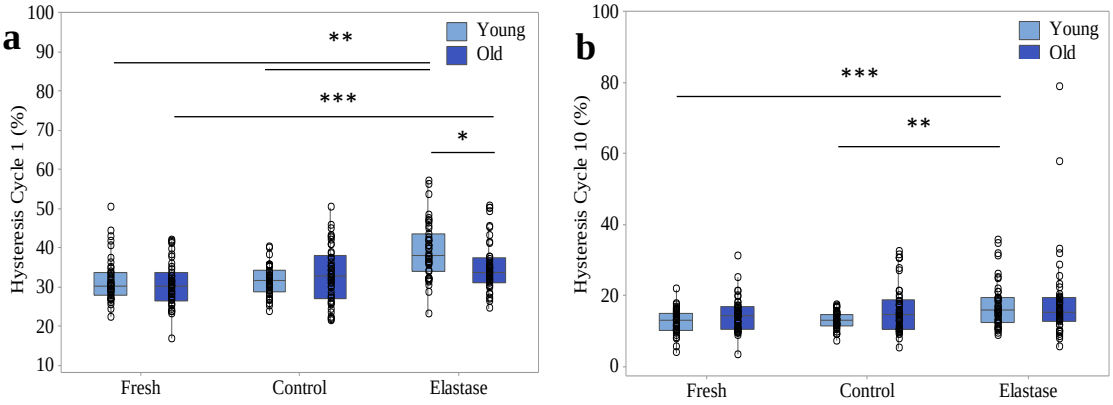

Figure 42: Hysteresis Cycle 1 (a), Hysteresis Cycle 10 (b) of young and old SDFT IFM samples subject to different treatments: Fresh, Control and Elastase (n=5/age group; total samples tested: 15/treatment/tendon). Significant differences are flagged with: *p<0.05; **p<0.01 and ***p<0.001 (Hysteresis Cycle 1 - normally distributed data – ANOVA; Hysteresis Cycle 10 – non-normally distributed data– Man-Whitney test).

4.6. Fatigue Properties of SDFT Fascicles and IFM Exposed to Elastase

4.6.1. Sample Preparation

SDFTs from 5 young (3 to 7 years) and 5 old (15 to 19 years) horses were used. Approximately 45 fascicles and 45 IFM samples were dissected from longitudinal tendon sections previously prepared, as described in Chapter 2. Tendons used for fatigue testing were matched with those used for failure tests (shown in section 4.5), taking different longitudinal sections from the same tendon. Fascicles and IFM samples were equally separated into three groups: Fresh, Control and Elastase (15 fascicles and 15 IFM samples/treatment/tendon used). After dissection, samples in the fresh group were tested within 16H and the remaining samples were incubated for 16H at room temperature in control buffer or control buffer and elastase.

4.6.2. Incubation Protocol

Fascicle and IFM samples in the Control group were placed in a petri dish and covered with 5 ml 1x PBS plus 0.1mg/ml SBTI solution. Samples in the elastase group were also placed in a petri dish, and 5 ml 2U/ml elastase (trypsin-free porcine pancreatic elastase, EPC134, Elastin Products Co., Owensville, MO) in 1x PBS plus 0.1mg/ml SBTI solution was added. Samples were incubated for 16H, at room temperature, with moderate agitation.

4.6.3. Fascicles and IFM Fatigue Properties – Protocol for Testing

After incubation, samples were removed from the solutions, rinsed twice in PBS and transferred to a new petri dish with tissue paper dampened with PBS. After incubation, fascicle diameter was measured and CSA calculated as previously described (Section: 4.5.3; Figure 36).

The fatigue properties of fresh, control and elastase treated fascicles and IFM samples were investigated. For mechanically testing these samples, a mechanical testing machine (Electroforce 5500, TA instruments, Delaware, USA) (Figure 43a) with a 22N load cell, was used (Figure 43a). This machine functions inside a cell culture incubator (37 °C, 20% O_2, 5% CO_2).

Each sample was secured in a custom designed chamber (Figure 43b). Samples were first secured in the top grip and then the bottom grip, with a grip to grip distance of 10mm. Once samples were secured, chambers were filled with PBS to prevent samples from drying out, and attached to the machine (Figure 43c). The test method was set using the Bose software *WinTest®7 Controls.*

Fascicles were preloaded to 0.1N to remove any slack in the samples. As failure strain is more consistent between cycles than failure stress (Thorpe et al., 2012), one loading cycle of 1 mm displacement was applied, which corresponds to approximately 10% strain, and 50% of the predicted failure strain (Thorpe et al., 2012). The peak load during the cycle was recorded, and used as the target load for the creep tests.

IFM samples were pre-loaded to 0.02N to also remove any slack, and in the same manner, the load for creep tests was determined from a single loading cycle to 1mm displacement, equivalent to approximately 50% of the predicted failure extension (Thorpe et al., 2012).

In both fascicle and IFM tests, the identified load was applied cyclically to the samples at a frequency of 1 Hz until sample failure, with force and maximum and minimum displacement data, continuously recorded at 100 Hz throughout the tests.

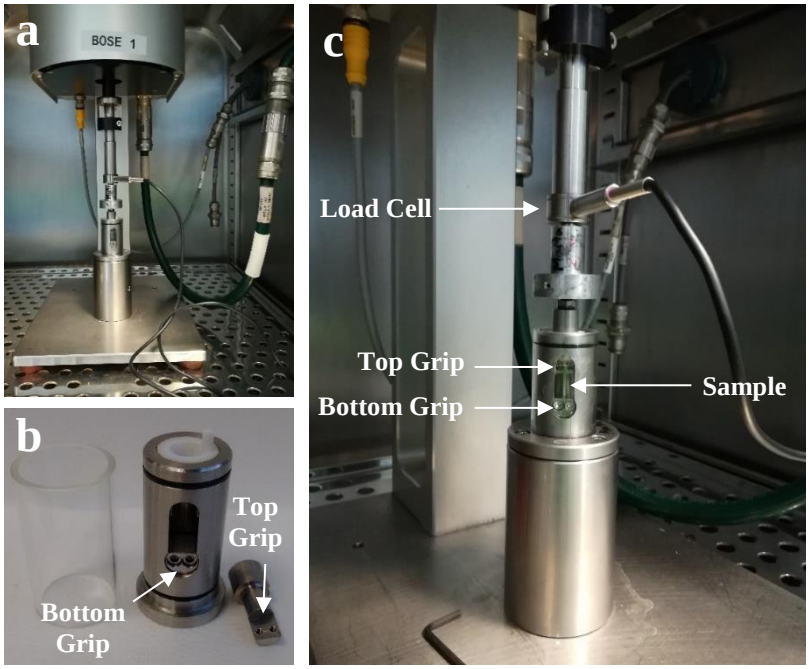

Figure 43: Images of the fatigue testing set up. The mechanical testing machine (Electroforce 5500) sits inside the incubator (a). Samples are secured in the metal chamber (b) where the load cell and other connectors attach (c).

4.6.4. Calculation of Fascicle and IFM Fatigue Properties

For each test, the number of cycles to failure was recorded and creep curves to failure were drawn using the maximum and minimum displacement data. The creep rate (mm/cycle) of the first 10 loading cycles, as well as the secondary creep rate of both maximum and minimum displacements (mm/cycle) were calculated (Figure 44). Data from fascicle and IFM samples were compared between treatments and age groups. Samples that did not fail or where curves showed a clearly atypical shape (examples shown in Figure 45), were rejected from the data set.

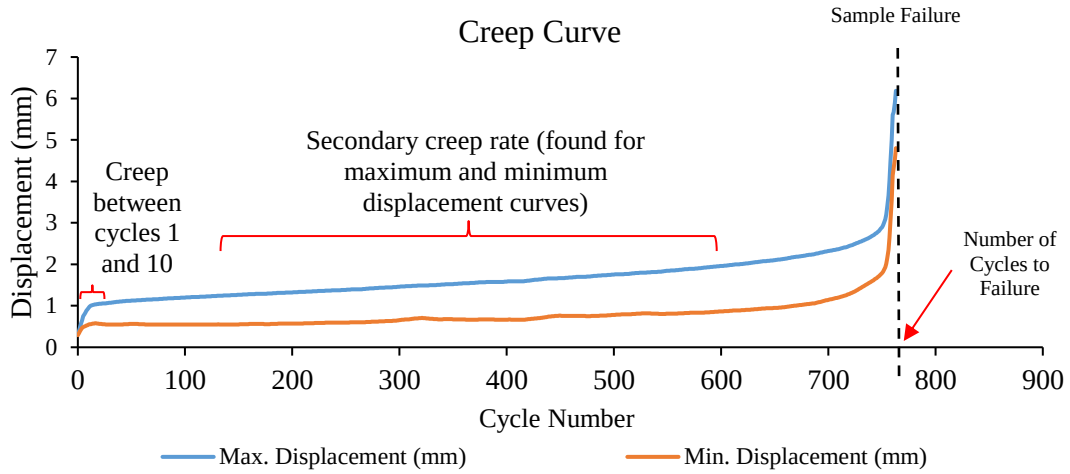

Figure 44: Representative creep curve of a young SDFT fascicle. Minimum and maximum displacement for each cycle is plotted against the cycle number.

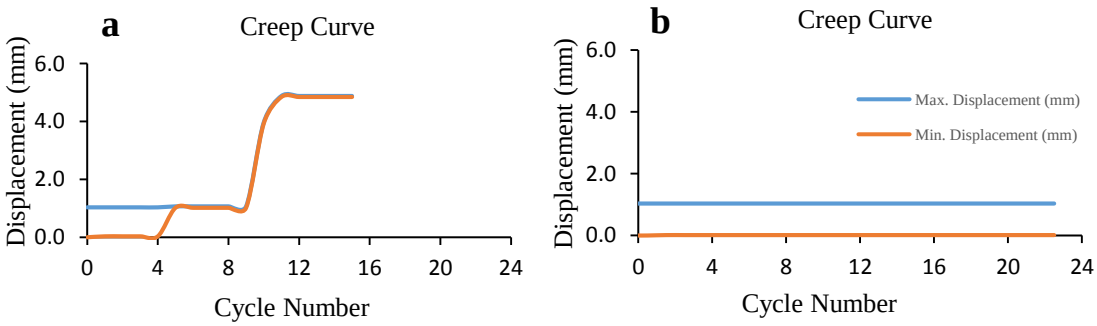

Figure 45: Representative curves that have been excluded from the data set. These curves were very different from the majority and showed a clear atypical behaviour. In some instances, friction in the grips or immediate overload of samples was evident (a); in other instances, the sample was not loaded, reporting no data at all (b).

4.6.5. Fascicle Fatigue Properties – Preliminary Results and Discussion

The fatigue properties of fascicles are shown in Figure 46. Due to time constraints, only fascicles from two young and one old SDFTs were tested. Data showed considerable variability but no significant differences between treatments in any of the fatigue parameters calculated (Figure 46). With ageing, fascicles in the fresh group showed a significant increase in creep between cycles 1 and 10 (Figure 46b), which indicates, as seen in trends in other creep parameters, that old SDFT fascicles are more prone to creep than young fascicles. However, no differences in cycles to failure were seen. These results support the hypothesis that fascicle fatigue properties are not elastin content dependent.

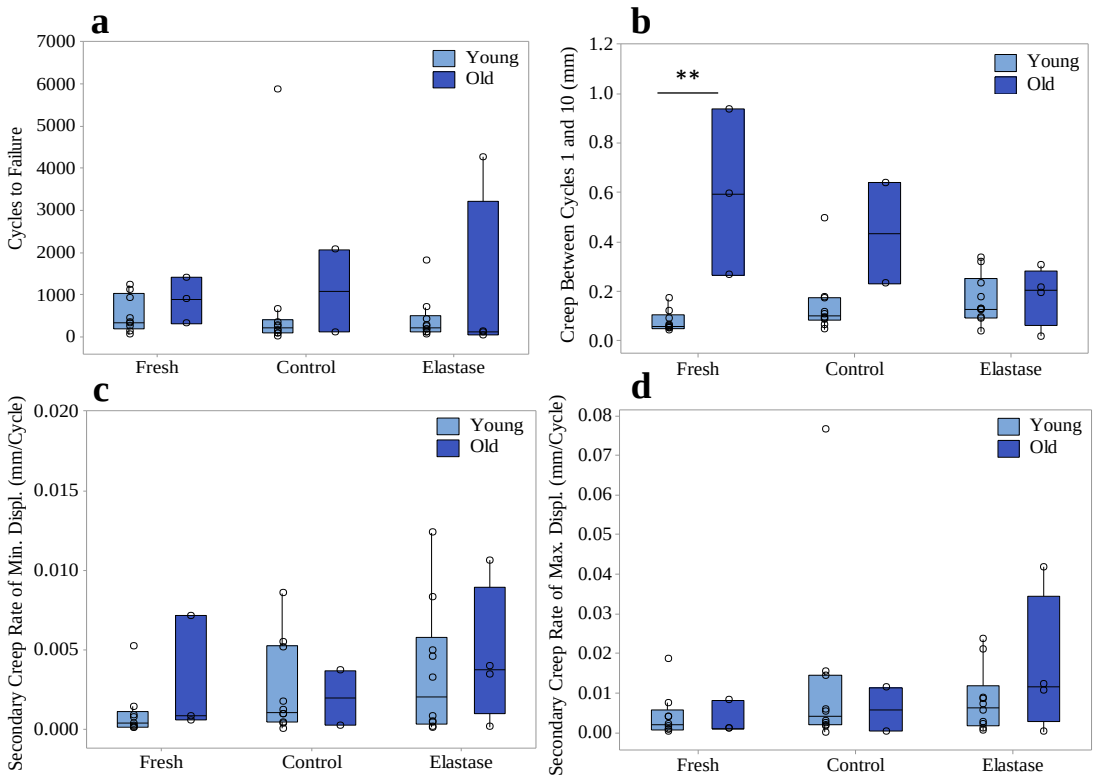

Figure 46: Cycles to failure (a), creep between cycles 1 and 10 (b), secondary creep rate of minimum (c) and maximum (d) displacement of young and old SDFT fascicles subject to different treatments: Fresh, Control and Elastase (n=2 (young group), n=1 (old group); total samples tested: 15/treatment/tendon). Significant differences are flagged with: **p<0.01 (all normally distributed data – ANOVA).

4.6.6. IFM Fatigue Properties – Results

SDFT IFM fatigue properties are shown in Figure 47. Representative creep curves for young and old SDFT IFM samples are also shown in Figure 48.

Data shows a significant reduction in the number of cycles to failure in elastase treated samples compared to both fresh and control groups (Figure 47a, Figure 48a). Results also show a significant increase in creep between cycles 1 and 10 (Figure 47b, Figure 48a) and also an increase in the secondary creep rate for minimum and maximum displacement, compared to both fresh and control groups (Figure 47c and d, respectively).

With ageing, there was a trend towards the decrease in the number of cycles to failure in both fresh and control groups, as reported previously. However, after elastase treatment, samples showed the same significant decrease in the number of cycles to failure, and increase in all creep parameters (Figure 47, Figure 48b).

No changes were seen between fresh and control groups in any of the parameters calculated, which supports the hypothesis that changes between treatments are caused by the presence of elastase and not by the incubation itself. Overall, these results support the hypothesis that, while fascicle fatigue properties are not affected by elastin depletion, IFM fatigue properties are directly influenced by elastin content.

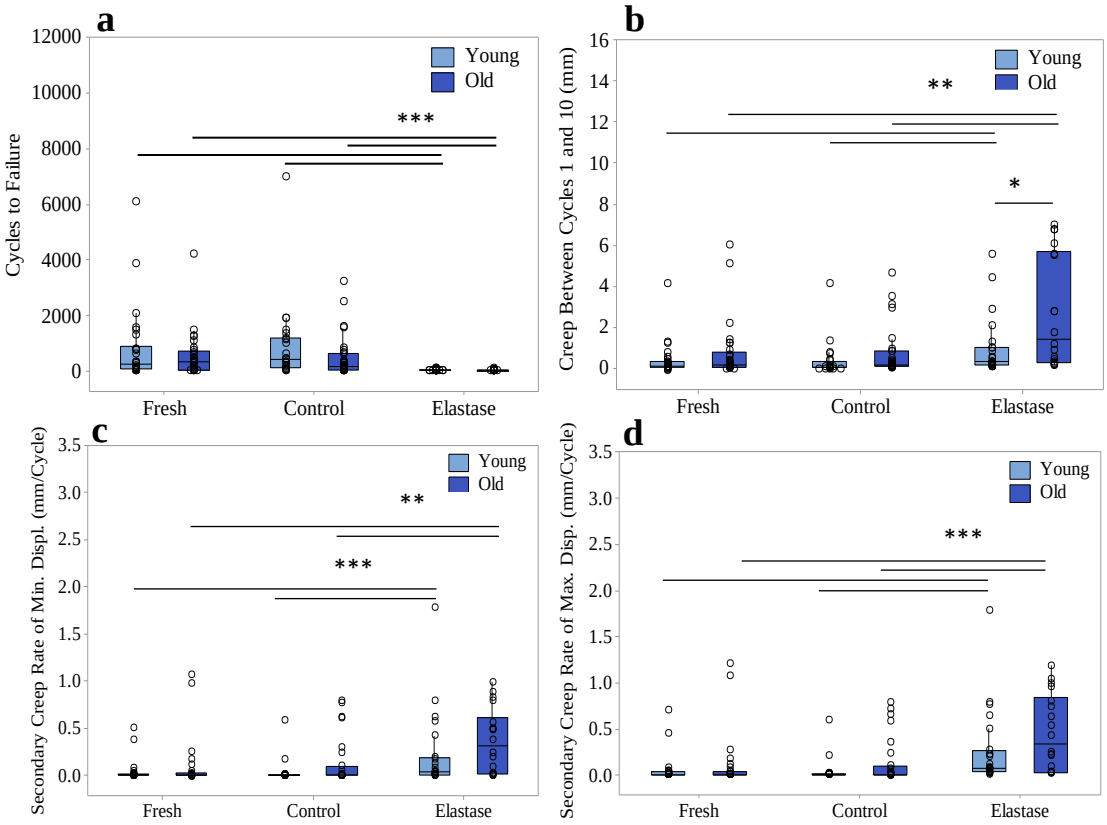

Figure 47: Cycles to failure (a), creep between cycles 1 and 10 (b), secondary creep rate of minimum (c) and maximum (d) displacement of young and old SDFT IFM samples subject to different treatments: Fresh, Control and Elastase (n=5/age group; total samples tested: 15/treatment/tendon). Significant differences are flagged with: **p<0.01 and ***p<0.001 (Cycles to Failure: normally distributed – ANOVA, all remaining IFM fatigue data not normally distributed –

a

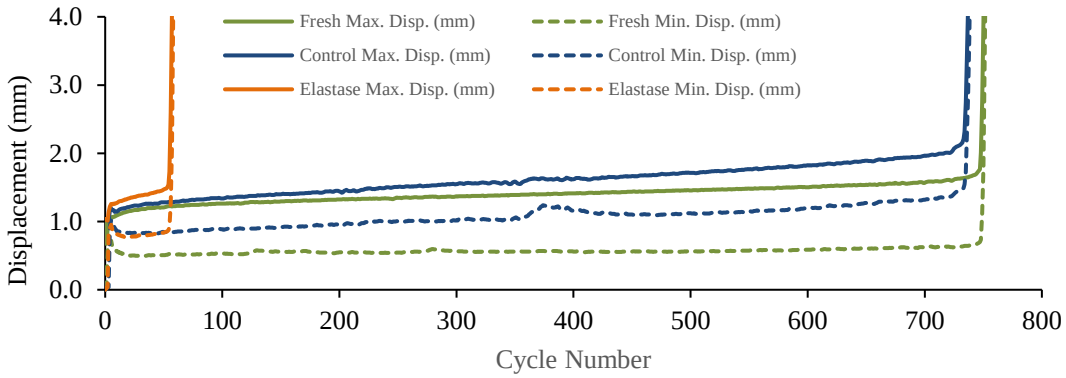

b

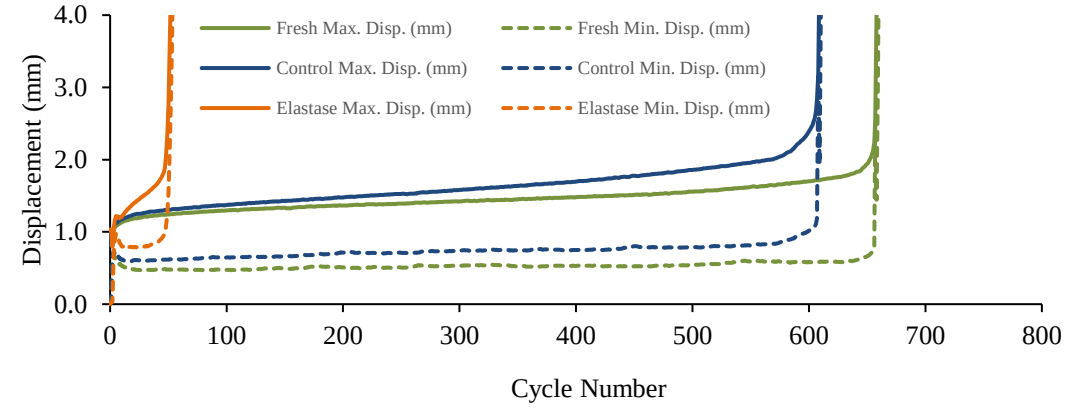

Figure 48: Typical creep curves of young SDFT IFM (a) and old SDFT IFM (b). Maximum and minimum displacement for each treatment Fresh, Control and Elastase are represented.

4.7. Recovery Properties of SDFT IFM Exposed to Elastase

4.7.1. Sample Preparation

SDFTs from 5 young (3 to 7 years) and 5 old (15 to 19 years) horses were used. Approximately 16 IFM samples were dissected from longitudinal tendon sections previously prepared, as described in Chapter 2. All samples used in recovery tests were matched with the ones used in the failure and fatigue testing (shown in section 4.5 and 4.6, respectively). IFM samples were separated into three groups: Fresh, Control and Elastase (6 IFM samples/treatment/tendon used). After dissection, samples in the fresh group were tested within 16H and the remaining samples were incubated for 16H at room temperature in control buffer or control buffer and elastase, following the procedure outlined in section 4.6.2.

4.7.2. IFM Recovery Properties - Protocol for testing

Previously prepared and treated samples were divided in three testing groups as described in the schematic below.

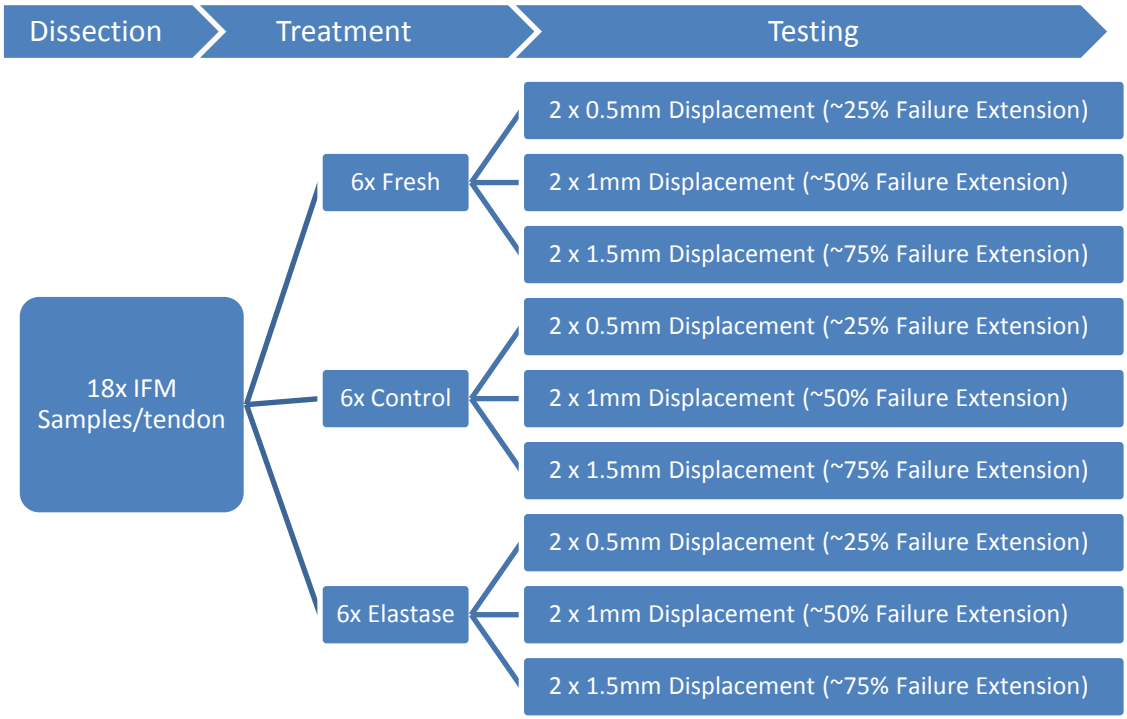

Figure 49: Schematic showing how samples were divided for the IFM recovery testing.

A custom designed tensile straining rig (Figure 50) with a 10N load cell was used to investigate the ability of IFM samples to recover initial dimensions after cyclic loading. The rig was developed and validated by Screen's group and previously used to measure the microstructural response of tendon fascicles when subjected to different strains (Cheng & Screen 2007).

Stainless steel grips were secured at a 15mm grip to grip length, using a metal spacer (Figure 50a), and the sample secured in the grips, such that a single intact fascicle was held at each end, with the IFM testing region in the middle (Figure 50b).Once samples were secured in the grips, grips were turned upside down and four vertical lines (equally spaced) were manually drawn across the 10mm IFM testing region using a permanent marker pen, so that they would be visible when observed from above (Figure 50c). Grips were then secured into the rig and the sample immersed in PBS (Figure 50d).

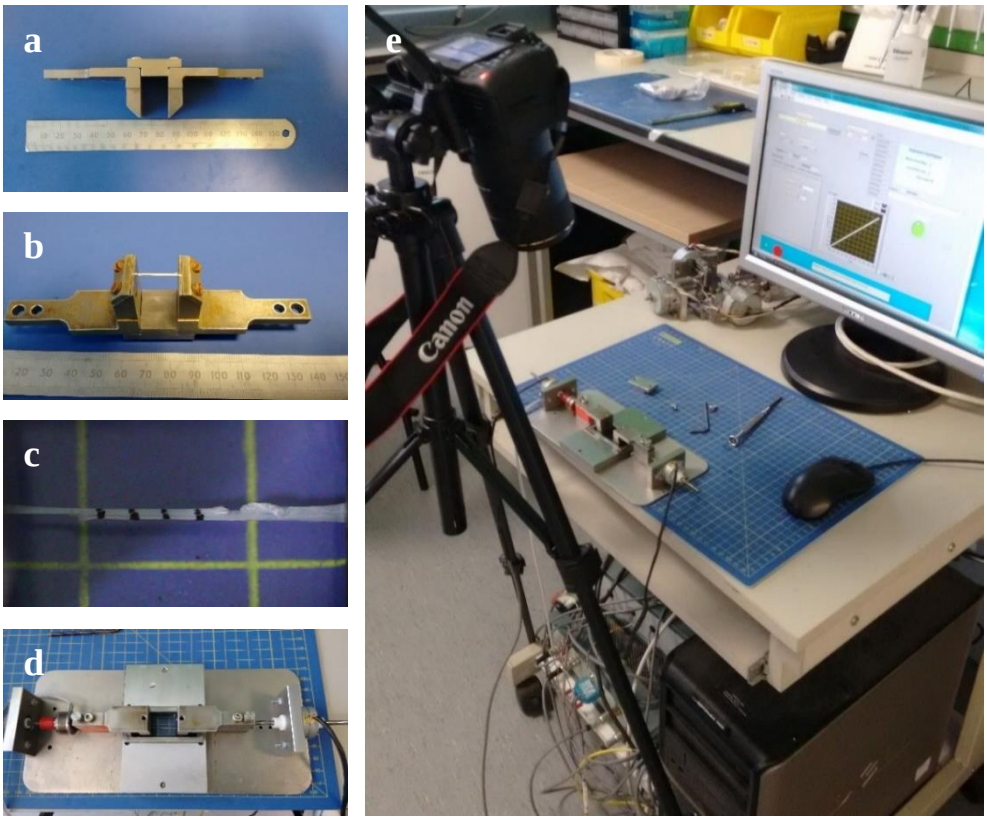

Figure 50: Images showing the preparation of samples for IFM recovery testing. Grips were secured using a 15mm spacer (a) and the sample secured in the grips (b). Four lines were drawn transversely across the 10mm testing region of the samples (c), then grips were transferred to the rig (d). A camera is positioned so that the test could be recorded from above (e).

A Canon EOS 700D camera with a Sigma 105mm F2.8 EX DG MACRO OS lens was secured in a tripod and placed over the sample to allow visualisation of sample movement. Controlled by linear actuators, the grips were slowly moved apart, applying 0.05mm increments of displacement, whilst visually monitoring the sample until it lifted slightly off the base of the rig (Screen et al., 2004). This provided a consistent start point for tests and removed any slack.

Samples were subjected to 10 loading cycles at 0.5Hz between 0mm and 0.5mm, 1mm or 1.5mm, which corresponds to approximately, 25, 50 or 75% of IFM predicted failure extension, respectively, followed by a ten second hold period to allow for any IFM recovery. Video footage was recorded throughout the test. At the end of the test, samples were pulled to failure at a rate of 1mm/s, to ensure there were no intact fascicles in the test region. Samples that did not fail properly or that had intact fascicles in the testing region were excluded from the data set.

4.7.3. IFM Recovery Properties - Data analysis

The video of each test was split into frames, from which four specific time points during the test were selected and further analysed (Figure 51):

A - Initial point (after pre load and before cyclic loading to serve as a reference);

B - Maximum displacement (taken as the peak of the last loading cycle);

C - After loading (recovery immediately after load is removed);

D – Holding period (recovery ten seconds after load is removed).

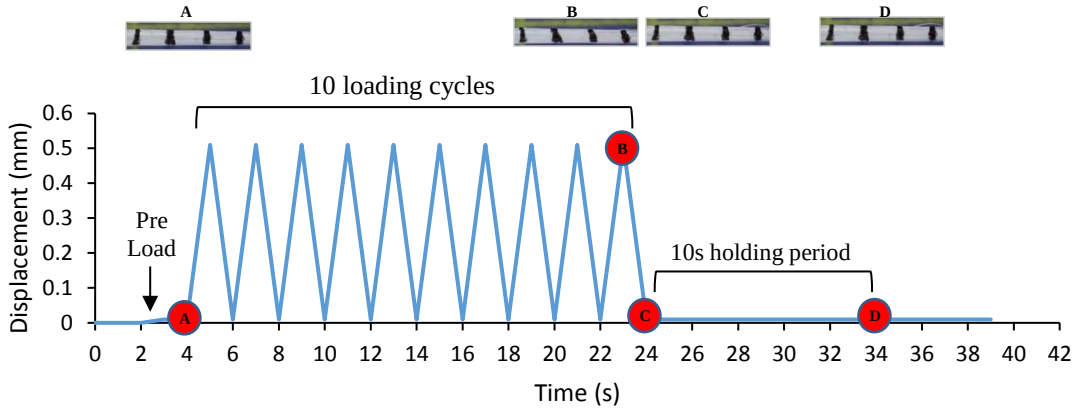

Figure 51: Representative displacement over time graph of an IFM sample being cyclically loaded between 0 and 25% of its predicted failure extension. For this case, thirty-nine frames in total were extracted from the video and from those, four were extracted at the specified moments for further analysis (identified with the red circles and corresponding images); A: initial point, B: maximum displacement, C: after loading and D: holding period.

A cutting board was placed under the rig, where 1 square equals 10 mm, (Figure 50c) to provide a scale for images.

A MATLAB code was then written and validated by a member of Screen's research group, to analyse the angular deviation of lines, comparing images taken at different moments of the testing. The code was able to automatically identify each line (also called marker), trace its orientation and then detect its angle relative to the vertical. The code was divided into two sections: one to "find the marker" (Appendix C1.1) and another to "analyse the image" (Appendix C1.2).

To briefly describe the process, Fiji (ImageJ) was used to draw a region of interest (ROI) around the lines, using ROI manager function, allowing the relevant image region to be cropped (Figure 52). The same ROI was then applied to the other selected images of that sample.

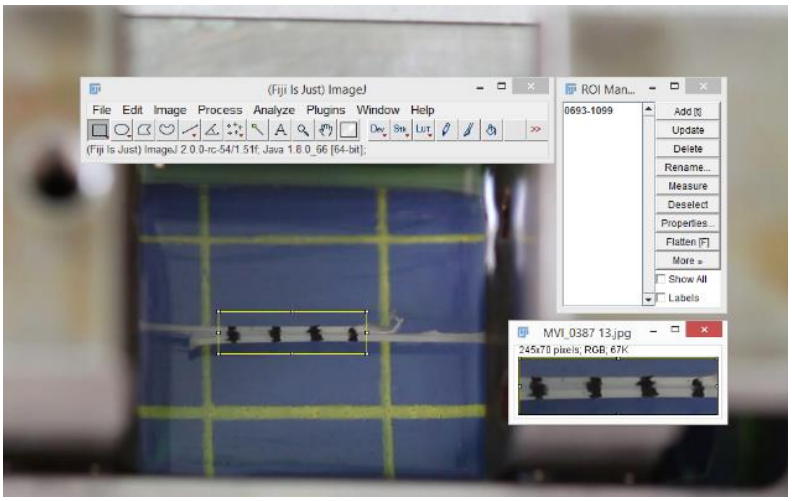

Figure 52: Print screen of the method used to crop the images for MATLAB analysis.

Original images (Figure 53a) were smoothed in MATLAB using a Gaussian filter and then thresholded, using the same parameters for all images (sensitivity 0.1; marker margin 10, chosen from empirical data) (Figure 53b). Each marker was divided into multiple horizontal rectangles, and for each one, the centre of mass was found (position in x axis) (Figure 53c) and the interpolated line drawn (Figure 53d). Then, the interpolated lines generated from the first image (initial point – called "Ref=A") were compared with those in the second image (maximum displacement – called "set1=B", Figure 53e), third image (after loading – called "set2=C", Figure 53f) and finally fourth image (holding period – called "set3=D", Figure 53g). The displacement of each line, and angle relative to that in the reference image (initial point - "ref "), were calculated. Efforts were made to adjust images for some motion of the entire rig. However, it was not possible to do this robustly. As involuntary motion will only affect absolute measurement of displacement, it was decided to report only angle deviation of lines in further analysis, as this variable is not affected by vertical or horizontal motion.

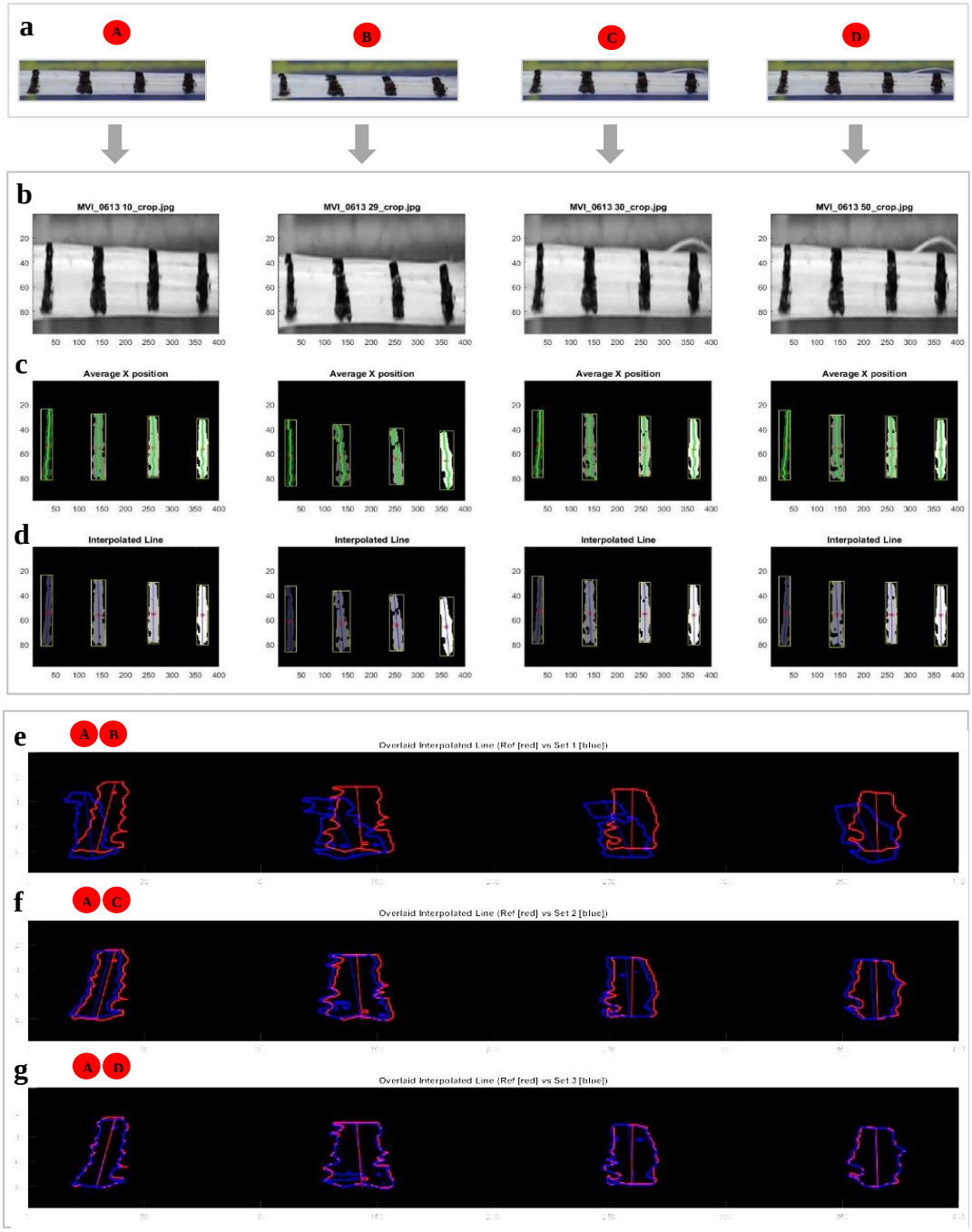

Figure 53: Images showing the step-by-step procedure for data analysis using MATLAB. Original images (a) were smoothed and thresholded (b). Each marker was divided into multiple horizontal rectangles, and for each one, the centre of mass was found (c) and the interpolated line drawn (d). Then, the interpolated lines generated from the first image (Ref=A) were compared with those in the second image (e) (set1=B), third image (f) (set2=C) and finally fourth image (g) (set3=D).

Once the angle deviation between “A & B”, “A & C” and “A & D” for every line on a single image was calculated, data from the four lines was averaged, and used as the overall angle deviation of the sample at maximum displacement (“B”), after loading (“C”) and holding period (“D”). From this, other variables were calculated such as: percentage recovery after loading (at “C”) and the total percentage recovery after holding period (10s of extra recovery - at “D”).

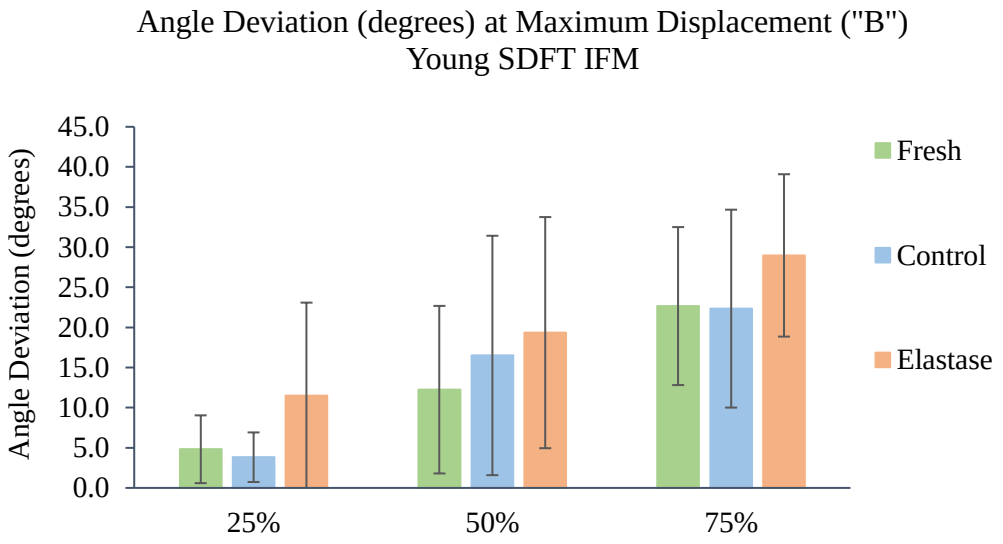

Figure 54: Angle deviation at maximum displacement for young SDFT IFM samples (n=5; total samples tested: 2/treatment/testing condition/tendon). Data are displayed as mean ± standard deviation.

Deviation of lines was evident when analysing all videos, however in many instances, particularly with smaller applied displacements, the angles were very small.

Validation of possible error in the MATLAB code showed that shifting the interpolated lines by 1 pixel, would affect the calculated angle by approximately 0.2 degrees. Thus, from the data set, any values lower than 0.2 degrees were excluded from the data set. Most of these cases happened in samples that had been cyclically loaded up to 25% or 50% of the predicted sample failure extension. For these cases, the angle deviation was very small and data was extremely variable (Figure 54). Hence, further detailed analysis focusses on samples only loaded up to 75% of their predicted failure extension.

4.7.4. IFM Recovery Properties - Results

IFM recovery properties are shown in Figure 55 - Figure 57. Data showed a significant increase in the angle deviation in the elastase group compared to both fresh and control groups (Figure 55). The percentage recovery after loading was also significantly lower in the elastase group compared to either of the other groups, both immediately after loading (Figure 56) and total recovery including the holding period (Figure 57). In aged samples, similar overall trends were evident, but it was notable that immediate recovery after loading was significantly better in the aged then young elastase treatment group (Figure 56). Total recovery showed no age related changes, however results showed no significant differences between fresh and control groups in any of the calculated parameters, suggesting that the changes in the IFM recovery properties between groups are specific to the elastase treatment and not the incubation. These results support the hypothesis that elastin functions to transfer stress between fascicles providing an extensible interface with high recoil ability in the IFM of energy storing tendons.

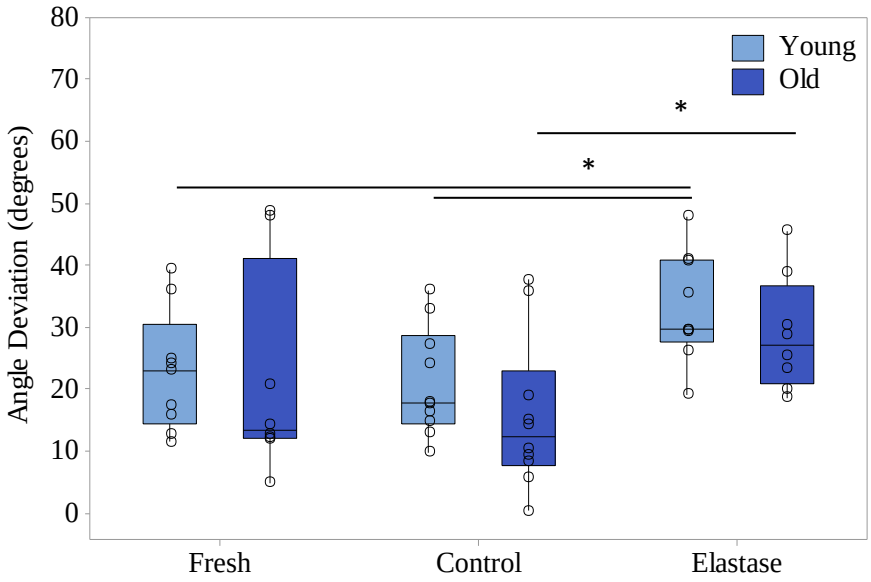

Figure 55: Angle deviation (degrees) calculated at the point application of 75% of the failure extension ("B: Maximum displacement - taken as the peak of the last loading cycle") for young and old SDFT IFM samples subject to different treatments: Fresh, Control and Elastase. Samples were stretched up to 75% of their predicted failure extension. Significant differences are flagged with: *p<0.05 (data non-normally distributed – Mann-Whitney test).

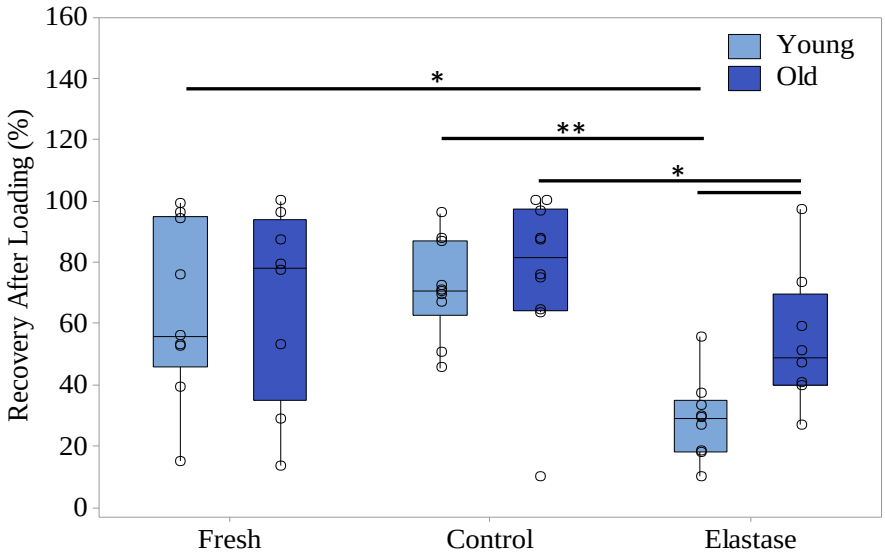

Figure 56: Recovery after loading to 75% of the failure extension ("C: After loading - recovery immediately after load is removed") for young and old SDFT IFM samples subject to different treatments: Fresh, Control and Elastase. Samples were stretched up to 75% of their predicted failure extension. Significant differences are flagged with: *p<0.05 and **p<0.01 (data non-normally distributed – Mann-Whitney test).

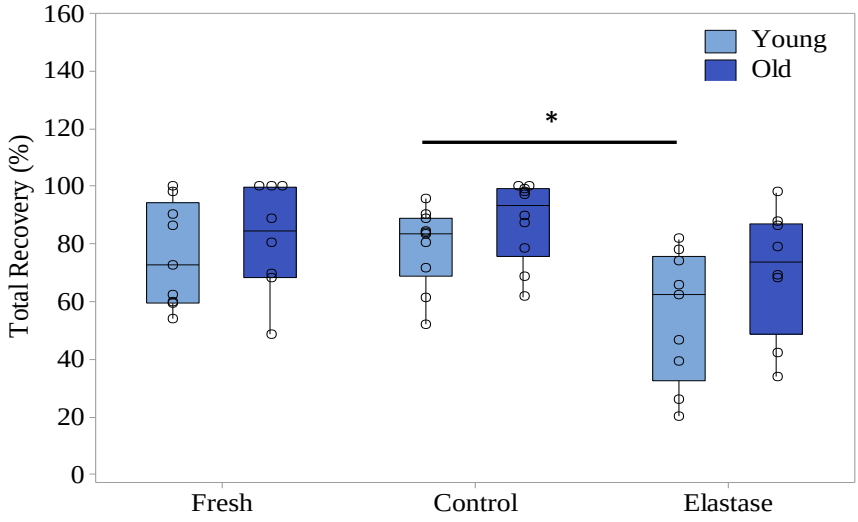

Figure 57: Total Recovery to 75% of the failure extension ("D: Holding period - recovery ten seconds after load is removed") for young and old SDFT IFM samples subject to different treatments: Fresh, Control and Elastase. Samples were stretched up to 75% of their predicted failure extension. Significant differences are flagged with: *p<0.05 (data non-normally distributed – Mann-Whitney test).

4.8. Failure Properties of SDFT Quarter Sections

4.8.1. Sample Preparation for Validation of Elastin Removal

SDFT quarter sections, previously prepared (Chapter 2), were used to first validate the ability to remove elastin with elastase from these much larger sections of tendon. Four sections from a young (n=1; 7 years old) and four from an old (n=1; 17 years old) SDFT were removed from the freezer and allowed to thaw for 30 minutes at room temperature. During this period, tissue was kept hydrated by spraying several times with PBS. Samples served as their own controls by comparing analysis with and without treatment.

4.8.2. Elastase Treatment Validation Protocol

To validate the elastase treatment, dose response experiments (enzyme concentration) were performed to determine the amount of elastase needed to digest the elastin in a pre-set incubation period of 24H. One young and one old sections were allocated to a fresh group, with the remaining six samples utilised for elastase treatment. Fresh samples were immediately dissected, to remove small squared samples (5x5x5mm), from the mid-metacarpal region of the section, which were then stored in cryotubes. Samples in the "elastase" group were incubated in the buffer solution (1x PBS plus 0.1mg/ml SBTI solution) with elastase (trypsin-free porcine pancreatic elastase, EPC134m Elastin Products Co., Owensville, MO), for 24 hours at room temperature, in either 1 U/ml, 5U/ml or 10U/ml elastase (1 young and 1 old section/condition), with mild agitation.

SDFT quarter sections are roughly 10 times the volume of IFM samples, which means that a much greater volume of solution would be needed. As elastase is such an expensive enzyme, a special container was designed and manufactured, especially to fit these samples and use the least amount of solution possible (Figure 58).

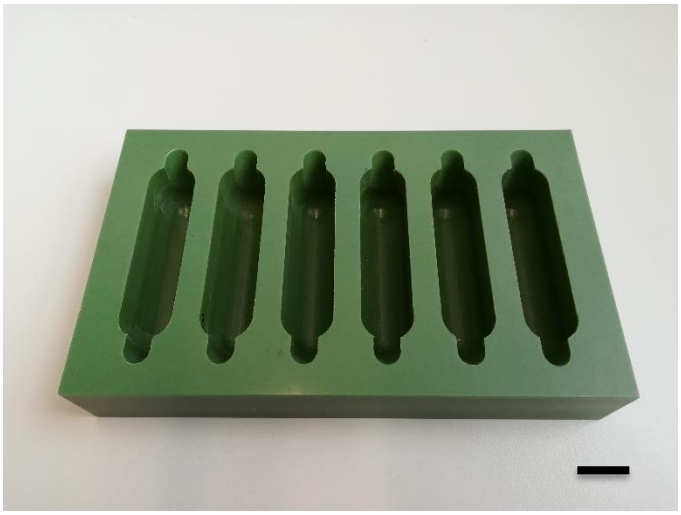

Figure 58: Plastic container designed for the incubation of longitudinal quarter tendon sections. Scale bar: 30mm.

It was calculated that for each cavity, 20ml of solution would be needed, and appropriate concentrations of elastase in buffer were prepared accordingly. Longitudinal sections (Figure 59a) were incubated in the control buffer with elastase. Taking into account the design of the container, only the middle region of the section (the region of interest) was immersed in the solution (Figure 59b). To prevent samples from drying out, the ends of the sections were wrapped in tissue (dampened in PBS) (Figure 59b) and the whole container in foil (Figure 59c). More foil was then added on top of the container, to prevent evaporation of the solution.

After treatment, samples were rinsed three times in PBS, and small squared samples (5x5x5mm) dissected from the middle region of the section and stored at -20°C in cryotubes, as described for fresh samples.

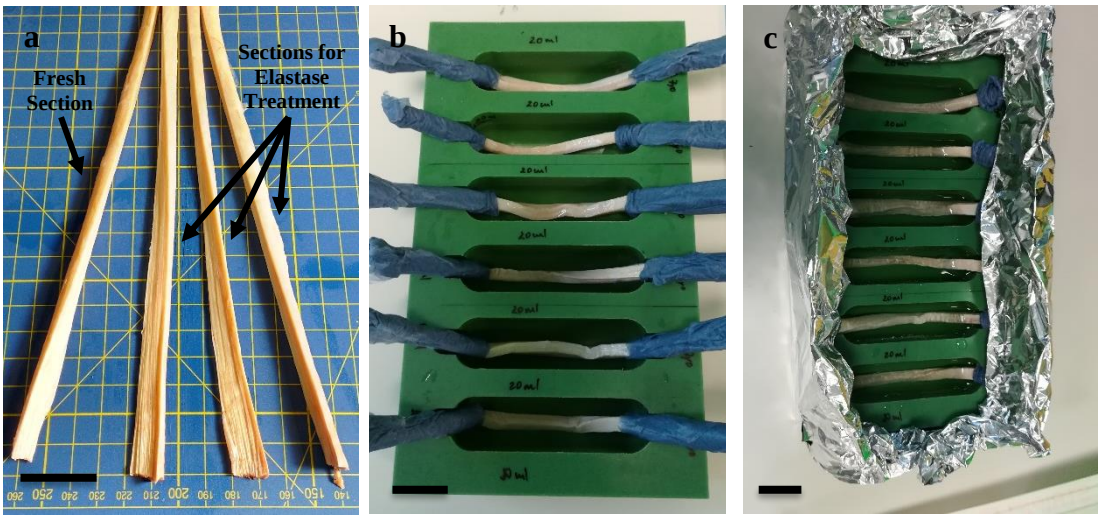

Figure 59: Images showing SDFT quarter sections (a) being submerged for elastase treatment incubation (b). The ends of each section were wrapped in tissue and covered in foil (c) to avoid sample dehydration. Scale bar: 30mm.

4.8.3. Biochemical Analysis

A Fastin Elastin assay (Fastin Elastin Assay Kit, Biocolour, UK), hydroxyproline assay (Birch et al., 1998) and a DMMB assay (Farndale et al., 1986) were used to quantify the amount of elastin, collagen type I and sulphated GAG, respectively. When needed, samples were removed from the freezer, and organised in groups according to the treatment (fresh, 1U/ml, 5U/ml and 10U/ml). In each group, at least 4 small squared samples were included in the analysis, to make up enough tissue to perform all three biochemical assays. All samples were powdered using a Micro dismembrator and then freeze dried. From each group, approximately 2x3mg (dry weight) was measured and stored in 2 different tubes for the Fastin Elastin assay. The remaining tissue (10-20mg dry weight) was solubilised in papain (as described in Section 3.3.3) in preparation for the hydroxyproline and DMMB assays. Samples were assayed following protocols described in section 3.3. Statistical analysis was only conducted for elastin content, due to the limited number of samples in the hydroxyproline and DMMB assays.

4.8.4. Elastase Treatment Validation – Results and Discussion

Results from the Fastin elastin assay are shown in Figure 60. No significant differences were seen between treatments or age groups. Although there was a trend towards elastin reduction in both young and old groups with elastase treatments, that reduction was not significant and only reached about 30% in the young samples and 44% in the old samples, compared to fresh SDFT samples (Figure 60).

Results from the DMMB assay (Figure 61) and hydroxyproline assay (Figure 62) were not statistically analysed due to the fact that only one sample was measured. However, similar to previous observations, elastase treatments seem to induce some GAG release from the tendon tissue (Figure 61) but not collagen. Collagen content increased in the elastase treated samples, compared to fresh samples in both young and old samples (Figure 62).

Although these results supported the previous elastase treatment validation in smaller SDFT samples, the percentage of elastin digested from the tissue was lower. This can be explained by the fact that these samples are much longer and thicker than IFM samples and so, much harder for the enzyme to penetrate the tissue. Indeed, digestion efficacy matched other published studies, highlighting the difficulties in removing the protein. Previous studies have attempted to quantify the mechanical effects of the partial digestion, but results analysis can be challenging.

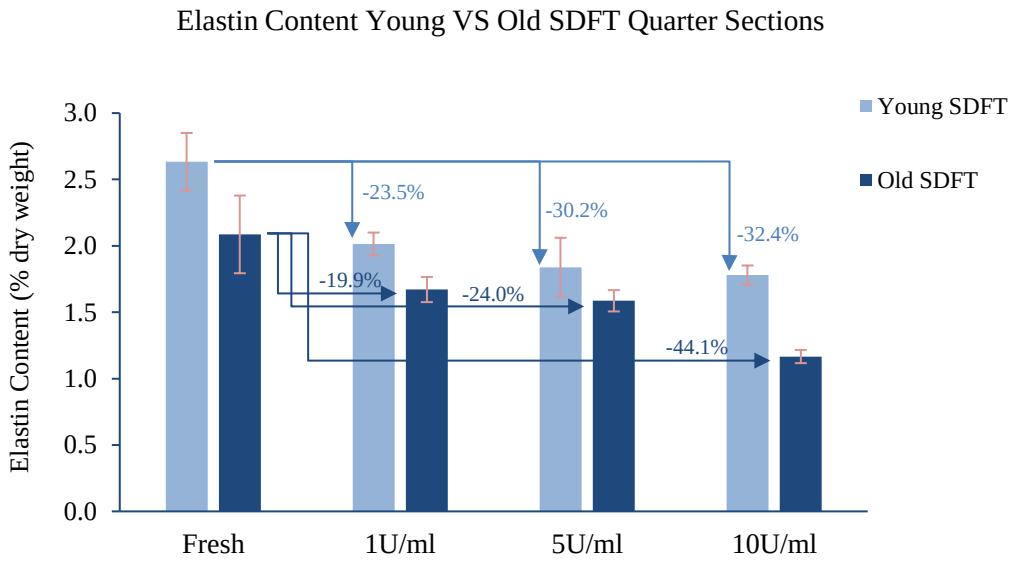

Figure 60: Elastin content, expressed as a percentage of dry weight tendon tissue, and the percentage of elastin reduction. Samples from one young horse (7 years) and one old horse (17 years) were used. No significant differences were found (all data normally distributed – ANOVA). Data are displayed as mean ± standard deviation.

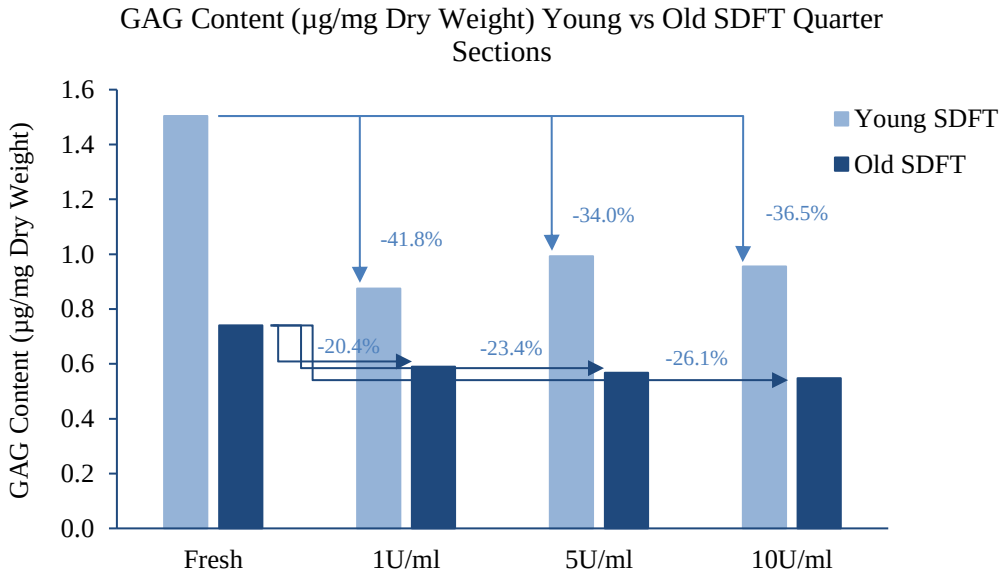

Figure 61: GAG content, expressed as µg/mg of dry weight tendon tissue, and the percentage of GAG reduction. Sample from one young horse (7 years) and one old horse (17 years) were used.

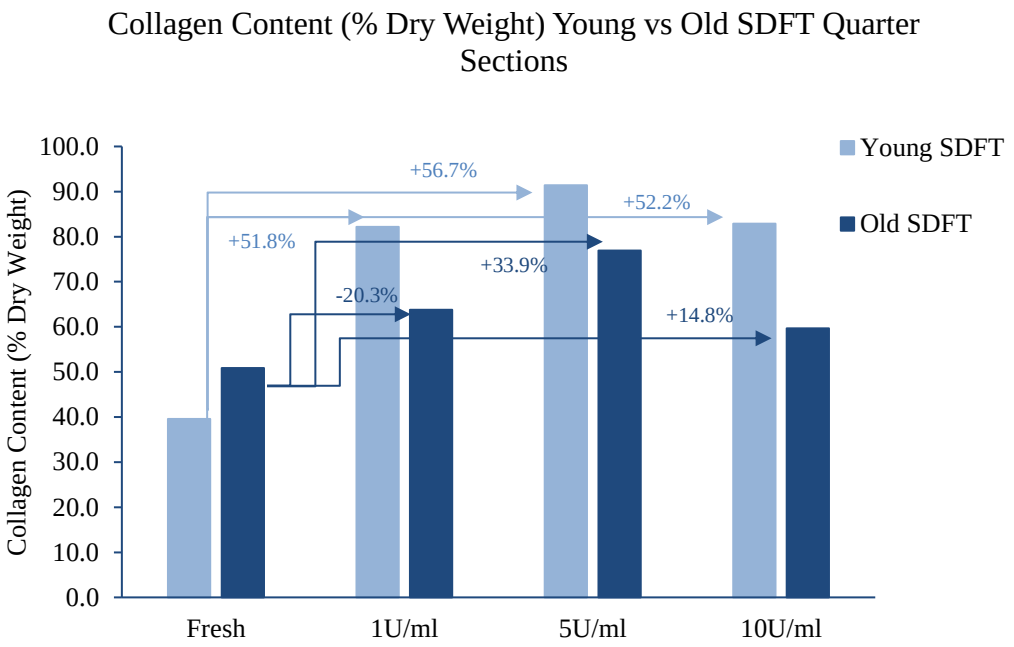

Figure 62: Collagen content, expressed as percentage dry weight tendon tissue, and the percentage of collagen reduction. Sample from one young horse (7 years) and one old horse (17 years) were used.

4.8.5. Failure Properties of SDFT Quarter Sections

Protocols for mechanically testing large tendon sections were next established, and the mechanical properties of fresh quarter tendon sections first investigated.

4.8.5.1. Sample Preparation

SDFTs from 5 young (3 to 7 years – young group) and 5 old (15 to 19 years - old group) horses were used. A single longitudinal tendon section from each tendon (as described in Chapter 2) was removed from the freezer and allowed to thaw for 30 minutes. Sections were kept hydrated by spraying several times with PBS. Once defrosted, the CSA of each section was measured, simple and non-destructive method using alginate paste (Goodship & Birch, 2005). This paste was used to create a cast around the tendon cross section, then after removal, transverse sections were cut along the cast, and digital images were taken (Figure 63). Using image analysis software (ImageJ) the CSA was determined by measuring the area that had been occupied by the tendon section.

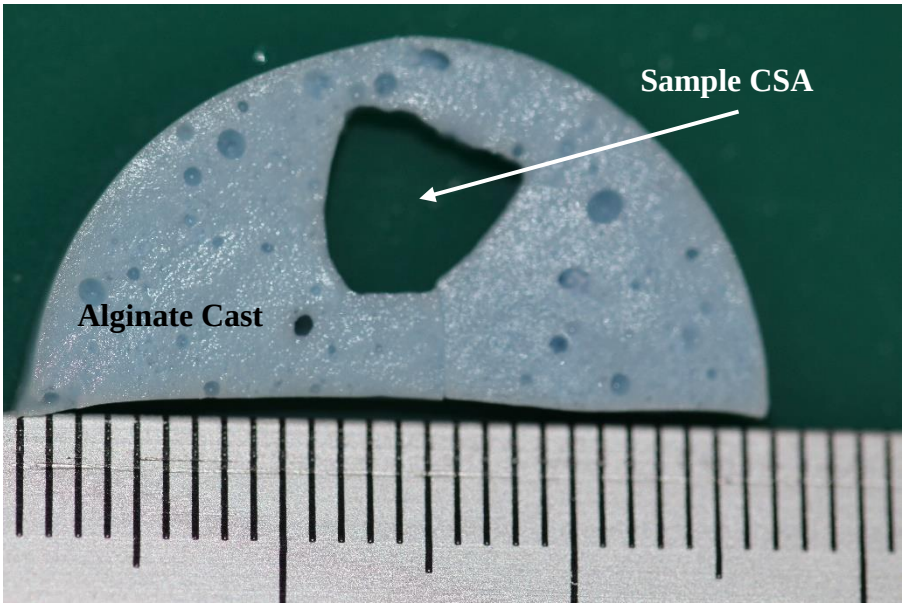

Figure 63: Transverse cut of the alginate cast formed around the tendon section. The scale (created with a ruler) is used to calculate the cross sectional area corresponding to the tendon section.

4.8.5.2. Protocol for Testing

Gripping large tendon specimens is difficult, as failure forces are large. Also, tendon is highly hydrated, hence the forces required to prevent slippage are very large. In order to mechanically test large tendon sections, it was first necessary to optimise a gripping method to securely grip samples during testing, whilst minimizing both slippage and sample damage. Multiple attempts were made to use classic wedge-shaped compressions grips, and increase the coefficient of friction at the grip surface with sandpaper or cardboard to balance gripping force and friction to secure the samples without slippage or excess damage. After a series of failures, cryogrips (Figure 64a) were custom made for these samples, freezing the ends, to enable tighter compression gripping without damage (Riemersa & Schamhardt, 1982).

The failure properties of fresh longitudinal SDFT quarter sections were investigated. For mechanically testing these samples, a hydraulic testing machine (Instron 8801) with a 50KN load cell, was used (Figure 64b). Cryogrips were installed in the testing machine, with a grip to grip distance of approximately 100mm and cooled down using CO_2 provided by cylinders connected to the grips. Once the grip surfaces were frozen, tendon samples were quickly placed between them (Figure 64c) and grips

lightly tightened. Grips were kept frozen by controlling the CO_2 flow and the samples hydrated by spraying several times with PBS. After a few minutes, the ends of the samples within the grip surfaces started freezing, and a freezing line started forming. The grips were then manually fully tightened and the freezing line identified using a marker pen. This way, it was possible to identify any slippage that may have occurred. The distance between the grips (initially set to 100mm) was adjusted as needed during the tightening of the grips, so that the samples were not in tension.

Once fully secured, samples were pre-loaded to 25N, which represents approximately 1% of the predicted failure load. The grip to grip distance, was recorded after the application of pre-load to give the correct value of gauge length. Sections were then preconditioned with 10 loading cycles between 0 and 5% strain (approx. 25% of expected failure strain) using a sine wave at a frequency of 1Hz, before pulling to failure at room temperature at a strain rate of 5% per second. Force and extension data were continuously recorded at 100Hz during preconditioning and the pull to failure.

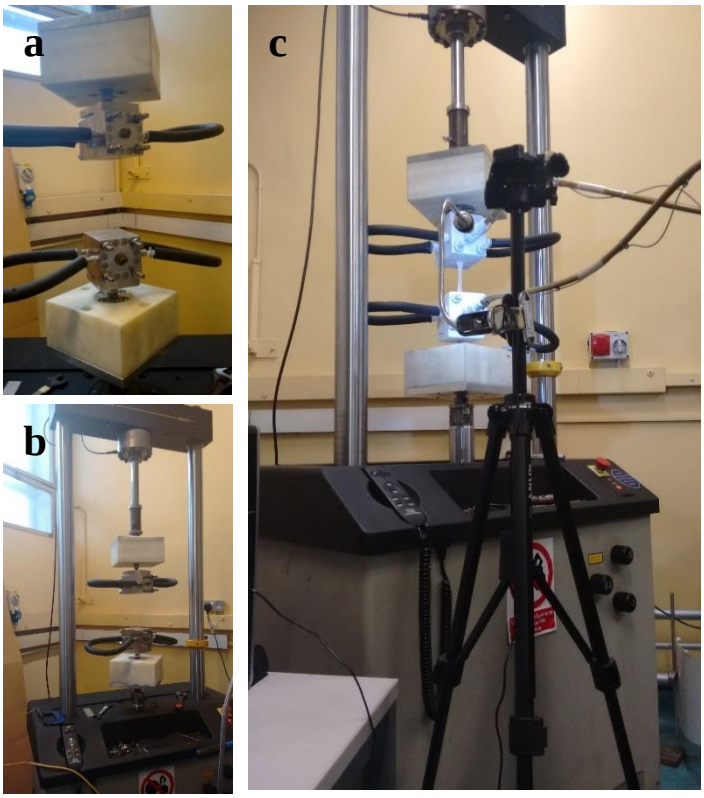

Figure 64: Images of the cryogrips designed and used for the failure tests of SDFT quarter sections (a). Cryogrips were installed in a hydraulic testing machine (b) (Instron 8801). Sample's ends were frozen in the grips and pulled to failure (c).

4.8.5.3. Failure Properties Calculations

Displacement at which the initial pre-load was reached was taken as the start point for the test to failure.

Failure load was determined as the maximum load sustained by the sample, and failure extension as the extension at this point. For each sample, engineering stress and strain were calculated using the CSA (determined as described in section 4.8.5.1) and effective gauge length, respectively. A continuous modulus was calculated across every 10 data points of each stress strain curve and smoothed using a 9-point moving average filter. From these data, a maximum modulus value was determined.

Percentage hysteresis in the first and tenth cycles was also calculated, as the percentage difference in the area between the loading and unloading curves for each cycle.

4.8.6. Failure Properties of SDFT Quarter Sections - Results

Results showed no significant differences in any of the failure variables (Figure 65) nor viscoelastic properties (Figure 66) of young and old SDFT sections. These results correlate well with previous studies, where no ageing changes were identified in whole SDFTs subjected to quasi-static testing (Thorpe et al., 2013a). Of additional importance, the parameters reported for quarter sections tests matched those determined in whole tendon tests (Thorpe et al., 2013a).

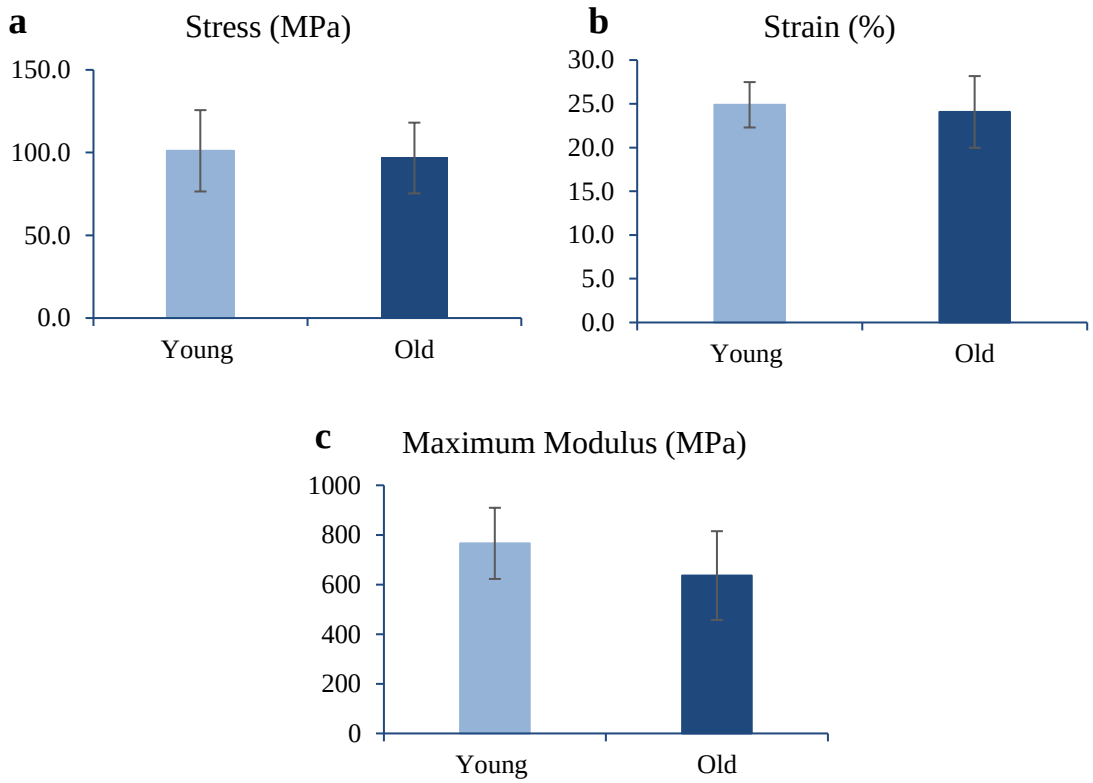

Figure 65: Stress (a), Strain (b) and maximum modulus (c) of young and old SDFT quarter sections. No significant differences were identified (all normally distributed data – ANOVA). Data is displayed as mean ± standard deviation.

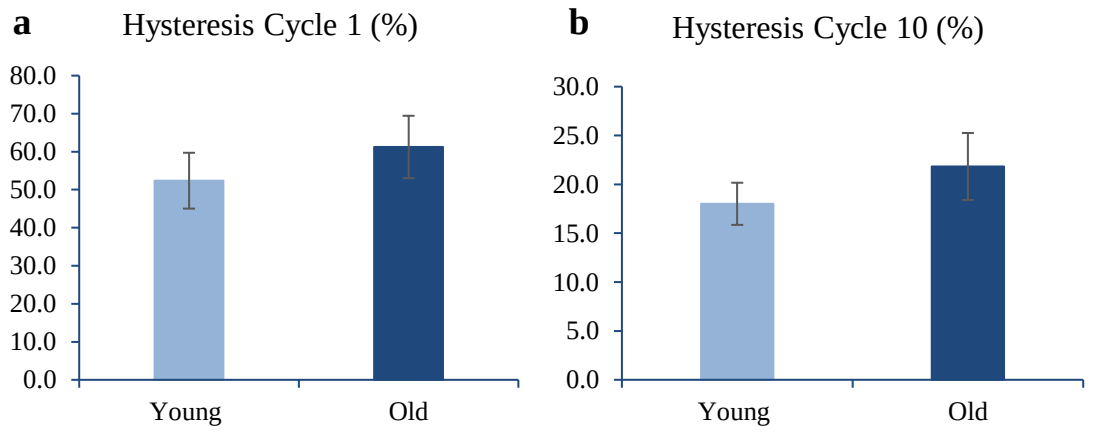

Figure 66: Hysteresis Cycle 1 (a) and Hysteresis Cycle 10 (b) of young and old SDFT quarter sections. No significant differences were identified (all normally distributed data – ANOVA). Data is displayed as mean ± standard deviation.

4.9. Discussion

This is the first study to investigate how elastin depletion affects the mechanical properties of fascicles and IFM samples from energy storing tendons. It is also the first study to investigate how elastase treatments differentially affect different aged tendon samples. Furthermore, methods were optimised to investigate the effects of elastase treatment on quarter tendon samples, providing the opportunity to characterise multi-scale tissue response. Time constraints prevented completion of these studies prior to submission but these are ongoing.

The failure, fatigue and recovery properties of fascicles and IFM samples from young and old energy storing SDFTs were investigated. The results generally support the hypothesis, showing a significant decrease in IFM mechanical properties with elastase treatments, whereas fascicle mechanical properties remain unchanged. With ageing, these changes in the elastase group were maintained, with all elastase treated IFM samples consistently showing a significantly lower ability to withstand load and resist fatigue loading, as well as a lower ability to recover after loading.

Enzyme efficacy and specificity should be questioned when carrying out targeted digestion assays such as this. Further, it is important to investigate possible effects of the buffer solution, particularly swelling, or consider if the enzyme may cause structural disruption in the tissue, and subsequently affect mechanical properties.

IFM is mainly composed of collagen type III, proteoglycans and elastin. Elastase treatment validation reported a significant reduction of elastin (>70%) but also of GAGs (>80%). These data lead to concern as to whether the reported loss of mechanical properties stems from changes in collagen or GAG content. Previous studies have reported that GAGs interact with collagens, supporting its fibril network, but also with elastin, where they are believed to associate with microfibrils and contribute to their integration into the ECM (Kielty, Sherratt and Shuttleworth, 2002). It is possible that changes in GAG content affected IFM mechanics, however, previous studies have failed to prove that tendon mechanical properties are affected by GAG digestion (Legerlotz et al., 2013, Lujan et al., 2009). Furthermore, a preliminary trial of GAG digestion in IFM samples showed no effects of 90% GAG removal on IFM mechanical behaviour. Structural imaging of the current samples, demonstrate no clear disruption to the tissue and collagen content was not altered. Taken together, data suggest that any changes in tissue mechanics originate from loss of elastin and not

GAG. Further, the inclusion of a control group, maintained in the incubation media provides confidence that swelling, or water modification effects are accounted for.

Data demonstrates no changes to fascicle failure or fatigue properties post-elastase treatment. With fascicles comprising in excess of 90% collagen, these findings are perhaps not surprising. By contrast, after elastase treatment, IFM failure load and stiffness were both significantly reduced compared to both fresh and control groups. There are few relevant studies with which to compare these findings, but they do correlate well with previous studies in tendon that reported a significant reduction in whole tendon stiffness after elastase digestion (Millesi *et al.*, 1995). With ageing, although not significant, there was a trend towards maximum stiffness increasing in both fresh and control samples. These results support previous findings where IFM samples were observed to become stiffer with ageing in SDFTs (Thorpe et al., 2015c) and it was interesting to note that elastase treatment masked any ageing changes.

Interestingly, no changes were observed in the failure extension of young or old SDFT IFM samples after elastase treatment. Although changes with ageing were not expected (Thorpe et al., 2015c), the fact that failure extension did not change with elastase treatment was surprising and requires further discussion. This might be explained by the preconditioning step. Samples were preconditioned with 10 loading cycles prior to pull to failure, and extension was normalised after the preconditioning, as per other studies (Thorpe et al., 2015c). Such an approach means that any extension that occurred during the preconditioning cycles was not included in final values. With other datasets demonstrating poor recoverability of IFM in elastase treated samples, it seems likely that the elastase treated IFM samples extended notably during those initial cycles, perhaps more so than any other samples, as the IFM was less able to sustain applied load.

Elastase treatments also influenced the viscoelastic properties of IFM samples specifically. Data showed a significant increase in hysteresis in both cycle 1 and 10 in elastase treated IFM samples, and a severe reduction in fatigue resistance such that most elastase treated samples failed immediately. Similar to previous studies, no changes in the IFM hysteresis were observed between age groups (Thorpe et al., 2015c), and it was also notable that fascicle fatigue properties were not affected by the elastase treatment.

It is important to note that all IFM samples, regardless of what treatment they were subject to, were fatigue loaded from zero to the peak load found by applying one

cycle between 0 and 50% of IFM predicted failure extension. This protocol was based on previously published data (Thorpe et al., 2015c), but might have caused some samples to be over-loaded and others under-loaded. However, large numbers of samples were tested to help account for this, and the fact that no differences were observed between fresh and control groups, whilst elastase treated samples were so significantly different ($p=0$), gives confidence in treatment effects. Indeed, it was also notable that elastase treated samples showed a significant increase in creep between cycles 1 and 10 and in both minimum and maximum displacement creep curves, all indicated reduced fatigue resistance. Taken together, both failure and fatigue data suggest that IFM samples become less able to withstand load and more viscoelastic with reduced fatigue resistant when subject to elastase treatments.

In order to directly explore how the IFM loads and recovers when subject to elastase treatments, further experiments combining imaging and mechanics were designed and performed. An experimental protocol stretching IFM samples under a camera was conceived, and Digital Image Correlation (DIC) developed in order to investigate sample response to loading and recovery. With these experiments it was possible to compare IFM sliding and recoil when samples were stretched up to 75% of the IFM predicted failure extension, between fresh, control and elastase treated samples in both young and old samples. It would have been very useful if force and displacement data had been recorded throughout the test, such that hysteresis could have been calculated and compared to previous data. However, the load cell attached to the rig was not working. This provided an additional concern, that it was not possible to guarantee that all samples were preloaded with exactly the same amount of load prior to testing. However, a previously published protocol which looked for lifting of samples from the base of the rig to define the start point was adapted, which has shown good repeatability (Thorpe et al., 2013b). Finally, it should be noted that the displacement applied to all samples was based on average values from previous publications. Thus, similar to the scenario described for fatigue tests, some samples may have been over loaded, and others under loaded. However, the consistency in response, once again, provides confidence in the data.

Data showed a significant increase in the angle deviation in the elastase group compared to both fresh and control groups, suggesting that elastase treated IFM samples stretched more than fresh and control samples, when subject to similar displacements. This additional IFM extensibility in elastase treated IFM samples

appears contradictory to earlier studies of IFM mechanical properties, but is more intuitive as a sample response. As IFM extension was not normalised in these tests, but is a report of all extension from the first loading cycle, it adds further evidence in support of the previous hypothesis that, after elastase treatment, the IFM responds immediately to applied load with irrecoverable extension and shear. Further corroborating this behaviour, results also showed a significant decrease in the percentage recovery of IFM sliding after load is removed in the elastase group compared to all other treatment groups. Indeed, while recovery in fresh and control samples was close to 70%, elastase treated samples showed a much lower percentage recovery (30%, approximately). After an unloaded hold period, fresh and control samples showed little further recovery, as most of the recovery was observed immediately after load was removed. On the other hand, it was interesting to note that elastase treated samples did show a continual gradual recovery with time, from approximately 30% to 55%, as a result of the holding period. However, the total ability to recover for these samples was still significantly lower compared to the control group. Taken together, data implies that elastase treatment results in increase IFM sliding and reduced ability for the IFM to withstand or recoil after loading, all contributing to reduce fatigue resistance. These findings are of crucial importance to structure-function studies, allowing a new level of insight into the hierarchical mechanics of tendon.

Unfortunately, complete elastin removal is not achieved in SDFT quarter sections. However, the reported >30% removal of elastin is in line with that demonstrated in other published papers, where the ability to interpret such a graded loss is argued. Here, protocols are prepared to investigate the response of these samples, and it will be interesting to investigate how elastase treatments affect the whole SDFT and the contribution from fascicles and IFM.

Chapter 5 - Overall Discussion and Future Work

5.1. Main Findings

This body of research has shown that most of the elastin (>90%) in equine tendon is localised to the IFM, but has also demonstrated differences in elastin associated with functionally distinct tendons. Overall tendon elastin content was greater in the SDFT compared to the CDET, and with ageing, there was a decrease in elastin content and organisation in the energy storing SDFT, whilst no changes were seen in the CDET (Godinho et al., 2017). These results support previous studies in other species, that have shown that the IFM is comparatively rich in elastin (Grant et al., 2013, Smith et al., 2011), and have also suggested that enrichment is particularly evident in energy storing tendons (Thorpe et al., 2016a).

In this study, immunohistochemistry followed by confocal microscopy was used to establish regional elastin organisation and structure in tendon. However, the amount of processing these samples have to undergo prior to imaging should be considered. Tissue had to be snap frozen, sectioned, fixed and stained, and whilst arguably less destructive than the dehydration stages of wax embedding, it may cause damage to the structure of the tissue. During sectioning, for instance, it is very common that regions of the IFM, tear apart. Various other techniques have been suggested for elastin visualisation.

5.2. Alternative Techniques for Elastin Visualisation

Early studies used transmission electron microscopy (TEM), and scanning electron microscopy (SEM) to investigate the ultrastructure of elastic fibres in tendon (Parry and Craig, 1978), however these techniques also have limitations. Both approaches require complete tissue dehydration, and SEM is limited to surface imaging, while TEM requires ultra-sectioning of tendon tissue (Pang et al., 2016). Furthermore, although the substructures of elastin can be well visualised with these techniques, the magnification range is too high to clearly visualise elastic fibres, which are the functional unit of the elastin structure. Hence imaging of fibre organisation is not easily achievable. Other techniques that require minimal tissue processing and

enable good elastin visualisation were also considered. Multiphoton high resolution imaging is a very promising technique as it allows elastic fibres detection within intact tissue specimens, without any need for preparation processes that may damage the tissue and compromise the visualisation of certain structures. By changing the laser excitation wavelengths, elastic fibres can be differentiated from collagenous structures and other matrix elements without having to use any staining (Press, 2005). In the current thesis, multiphoton microscopy was investigated, however, images from tendon samples showed substantial background fluorescence, making it impossible to see elastin fibres.

5.3. Elastin Organisation in Tendon

Despite the limitations, clear images of elastin fibres were acquired using immunohistochemistry. Automated image analysis of these samples suggested predominant fibre orientation parallel to the IFM. However, when blind scorers were asked to identify elastin organisation, they reported that there were a greater number of elastin fibres aligned perpendicular to the IFM in the young SDFT than in the CDET. The presence of perpendicularly aligned elastin fibres, particularly in the SDFT IFM, suggests that, elastin orientation may specifically facilitate mechanical function. Elastin fibres oriented in this perpendicular manner may serve as a "bridge" between adjacent fascicles, which would assist in returning fascicles to their initial location once external forces have been removed. However, the question remains: how exactly does elastin bridge the IFM? The schematic in Figure 67 illustrates a hypothesis of how elastin might function to connect fascicles, and how it is affected by ageing. In the unloaded condition, elastic fibres are shown to bridge fascicles, in a coiled conformation (Figure 67a). When external forces are applied, the elastin network can unfold and stretch as the fascicles slide (Figure 67b_1), providing initial low stiffness fascicle sliding with a clear increase in stiffness as the collagen and elastin bridging the IFM are directly loaded. Once load is removed, elastin fibres recoil and help fascicles return to their original position (Figure 67b_2). However, with ageing, IFM elastin content reduces and organisation is lost, accompanied by decreased protein turnover in the IFM, meaning that regions of damage may not be repaired as effectively. Together, these changes likely reduce capacity for low stiffness fascicle sliding (Figure 67c_1). Therefore the fascicles themselves will be stretched more

readily, and so, both IFM and fascicles become more likely to be damaged, which is likely to contribute to the age-related increase in tendon injury (Figure 67c_2).

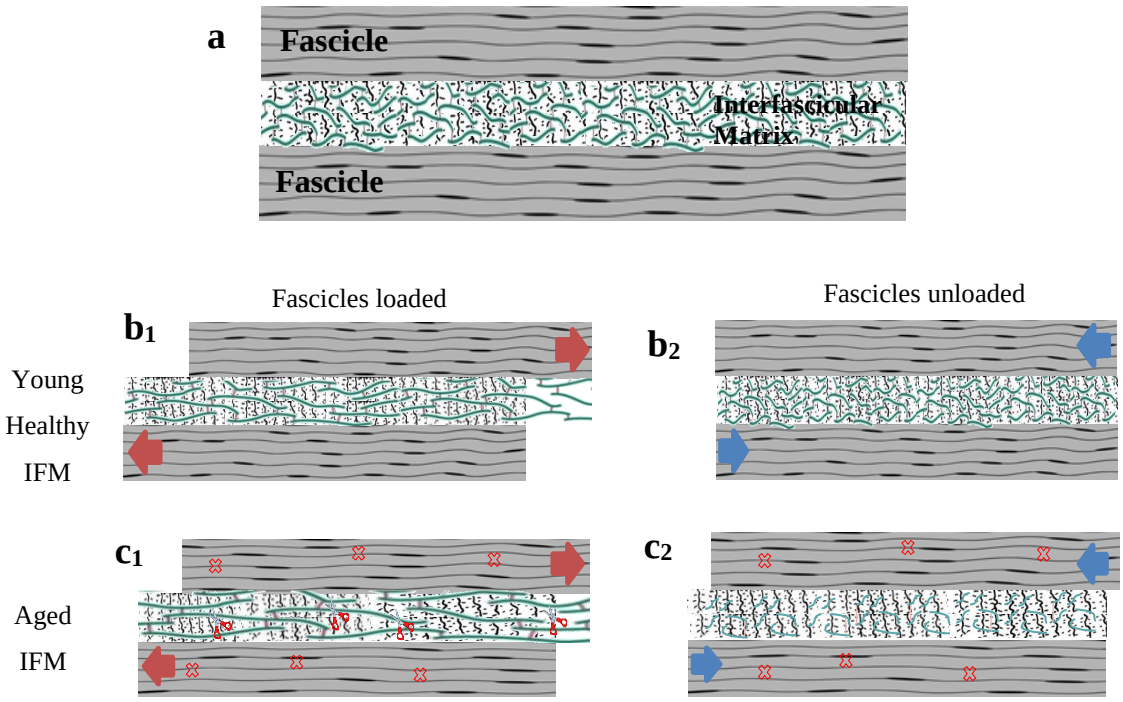

Figure 67: Schematic of the IFM in tendon mainly composed of collagen type III proteoglycans and elastin (green fibres) (a). When two adjacent fascicles are pulled in different directions (b1), the IFM stretches and the elastin fibres unfold adopting a more elongated configuration. Once the load is removed (b2), fascicles slide back, and elastin folds again, returning to its original configuration. With ageing (c_1), elastin content is reduced and remaining elastin shows signs of fragmentation. Together, these changes reduce capacity to control fascicle sliding and recoil, which leads to fascicle overload and damage (c_2). Adapted from schematic by C Thorpe.

To investigate this hypothesis in further detail, a custom designed tensile straining rig (Figure 50) was used to investigate the recoverability of IFM samples after cyclic loading, imaging local tissue mechanics during loading and recovery. This system was previously used by Screen's group to measure the microstructure response of tendon fascicles when subject to different strains (Cheng & Screen 2007), and allows fresh samples to be loaded while in situ on the stage of a confocal microscope. Preliminary studies clearly showed sliding and recoil in the IFM, with a series of elastase treatment experiments specifically implicating elastin in this response. If

multiphoton imaging difficulties could be overcome, future studies could potentially use this technique to directly visualise elastin organisation and strain response in the IFM samples to more fully probe the hypothesised model in Figure 67. Staining could be used to identify other IFM proteins or cells also, to create a more detailed description of how the different matrix components respond to loading and unloading, and also investigate how elastin influences that response. Ideally, samples of different ages and from functionally distinct tendons would allow a clear structure-function investigation.

5.4. Importance of Elastin Models

As a compliment to experimental work, several studies have been focussing on developing models of protein behaviour, and elastin being such an important ECM protein is no exception (Tarakanova & Buehler, 2013). Initially, computational models of elastin-like polymers were developed to study the source of elastin elasticity and provide fundamental understanding of the molecular mechanisms behind the biological function of elastin (Hoeve & Flory 1958, Venkatachalam et al., 1981). More recent approaches have aimed to model elastin interactions using an atomistic modelling approach, in which molecular dynamics can be used to predict protein response to loading (Rousseau et al., 2004). Being able to use computational modelling to investigate elastin functionality at a molecular level has contributed massively to the development of demanding biomaterials, and here, it may help establish how elastin controls collagen sliding and how elastin conformational changes with age or disease may impact IFM function.

Most of the elastin in the body is produced in the early stages of development of life. This means that any damage or injury to the elastin rich tissues is very difficult to repair (Swee et al., 1995). As a consequence, various diseases including emphysema and cutis laxa are related to mutations within or malfunction of elastic fibres (Vrhovski and Weiss, 1998). Tissue replacements using elastin-based biomaterials are in high demand. In addition to physiological compatibility, elastin-based peptides show excellent material properties that can be used to create smarter biomedical applications. Some examples are elastin hydrogels, developed as matrices for controlled drug delivery, or elastin-based synthetic fibres to be used as prototypes for tissue engineering and artificial cardiovascular tissue (Swee et al., 1995). The most

important aspect of elastin, in terms of biomedical applications, is its ability to undergo a lifetime of extensions, to strains several times its resting length, and to reversibly return to its original length. As such, most computational models have focussed on investigating the source of this elasticity. However, how elastin interacts with the surrounding components, such as other proteins or even cells, is not yet known. Tissue extensibility often arises from reordering of tissue fibres (collagen or elastin) as well as directly from stretching of resident fibres, so investigating matrix interactions is as important as the properties of the elastin itself.

Previous studies in tendon have suggested that elastin also regulates the interactions between cells and extracellular matrix (Pang et al., 2016, Grant et al., 2013). Data have shown elastic fibres localised around tenocytes, forming a sparse meshwork style configuration. This close interaction between elastic fibres and cells in the tendon pericellular matrix, is likely to have a substantial effect on the forces experienced by cells, and therefore, their mechanobiological response to load. Tendon cells have previously been reported to attach to collagen fibres, and thus slide on one fibre relative to another during deformation (Screen et al., 2004). Elastin may also serve to protect cells during this mechanical loading and sliding, by helping them glide relative to adjacent fibres, and to return to their original configuration following unloading. Elastin has also been suggested to play a crucial role in cell attachment, working as an intermediate link between cells and collagen (Grant et al., 2013). Previous studies have demonstrated that elastin functionalised substrates are useful tools to investigate cellular adhesion and proliferation (Vassalli et al., 2013, Ito et al., 1998). Indeed, studies with elastin coated substrates showed excellent fibroblast proliferation and adhesion, compared to un-functionalised substrates, where cells remained round-shaped (Barenghi et al., 2014). These results support previous work showing that tropoelastin, a precursor of elastin, promotes fibroblast adhesion, proliferation, and spreading (Rnjak et al., 2009).

Another useful approach to investigate the influence of specific proteins on tissue function is to adopt either direct enzymatic treatments, or use genetic knockout models, and carry out testing with these. Integrating these approaches with the novel local mechanics assessments described in this thesis, could provide exciting insight into the specific effects of different treatments.

Genetic knockout models have been used mainly to investigate the role of minor tissue components, such as specific proteoglycans and glycoproteins (Robinson

et al., 2005, Waller et al., 2013), as elastin knockout models can only be partial. It has been shown that when levels of elastin in a knockout drop below 30%, animal viability is compromised, owing to its crucial role in the lungs and circulatory system (Hirano et al., 2007, Wagenseil et al., 2005). As an attempt to overcome this problem, some studies are using site-specific recombination to generate conditional gene knockouts and thus, targeting specific cell types, tissues or even specific time points (Pappas et al., 2018).

Whilst a highly successful approach in many tissues, its successful implementation necessitates clear cell markers in the tissue of interest to target the treatment, and to date, such markers have not been identified for tendon. Furthermore, knockout studies all adopt mouse models, and mouse tendons are so small they do not have a clear IFM structure, which provides a further substantial limitation. Recent advances such as Clustered Regularly Interspaced Short Palindromic Repeats (CRISPR), offer opportunity here, in which knockout approaches can be translated into other larger animals (Ma et al., 2014). The rat has been identified as an ideal model system, with the appropriate IFM structure present. However, the absence of clear cell markers for tendon, means this approach remains challenging.

5.5. Advantages and Disadvantages of Elastase Treatments

In this thesis, it has been shown that elastin depletion has a significant effect on overall tendon mechanics, but specifically through an influence on IFM mechanics, where elastin is predominantly localised. Failure and fatigue tests showed a significant reduction in the ability of the IFM to withstand load, as well as a significant reduction in the IFM fatigue resistance when elastin is partially removed. Additionally, direct assessment of IFM recovery properties, showed that elastase treatment strongly impaired the ability of IFM samples to recoil. These results are very promising as they support the hypothesis that elastin is a key contributor to all aspects of the tendon mechanical behaviour. However, enzymatic treatments can be challenging, as they can have a non-specific effect on other ECM components and can also compromise the structure of the tissue. Despite typical limitations of the enzymatic treatments, results were promising. In the validation process, changes in tendon structure and composition were investigated and results showed very few non-specific changes with elastase treatments. Also, the addition of a control group supported the hypothesis that changes

in the mechanical properties are caused by enzyme treatments and not by the swelling. Taking these observations together, this thesis suggests that combining elastase treatments with the detailed structure-function microscopy studies, described earlier in this work, would provide unprecedented insights into how elastin governs fascicle sliding and interacts with other proteins and cells to enable energy storing tendons to stretch further than positional tendons.

5.6. Elastin Contribution to Overall Tendon Mechanics

Over the years, most studies of elastin have focused on the cardiovascular system, where elastin is a major structural component. In these tissues, such as arteries and smaller blood vessels, elastin is thought to provide tissue stiffness at low strains. As the tissue is first strained, elastin is straightened and loaded, while only 10% of the collagen is straightened and loaded (Clark and Glagov, 1985). Only when pressure increases above physiological loads, do the collagen fibres become straight and load bearing also (Clark & Glagov 1985, Carta et al., 2009). Similarly, in the skin, while collagen is the main source for the mechanical strength, elastin is thought to be responsible for the initial extensibility of the tissue (Oxlund et al., 1988). Differences in how elastin contributes to the overall tissue mechanics, may be reflected in how elastin is organised in the tissue. Indeed, while in the cardiovascular tissue elastin is arranged in an interconnecting fenestrated network, called a lamellar unit (Wagenseil & Mecham, 2013), in skin, elastin forms a branching network between bundles of collagen (Oxlund et al., 1988). In tendon, elastin seems well organised, with specific localisation to the IFM and very often located around cells (Godinho et al., 2017, Grant et al., 2013), which might explain why changes to the mechanics with elastin depletion were only significant in the IFM and not in the fascicles.

Taken together, given the unique ability of elastin to undergo large deformations, and considering the findings presented in this work, it is believed that elastin provides tendon with elastic recoil and resilience. In this study, it was demonstrated that, despite the low amounts of elastin in tendon, elastin plays a role in its mechanical properties, which is consistent with previous studies of soft tissues, such as tendon (Grant et al., 2015) and ligament (Henninger et al., 2013). For rat tail tendon fascicles and human supraspinatus tendon, elastin depletion affected the mechanical properties of the tissue, including a significant decrease in the stress values (Grant et

al. 2015, Fang & Lake, 2016). Ligament was also shown to have smaller stresses after elastin digestion under tensile and shear loading (Henninger *et al.*, 2013). As previous mentioned, energy storing tendon deformation is governed by sliding of fascicles, and the concentrated distribution of elastic fibres in the interfascicular space is likely to provide this region with elastic recoil, by "bridging the fascicles" and transferring stress. Unfortunately, it is still unclear how elastin and collagen interact to enable its function. It is known that type VI collagen, although only 0.33% (wet weight) of tendon (Carvalho et al., 2006), is a major constituent of the pericellular matrix (Ritty et al., 2003). Interestingly, FBN-1 (an important constituent of elastic fibres) has been shown to bind to type VI collagen (Midwood and Schwarzbauer, 2002). Therefore, elastic fibres may form an intermediate link between the cell and type VI collagen, which binds to collagen fibrils.

5.7. Future work

As a final body of further work, it would be interesting to probe IFM composition and function and the role of elastin in tendons from other species. Recent studies are providing increasing evidence of variation in hierarchical structure and composition between tendons from different species and with different functions (Thorpe et al., 2015a, Thorpe et al., 2016a). However, horse tendons have been shown to have a similar epidemiology and aetiology to human tendon injury (Ely et al., 2009), and recent still unpublished work from QMUL group indicated similar arrangements of elastin in human and equine energy storing tendons. Indeed, as the equine SDFT is an extreme example of an energy storing tendon, it arguably provides one of the best models for studying key structure-function relationships. This kind of work to further understand human tendon injury is very important as such injuries are still a big clinical problem.

Future work could also focus on further probing elastin contribution to specific tendon structure-function, by looking in more detail at elastin organisation and interaction with other proteins, such as collagen and PGs, using scanning electron microscopy or multiphoton microscopy. Whilst some investigations of such relationships have been carried out in cardiovascular tissues, relationships remain unexplored in tendon (Midwood and Schwarzbauer, 2002).

Making use of the already validated methods for elastin depletion, it would also be interesting to investigate how mechanical and fatigue properties of whole tendons change when elastin is removed from those samples. The same elastin depletion methods could be further used to determine the impact of elastin on whole tendon local strain patterns, or investigate changes in the transverse mechanics perhaps more specifically targeting mechanics of the elastin-rich IFM region.

Elastin ageing process remain under explored, and it would be of benefit here to establish the impact of elastin ageing on overall tendon mechanics.

Understanding how minor components of tissues, such as elastin in tendon, contribute to the overall tendon function, will help identify key structure and function relationships in different tendons. This way, new approaches can be proposed to target specific matrix components or cells to support healthy function, or even avoid or treat tendinopathies. With a better knowledge of elastin's role in tendon, new approaches for modulation of exercise could be developed to maintain a heathy IFM. Perhaps a lubricant could be used to prevent elastin overload and damage. Similarly, synthetic biology could create an elastin analogue to replace the dysfunctional one, or even new approaches to manipulate elastin turnover and ageing could be adopted.

Chapter 6 - References

Akagawa, M. and Suyama, K. (2000) 'Mechanism of formation of elastin crosslinks.', *Connective Tissue Research*, 41, pp. 131–141.

Alexander, R. (1991) 'Energy-saving mechanisms in walking and running', *Journal of Experimental Biology*, 69, pp. 55–69.

Ali, O. J. *et al.* (2018) 'Variations during ageing in the three-dimensional anatomical arrangement of fascicles within the equine superficial digital flexor tendon', *Eur Cell Mater*, 35, pp. 87–102.

Almeikinders, L. C. and Temple, J. D. (1998) 'Etiology, diagnosis, and treatment of tendonitis: an analysis of the literature', *Medicine and science in sports and exercise*, 30(8), pp. 1183–1190.

Andres, B. M. and Murrell, G. C. (2008) 'Treatment of tendinopathy: what works, what does not, and what is on the horizon.', *Clinical orthopaedics and related research*, 466(7), pp. 1539–54.

Anwar, R. A. (1990) 'Elastin: A brief review', in *Biochemical Education*, pp. 162–166.

Avery, N. C. and Bailey, A. J. (2005) 'Enzymic and non-enzymic cross-linking mechanisms in relation to turnover of collagen: relevance to aging and exercise.', *Scandinavian journal of medicine & science in sports*, 15(4), pp. 231–40.

Bannister, D. W. and Burns, A. B. (1970) 'Adaptation of the bergman and loxley technique for hydroxyproline determination to the auto analyzer and its use in determining plasma hydroxyproline in the domestic fowl', *The Analyst*, 95(1131), pp. 596–600.

Banos, C., Thomas, A. and Kuo, C. (2008) 'Collagen fibrillogenesis in tendon development: Current models and regulation of fibril assembly', *Birth Defects Research Part C - Embryo Today: Reviews*, 84, pp. 228–244.

Barbir, A. *et al.* (2010) 'Effects of enzymatic digestion on compressive properties of rat intervertebral discs.', *Journal of Biomechanics*. Elsevier, 43(6), pp. 1067–73.

Barenghi, R. *et al.* (2014) 'Elastin-coated biodegradable photopolymer scaffolds for tissue engineering applications', *BioMed Research International*, 624645–54.

Batson, E. L. *et al.* (2003) 'Are the material properties and matrix composition of equine flexor and extensor tendons determined by their functions?', *Equine veterinary journal*, 35(3), pp. 314–8.

Bedell-Hogan, D. *et al.* (1993) 'Oxidation, cross-linking, and insolubilization of recombinant tropoelastin by purified lysyl oxidase', *Journal of Biological Chemistry*, 268(14), pp. 10345–10350.

Beenakker, J. W. M. *et al.* (2012) 'Mechanical properties of the extracellular matrix of the aorta studied by enzymatic treatments.', *Biophysical journal*. Biophysical Society, 102(8), pp. 1731–7.

Benjamin, M. & Ralphs, J. R. (1997) 'Tendon and ligaments: An overview.pdf', *Histology and Histopathology*. Histology and Histopathology, 12, pp. 1135–1144.

Berens, P. (2009) 'CircStat: A MATLAB Toolbox for Circular Statistics', *Journal of Statistical Software*, 31(10), pp. 1–21.

Bergman, I. and Loxley, R. (1963) 'Two Improved and Simplified Methods for the Spectrophotometric Determination of Hydroxyproline.', *Analytical Chemistry*, 35(12), pp. 1961–1965.

Berry, C. L., Looker, T. and Germain, J. (1972) 'Nucleic acid and scleroprotein

content of the developing human aorta', *The Journal of Pathology*, 108(4), pp. 265–274.

Betts, J. *et al.* (2013) *Anatomy and Physiology*. OpenStax Collage.

Birch, H. L. (2007) 'Tendon matrix composition and turnover in relation to functional requirements.', *International journal of experimental pathology*, 88(4), pp. 241–8.

Birch, H. L. *et al.* (2008a) 'Matrix metabolism rate differs in functionally distinct tendons', *Matrix Biology*, 27, pp. 182–189.

Birch, H. L. *et al.* (1999) 'Age-related changes to the molecular and cellular components of equine flexor tendons.', *Equine veterinary journal*, 31(5), pp. 391–6.

Birch, H. L., Bailey, A. J. and Goodship, A. E. (1998) 'Macroscopic "degeneration" of equine superficial digital flexor tendon is accompanied by a change in extracellular matrix composition.', *Equine veterinary journal*, 30(6), pp. 534–9.

Birch, H. L., Wilson, A. M. and Goodship, A. E. (2008b) 'Physical activity : does long-term , high-intensity exercise in horses result in tendon degeneration ?', pp. 1927–1933. doi: 10.1152/japplphysiol.00717.2007.

Blanchevoye, C. *et al.* (2013) 'Interaction between the elastin peptide VGVAPG and human elastin binding protein.', *The Journal of biological chemistry*, 288(2), pp. 1317–28.

Braverman, I. M. and Fonferko, E. (1982) 'Studies of cutaneous aging:I. The elastic fiber network.', *J. Invest. Dermatol.*, 78, pp. 434–443.

Bressan, G. M., Argos, P. and Stanley, K. K. (1987) 'Repeating structure of chick tropoelastin revealed by complementary DNA cloning', *Biochemistry*, 26, pp. 1497–1503.

Burgeson, R. E. (1988) 'New Collagens, New Concepts.', *Ann. Rev. Physiol.*, 4, pp. 551–577.

Cain, S. A. *et al.* (2006) 'Proteomic analysis of fibrillin-rich microfibrils.', *Proteomics*, 6, pp. 111–122.

Caldini, E. G. *et al.* (1990) 'Distribution of elastic system fibres in the Rat Tail Tendon and its associated sheaths', *Acto Anat*, 139, pp. 341–348.

Cantor, J. *et al.* (2006) 'Synergistic effect of hydrogen peroxide and elastase on elastic fiber injury in vitro.', *Experimental biology and medicine (Maywood, N.J.)*, 231, pp. 107–111.

Canty, E. G. and Kadler, K. E. (2005) 'Procollagen trafficking, processing and fibrillogenesis.', *Journal of cell science*, 118, pp. 1341–1353.

Carta, L. *et al.* (2009) 'Discrete contributions of elastic fiber components to arterial development and mechanical compliance', *Arterioscler Thromb Vasc Biol*, 29(12), pp. 2083–2089.

Carvalho, H. F. *et al.* (2006) 'Identification, content, and distribution of type VI collagen in bovine tendons', *Cell and Tissue Research*, 325(2), pp. 315–324.

Chakraborti, S. *et al.* (2003) 'Regulation of matrix metalloproteinases: an overview', *Molecular and cellular*, 253, pp. 269–285.

Chen, A. C. H. *et al.* (2011) 'Second harmonic generation and multiphoton microscopic detection of collagen without the need for species specific antibodies', *Burns*, 37(6), pp. 1001–1009.

Cheng, V. W. T. and Screen, H. R. C. (2007) 'The micro-structural strain response of tendon', *Journal of Materials Science*, 42(21), pp. 8957–8965.

Clark, J. M. and Glagov, S. (1985) 'Transmural Organization of the Arterial Media The Lamellar Unit Revisited', *Arteriosclerosis*, 5(1), pp. 19–34.

Clayton, R. and Court-Brown, C. (2008) 'The epidemiology of musculoskeletal tendinous and ligamentous injuries.', *Injury*, 39(12), pp. 1338–44.

Corr, D. T. *et al.* (2009) 'Biomechanical behavior of scar tissue and uninjured skin in a porcine model', *Wound Repair and Regeneration*, 17, pp. 250–259.

Corson, G. M. *et al.* (2004) 'Differential expression of fibrillin-3 adds to microfibril variety in human and avian, but not rodent, connective tissues.', *Genomics*, 83(3), pp. 461–72.

Csóka, T. B., Frost, G. I. and Stern, R. (1997) 'Hyaluronidases in tissue invasion', *Invasion Metastasis*, 17, pp. 297–311.

Dakin, S. G. *et al.* (2014) 'Proteomic analysis of tendon extracellular matrix reveals disease stage-specific fragmentation and differential cleavage of COMP (cartilage oligomeric matrix protein)', *Journal of Biological Chemistry*, 289(8), pp. 4919–4927.

Davidsons, J. M. *et al.* (1982) 'Elastin Synthesis in Developing Sheep Nuchal Ligament', *Journal of Biological Chemistry*, 257(2), pp. 747–754.

Dowling, B. A. *et al.* (2002) 'Recombinant equine growth hormone does not affect the in vitro biomechanical properties of equine superficial digital flexor tendon', *Veterinary Surgery*, 31(4), pp. 325–330.

Elliott, D. G. (1965) 'Structue Function of mammalian tendon', *Biol. Rev*, 40, pp. 392–421.

Ely, E. R. *et al.* (2009) 'Descriptive epidemiology of fracture , tendon and suspensory ligament injuries in National Hunt racehorses in training', 41, pp. 372–378.

Fallon, J. *et al.* (2002) 'Functional morphology of the supraspinatus tendon.', *Journal of orthopaedic research : official publication of the Orthopaedic Research Society*, 20(5), pp. 920–6.

Fang, F. and Lake, S. P. (2016) 'Multiscale mechanical integrity of human supraspinatus tendon in shear after elastin depletion', *Journal of the Mechanical Behavior of Biomedical Materials*. Elsevier, 63, pp. 443–455.

Farndale, R. W., Buttle, D. J. and Barrett, A. J. (1986) 'Improved quantitation and discrimination of sulphated glycosaminoglycans by use of dimethylmethylene blue', 883, pp. 173–177.

Fazio, M. J. *et al.* (1991) 'Human Elastin Gene : New Evidence for Localization to the Long Arm of Chromosome 7', *Am. J. Hum. Genet.*, 48, pp. 696–703.

Fenwick, S. A., Hazleman, B. L. and Riley, G. P. (2002) 'The vasculature and its role in the damaged and healing tendon', *Arthritis Research*, 4(4), pp. 252–260.

Foster, J. A. *et al.* (1973) 'Isolation and Amino Acid Sequences of Tropoelastin Peptides.', *J. Biol. Chem.*, 248, pp. 2876–2879.

Foster, J. A. *et al.* (1974) 'Isolation and characterization of crosslinked peptides from elastin.', *J. Biol. Chem.*, 249, pp. 6191–6197.

Franchi, M. *et al.* (2007) 'Crimp morphology in relaxed and stretched rat Achilles tendon.', *Journal of anatomy*, 210(1), pp. 1–7.

Franchi, M. *et al.* (2010) 'Tendon and ligament fibrillar crimps give rise to left-handed helices of collagen fibrils in both planar and helical crimps', *Journal of Anatomy*, 216, pp. 301–309.

Funakoshi, T. *et al.* (2010) 'Distribution of lubricin in the ruptured human rotator cuff and biceps tendon: a pilot study.', *Clinical orthopaedics and related research*, 468(6), pp. 1588–99.

Gerard, M. P. *et al.* (2005) 'Effects of recombinant equine growth hormone on in vitro biomechanical properties of the superficial digital flexor tendon of Standardbred yearlings in training.', *Veterinary surgery : VS*, 34(3), pp. 253–9.

Godinho, M. S. C. *et al.* (2017) 'Elastin is Localised to the Interfascicular Matrix of

Energy Storing Tendons and Becomes Increasingly Disorganised With Ageing', *Scientific Reports*, 7(1), p. 9713.

Goodship, A. E. and Birch, H. L. (2005) 'Cross sectional area measurement of tendon and ligament in vitro: a simple, rapid, non-destructive technique.', *Journal of biomechanics*, 38(3), pp. 605–8.

Grant, T. M. *et al.* (2013) 'Elastic fibres are broadly distributed in tendon and highly localized around tenocytes', *Journal of anatomy*, 222(6), pp. 573–579.

Grant, T. M. *et al.* (2015a) 'The Mechanical, Structural, and Compositional Changes of Tendon Exposed to Elastase', *Annals of Biomedical Engineering*, 43(10), pp. 2477–2486.

Greenwald, S. E. (2002) 'Pulse pressure and arterial elasticity.', *QJM : monthly journal of the Association of Physicians*, 95(2), pp. 107–12.

Greenwald, S. E. (2007) 'Ageing of the conduit arteries', *Journal of Pathology*, 211, pp. 157–172.

Gunja-Smith, Z. (1985) 'An Enzyme-Linked lmmunosorbent Assay to Quantitate the Elastin Crosslink Desmosine in Tissue and Urine Samples', *Analytical Biochemistry*, 147, pp. 258–264.

Heinz, A. *et al.* (2011) 'Insights into the degradation of human elastin by matrilysin-1', *Biochimie*, 93(2), pp. 187–194.

Heinz, A. *et al.* (2013) 'In vitro cross-linking of elastin peptides and molecular characterization of the resultant biomaterials', *Biochimica et Biophysica Acta - General Subjects*, 1830(4), pp. 2994–3004.

Henninger, H. B. *et al.* (2013) 'Effect of elastin digestion on the quasi-static tensile response of medial collateral ligament.', *Journal of Orthopaedic Research*, 31(8), pp. 1226–33.

Hess, G. W. (2010) 'Achilles tendon rupture: a review of etiology, population, anatomy, risk factors, and injury prevention.', *Foot & ankle specialist*, 3(1), pp. 29–32.

Hinek, A. (1997) 'Elastin receptor and tropoelastin chaperone.', in Tamburro, A. M. (ed.) *Elastin and Elastic Tissue*., pp. 75–81.

Hinek, A. and Rabinovitch, M. (1994) 'The 67-kDa Elastin-binding Protein Is a Protective Companion of ExtraceUular Insoluble Elastin and Intracellular Tropoelastin', *J. Cell. Biol.*, 126(2), pp. 563–574.

Hirano, E. *et al.* (2007) 'Functional rescue of elastin insufficiency in mice by the human elastin gene: Implications for mouse models of human disease', *Circulation Research*, 101(5), pp. 523–531.

Hirokawa, S. and Hasezaki, H. (2010) 'Model analysis to investigate the contribution of ground substance to ligament stiffening.', *Medical engineering & physics*, 32(6), pp. 610–6.

Hoeve, C. A. J. and Flory, P. J. (1958) 'The Elastic Properties of Elastin', *Journal of the American Chemical Society*, 80(24), pp. 6523–6526.

Huang, T. F., Perry, S. M. and Soslowsky, L. J. (2004) 'The effect of overuse activity on Achilles tendon in an animal model: a biomechanical study.', *Annals of biomedical engineering*, 32(3), pp. 336–41.

Hunt, J. L. and Finkelstein, S. D. (2004) 'Microdissection techniques for molecular testing in surgical pathology', *Archives of Pathology and Laboratory Medicine*, 128(12), pp. 1372–1378.

Indik, Z. *et al.* (1987) 'Alternative splicing of human elastin mRNA indicated by sequence analysis of cloned genomic and complementary DNA', *Proc. Natl. Acad. Sci.*, 84, pp. 5680–5684.

Innes, J. F. and Clegg, P. (2010) ‘Comparative rheumatology: what can be learnt from naturally occurring musculoskeletal disorders in domestic animals?’, *Rheumatology*, 49(6), pp. 1030–9.

Ito, S., Ishimaru, S. and Wilson, S. E. (1998) ‘Effect of coacervated α-elastin on proliferation of vascular smooth muscle and endothelial cells’, *Angiology*, 49(4), pp. 289–297.

Jacob, M. P. and Hornebeck, W. (1985) ‘Isolation and characterization of insoluble and kappa-elastins’, *Front. Matrix Biol.*, 10, pp. 92–129.

Jacobs, N. T. *et al.* (2012) ‘Effect of orientation and targeted extracellular matrix degradation on annulus fibrosus shear mechanical properties’, *J Mech Behav Biomed Mater*, 4(8), pp. 1611–1619.

Järvinen, T. H. *et al.* (2005) ‘Achilles tendon disorders: etiology and epidemiology.’, *Foot and ankle clinics*, 10(2), pp. 255–66.

Jelinsky, S. A. *et al.* (2008) ‘Gene expression in rat supraspinatus tendon recovers from overuse with rest.’, *Clinical orthopaedics and related research*, 466(7), pp. 1612–7.

Kannus, P. *et al.* (1989) ‘Sports injuries in elderly athletes: a three-year prospective, controlled study.’, *Age and ageing*, 18, pp. 263–270.

Kannus, P. (2000) ‘Structure of the tendon connective tissue.’, *Scandinavian journal of medicine & science in sports*, 10(6), pp. 312–20.

Kasashima, Y. *et al.* (2004) ‘Prevalence of superficial digital flexor tendonitis and suspensory desmitis in Japanese Thoroughbred flat racehorses in 1999.’, *Equine veterinary journal*, 36(4), pp. 346–50.

Kastelic, J., Galeski, A. and Baer, E. (1978) ‘The multicomposite structure of tendon’, *Connective Tissue Research*, 6, pp. 11–23.

Kear, M. and Smith, R. N. (1975) ‘A method for recording tendon strain in sheep during locomotion’, *Acta Orthop. Scand*, pp. 896–905.

Keeley, F., Bellingham, C. and Woodhouse, K. (2002) ‘Elastin as a self-organizing biomaterial: use of recombinantly expressed human elastin polypeptides as a model for investigations of structure and self-assembly of elastin.’, *Philosophical transactions of the Royal Society of London. Series B, Biological sciences*, 357, pp. 185–189.

Ker, R. (2007) ‘Mechanics of tendon, from an engineering perspective’, *International Journal of Fatigue*, 29(6), pp. 1001–1009.

Khan, K. M. *et al.* (1999) ‘Histopathology of common tendinopathies. Update and implications for clinical management.’, *Sports medicine*, 27(6), pp. 393–408.

Khodabakhshi, G. *et al.* (2013) ‘Measuring three-dimensional strain distribution in tendon.’, *Journal of microscopy*, 249(3), pp. 195–205.

Kielty, C., Sherratt, M. and Shuttleworth, C. (2002) ‘Elastic fibres’, *J. Cell Sci.*, 115, pp. 2817–2828.

Kim, Y.-J. *et al.* (1988) ‘Fluorometric assay of DNA in cartilage explants using Hoechst 33258’, *Analytical Biochemistry*, 174(1), pp. 168–176.

Kjaer, M. (2004) ‘Role of extracellular matrix in adaptation of tendon and skeletal muscle to mechanical loading.’, *Physiological reviews*, 84(2), pp. 649–98.

Knobloch, K., Yoon, U. and Vogt, P. M. (2008) ‘Acute and Overuse Injuries Correlated to Hours of Training in Master Running Athletes’, *Foot & Ankle International*, 29(7), pp. 671–676.

Kohrs, R. T. *et al.* (2011) ‘Tendon fascicle gliding in wild type, heterozygous, and lubricin knockout mice.’, *Journal of orthopaedic research : official publication of the Orthopaedic Research Society*, 29(3), pp. 384–9.

Kubo, K. *et al.* (2002) 'Measurement of viscoelastic properties of tendon structures in vivo.', *Scandinavian journal of medicine & science in sports*, 12(1), pp. 3–8.

Lee, T. C. *et al.* (2001) 'The effect of elastin damage on the mechanics of the aortic valve', *Journal of Biomechanics*, 34, pp. 203–210.

Legerlotz, K., Riley, G. P. and Screen, H. R. C. (2010) 'Specimen dimensions influence the measurement of material properties in tendon fascicles.', *Journal of biomechanics*. Elsevier, 43(12), pp. 2274–80.

Legerlotz, K., Riley, G. P. and Screen, H. R. C. (2013) 'GAG depletion increases the stress-relaxation response of tendon fascicles, but does not influence recovery.', *Acta biomaterialia*, 9(6), pp. 6860–6.

Lichtwark, G. A. and Wilson, A. M. (2007) 'Is Achilles tendon compliance optimised for maximum muscle efficiency during locomotion?', *Journal of biomechanics*, 40(8), pp. 1768–75.

Lichtwark, G. A. and Wilson, A. M. (2005) 'In vivo mechanical properties of the human Achilles tendon during one-legged hopping.', *The Journal of experimental biology*, 208(Pt 24), pp. 4715–25.

Liu, Z. (1991) 'Scale space approach to directional analysis of images', *Applied Optics*, 30(11), pp. 1369–1373.

Lui, P. P. Y. *et al.* (2011) 'What are the validated animal models for tendinopathy?', *Scandinavian journal of medicine & science in sports*, 21(1), pp. 3–17.

Luisetti, M. *et al.* (2008) 'Desmosine as a biomarker of elastin degradation in COPD: current status and future directions', *European Respiratory Journal*, 32(5), pp. 1146–1157.

Lujan, T. J. *et al.* (2009) 'Contribution of glycosaminoglycans to viscoelastic tensile behavior of human ligament.', *Journal of Applied Physiology*, 106(2), pp. 423–31.

Ma, Y. *et al.* (2014) 'Generating rats with conditional alleles using CRISPR/Cas9', *Cell Research*, 24(1), pp. 122–125.

Maganaris, C. N. and Paul, J. P. (1999) 'In vivo human tendon mechanical properties', *J Physiol*, 521.1, pp. 307–313.

Markarian, G. G. *et al.* (1998) 'Anterior tibialis tendon ruptures: an outcome analysis of operative versus nonoperative treatment.', *Foot & Ankle International*, 19, pp. 792–802.

Mauch, J. C. *et al.* (1994) 'Extensive alternate exon usage at the 5th end of the sheep tropoelastin gene', *Matrix Biol.*, 14, pp. 635–641.

Midwood, K. S. and Schwarzbauer, J. E. (2002) 'Elastic Fibers : Building Bridges Between Cells and Their Matrix.', *Current Biology*, 12(2), pp. 279–281.

Millesi, H. *et al.* (1995) 'Biomechanical properties of normal tendons, normal palmar aponeuroses and palmar aponeuroses from patients with dupuytren's disease subjected to elastase and chondroitinase treatment', *Connective Tissue Research*, 31(2), pp. 109–115.

Montes, G. S. (1996) 'Structural biology of the fibres of the collagenous and elastic systems.', *Cell biology international*, 20(1), pp. 15–27.

Nimeskern, L. *et al.* (2016) 'Tissue composition regulates distinct viscoelastic responses in auricular and articular cartilage', *Journal of Biomechanics*, 49(3), pp. 344–352.

O'Rourke, M. and Hashimoto, J. (2007) 'Mechanical Factors in Arterial Aging. A Clinical Perspective', *Journal of the American College of Cardiology*, 50(1), pp. 1–13.

Oxlund, H., Manschot, J. and Vhdik, A. (1988) 'The role of elastin in the mechanical properties of skin', *Journal of biomechanics*, 21(3), pp. 213–218.

Pang, X. *et al.* (2016) 'The three dimensional microstructural network of elastin, collagen and cells in Achilles tendons', *Journal of Orthopaedic Research.*, 35(6):1203-1214.

Pappas, C. T. *et al.* (2018) "Cardiac-specific knockout of Lmod2 results in a severe reduction in myofilament force production and rapid cardiac failure.", *Journal of Molecular and Cellular Cardiology*, 122:88-97

Parry, D. A. and Craig, A. S. (1978) 'Collagen fibrils and elastic fibers in rat-tail tendon: an electron microscopic investigation.', *Biopolymers*, 17(3), pp. 843–845.

Pierce, J. A. and Hocott J B (1960) 'Studies on the collagen and elastin content of the human lung.', *J. Clin. Invest.*, 39, pp. 8–14.

Press, A. I. N. (2005) 'Multiphoton autofluorescence imaging of intratissue elastic fibers', *J Biomaterials*, 26, pp. 495–500.

Raju, K. and Anwar, R. A. (1987) 'Primary Structures of Bovine Elastin a, b, and c deduced from the sequences of cDNA clones', *J. Biol. Chem.*, 262, pp. 5755–5762.

Ramirez, F. and Pereira, L. (1999) 'The fibrillins.', *Int J Biochem Cell Biol*, 31, pp. 255–259.

Rees, S. G. *et al.* (2000) 'Catabolism of aggrecan, decorin and biglycan in tendon', *Biochem J.*, 188, pp. 181–188.

Reiser, K., McCormick, R. J. and Rucker, R. B. (1992) 'Enzymatic and nonenzymatic cross-linking of collagen and elastin.', *The FASEB journal : official publication of the Federation of American Societies for Experimental Biology*, 6, pp. 2439–2449.

Riemersa, D. J. and Schamhardt, H. C. (1982) 'The cryo-jaw, a clamp designed for in vitro rheology studies of horse digital flexor tendons', *Journal of Biomechanics*, 15(8), pp. 619–620.

Riley, G. (2004) 'The pathogenesis of tendinopathy. A molecular perspective', *Rheumatology*, 43(2), pp. 131–142.

Riley, G. (2008) 'Tendinopathy-from basic science to treatment.', *Nature clinical practice. Rheumatology*, 4(2), pp. 82–9.

Ritty, T. M., Roth, R. and Heuser, J. E. (2003) 'Tendon cell array isolation reveals a previously unknown fibrillin-2-containing macromolecular assembly', *Structure*, 11(9), pp. 1179–1188.

Ritz-Timme, S., Laumeier, I. and Collins, M. (2003) 'Aspartic acid racemization in human skin elastin: evidence for marked longevity of elastin in human skin', *British Journal of Dermatology*, 149, pp. 951–959.

Rnjak, J. *et al.* (2009) 'Primary human dermal fibroblast interactions with open weave three-dimensional scaffolds prepared from synthetic human elastin', *Biomaterials.*, 30(32), pp. 6469–6477.

Robert, L., Robert, A. M. and Fu, T. (2008) 'Rapid increase in human life expectancy : will it soon be limited by the aging of elastin ?', *Biogerontology*, 9, pp. 119–133.

Robinson, P. S. *et al.* (2005) 'Influence of Decorin and Biglycan on Mechanical Properties of Multiple Tendons in Knockout Mice', *Journal of Biomechanical Engineering*, 127(1), p. 181.

Ronchetti, I. P. *et al.* (1998) 'Study of Elastic Fiber Organization by Scanning Force Microscopy', *Matrix Biol*, 17, pp. 75–83.

Rousseau, R. *et al.* (2004) 'Temperature-Dependent Conformational Transitions and Hydrogen-Bond Dynamics of the Elastin-Like Octapeptide GVG(VPGVG): A Molecular-Dynamics Study', *Biophysical Journal.*, 86(3), pp. 1393–1407.

Schindelin, J. *et al.* (2013) 'Fiji - an Open Source platform for biological image analysis', *Nat Methods.*, 9(7).

Scott, J. E. (1995) 'Extracellular matrix, supramolecular organisation and shape.',

Journal of anatomy, 187, pp. 259–69.

Screen, H. R. C. *et al.* (2004) 'Local Strain Measurement within Tendon', *Strain*, 40(4), pp. 157–163.

Screen, H. R. C. *et al.* (2005) 'The influence of noncollagenous matrix components on the micromechanical environment of tendon fascicles.', *Annals of biomedical engineering*, 33(8), pp. 1090–9.

Screen, H. R. C. *et al.* (2015) 'Tendon Functional Extracellular Matrix', *Journal of Orthopaedic Research*, 33(6):793-9

Shepherd, J. H. and Screen, H. R. C. (2013) 'Fatigue loading of tendon.', *International journal of experimental pathology*, 94(4), pp. 260–70.

Sherratt, M. J. (2009) 'Tissue elasticity and the ageing elastic fibre.', *Age*, 31(4), pp. 305–25.

Sims, T. *et al.* (1996) 'The role of glycation cross-links in diabetic vascular stiffening', *Diabetologia*, 39, pp. 946–951.

Sivan, S. *et al.* (2008) 'Collagen turnover in normal and degenerate human intervertebral discs as determined by the racemization of aspartic acid', *Journal of Biological Chemistry*, 283(14), pp. 8796–8801.

Smith, K. D. *et al.* (2011) 'The organisation of elastin and fibrillins 1 and 2 in the cruciate ligament complex.', *Journal of Anatomy*, 218(6), pp. 600–7.

Smith, K. D. *et al.* (2014) 'Elastin content is high in the canine cruciate ligament and is associated with degeneration', *The Veterinary Journal*, 199(1), pp. 169–174.

Smith, L. J. *et al.* (2008) 'Elastic fibers enhance the mechanical integrity of the human lumbar anulus fibrosus in the radial direction.', *Annals of Biomedical Engineering*, 36(2), pp. 214–23.

Smith, R. K. *et al.* (2002a) 'The influence of ageing and exercise on tendon growth and degeneration — hypotheses for the initiation and prevention of strain', *Comp. Biochem. Physiol. A Mol. Tntegr. Physiol.*, 133, pp. 1039–1050.

Smith, R. K. W. *et al.* (2002b) 'Correlation of cartilage oligomeric matrix protein (COMP) levels in equine tendon with mechanical properties: a proposed role for COMP in determining function-specific mechanical characteristics of locomotor tendons.', *Equine veterinary journal. Supplement*, 34(34), pp. 241–4.

Soslowsky, L. J. *et al.* (2000) 'Neer Award 1999: Overuse activity injures the supraspinatus tendon in an animal model: A histologic and biomechanical study', *Journal of Shoulder and Elbow Surgery*, 9(2), pp. 79–84.

Spiesz, E. M. *et al.* (2015) 'Tendon extracellular matrix damage, degradation and inflammation in response to in-vitro overload exercise', *Journal of Orthopaedic Research*. 33(6):889-97.

Stephens, P. R., Nunamaker, D. M. and Butterweck, D. M. (1989) 'Application of a Hall-effect transducer for measurement of tendon strains in horses.', *American Journal of Veterinary Research*, 50, pp. 1089–1095.

Sullo, A. *et al.* (2001) 'The effects of prolonged peritendinous administration of PGE1 to the rat Achilles tendon: a possible animal model of chronic Achilles tendinopathy', *Journal of orthopaedic science : official journal of the Japanese Orthopaedic Association*, 6(4), pp. 349–57.

Swee, M. H. *et al.* (1995) 'Developmental Regulation of Elastin production', *J. Biol. Chem*, pp. 14899–14906.

Tarakanova, A. and Buehler, M. J. (2013) 'Molecular modeling of protein materials: Case study of elastin', *Modelling and Simulation in Materials Science and Engineering*, 21(6).

Tempelhof, S., Rupp, S. and Seil, R. (1999) 'Age-Related prevalence of rotator cuff tears in asymptomatic shoulders', *Journal of Shoulder and Elbow Surgery*, 8(4), pp. 296–299.

Tempfer, H. and Traweger, A. (2015) 'Tendon vasculature in health and disease', *Frontiers in Physiology*, 6, pp. 1–7.

Thorpe, C. T. *et al.* (2010b) 'Aspartic acid racemization and collagen degradation markers reveal an accumulation of damage in tendon collagen that is enhanced with aging', *The Journal of biological chemistry*, 285(21), pp. 15674–81.

Thorpe, C. T. *et al.* (2012) 'Specialization of tendon mechanical properties results from interfascicular differences.', *Journal of the Royal Society*, 9(76), pp. 3108–17.

Thorpe, C. T. *et al.* (2013a) 'Capacity for sliding between tendon fascicles decreases with ageing in injury prone equine tendons: a possible mechanism for age-related tendinopathy?', *European cells & materials*, 25(0), pp. 48–60.

Thorpe, C. T. *et al.* (2013b) 'Helical sub-structures in energy-storing tendons provide a possible mechanism for efficient energy storage and return.', *Acta biomaterialia*, 9(8), pp. 7948–7956.

Thorpe, C. T. *et al.* (2013c) 'The role of the non-collagenous matrix in tendon function.', *International journal of experimental pathology*, 94(4), pp. 248–59.

Thorpe, C. T. *et al.* (2014) 'Fascicles from energy-storing tendons show an age-specific response to cyclic fatigue loading', *Journal of the Royal Society*, 11: 201310.

Thorpe, C. T. *et al.* (2015c) 'The interfascicular matrix enables fascicle sliding and recovery in tendon, and behaves more elastically in energy storing tendons', *Journal of the Mechanical Behavior of Biomedical Materials*, 52, pp. 85–94.

Thorpe, C. T. *et al.* (2015b) 'Tendon overload results in alterations in cell shape and increased markers of inflammation and matrix degradation', *Scandinavian Journal of Medicine & Science in Sports*, 25(4):e381-91.

Thorpe, C. T. *et al.* (2015a) *Tendon Physiology and Mechanical Behavior: Structure–Function Relationships*. 1st Edition. Academic Press.

Thorpe, C. T. *et al.* (2016c) 'Anatomical heterogeneity of tendon : Fascicular and interfascicular tendon compartments have distinct proteomic composition', *Scientific Reports*, 6, p. 20455.

Thorpe, C. T. *et al.* (2016a) 'Distribution of proteins within different compartments of tendon varies according to tendon type', *J. Anat.*, 229(3), pp. 450–458.

Thorpe, C. T. *et al.* (2016b) 'Fascicles and the interfascicular matrix show adaptation for fatigue resistance in energy storing tendons', *Acta Biomaterialia*, 42, pp. 308–315.

Thorpe, C. T. *et al.* (2017) 'Fascicles and the interfascicular matrix show decreased fatigue life with ageing in energy storing tendons', *Acta Biomaterialia*, 56, pp. 58–64.

Thorpe, C. T., Clegg, P. D. and Birch, H. L. (2010a) 'A review of tendon injury: why is the equine superficial digital flexor tendon most at risk?', *Equine veterinary journal*, 42(2), pp. 174–80.

Toonkool, P. *et al.* (2006) 'Thermodynamic and hydrodynamic properties of human tropoelastin. Analytical ultracentrifuge and pulsed field-gradient spin-echo NMR studies.', *J. Biol. Chem.*, 276, pp. 28042–28050.

Tsuruga, E., Irie, K. and Yajima, T. (2007) 'Fibrillin-2 degradation by matrix metalloproteinase-2 in periodontium.', *Journal of dental research*, 86(4), pp. 352–356.

Umeda, H., Nakamura, F. and Suyama, K. (2001) 'Oxodesmosine and isooxodesmosine, candidates of oxidative metabolic intermediates of pyridinium cross-links in elastin.', *Archives of biochemistry and biophysics*, 385(1), pp. 209–219.

Vassalli, M. *et al.* (2013) 'Biological and structural characterization of a naturally inspired material engineered from elastin as a candidate for tissue engineering applications', *Langmuir*, 29(51), pp. 15898–15906.

Venkatachalam, C. M. *et al.* (1981) 'Nuclear Magnetic Resonance and Conformational Energy Calculations of Repeat Peptides of Elastin. Conformational Characterization of Cyclopentadecapeptide cyclo-(L-V al-L-Pro-Gly-L-V al-Gly)', *Journal of the American Chemical Society*, 103(9), pp. 2372–2379.

Verzijl, N. *et al.* (2000) 'Effect of collagen turnover on the accumulation of advanced glycation end products', *Journal of Biological Chemistry*, 275(50), pp. 39027–39031.

Viera, A. J. and Garrett, J. M. (2005) 'Understanding Interobserver Agreement : The Kappa Statistic', *Fam Med*, 37(5), pp. 360–363.

Vrhovski, B. and Weiss, A. S. (1998) 'Review: Biochemistry of tropoelastin', *Eur J Biochemi*, 258, pp. 1–18.

Wagenseil, J. E. *et al.* (2005) 'Effects of elastin haploinsufficiency on the mehcanical behavior of Mouse Arteries', *Am J Physiol Heart Circ Physiol*, 289(3):H1209-17.

Wagenseil, J. E. and Mecham, R. P. (2013) 'Elastin in large artery stiffness and hypertension', *Journal Cardiovascular Trans Res*, 5(3), pp. 264–273.

Waller, K. a *et al.* (2013) 'Role of lubricin and boundary lubrication in the prevention of chondrocyte apoptosis.', *Proceedings of the National Academy of Sciences of the United States of America*, 110(15), pp. 5852–7.

Watanabe, T. *et al.* (1989) 'An enzyme-linked immunosorbent assay (ELISA) for the quantitation of urinary desmosine.', *Tokai J Exp Clin Med*, 14, pp. 347–356.

Williams, R. B. *et al.* (2001) 'Racehorse injuries, clinical problems and fatalities recorded on British racecourses from flat racing and National Hunt racing during 1996, 1997 and 1998.', *Equine veterinary journal*, 33(5), pp. 478–86.

Wolinsky, H. and Glagov, S. (1964) 'Structural Basis for the Static Mechanical Properties of the Aortic Media', *Circ. Res.*, 14, pp. 400–413.

Wydner, K. S. *et al.* (1994) 'Use of an Intron Length Polymorphism to Localize the Tropoelastin Gene to Mouse Chromosome 5 in a Region of Linkage Conservation with Human Chromosome 7.pdf', *Genomics*, 23, pp. 125–131.

Yoon, J. H. and Halper, J. (2005) 'Tendon proteoglycans: Biochemistry and function', *Journal of Musculoskeletal Neuronal Interactions*, 5(1), pp. 22–34.

Zhang, H., Hu, W. and Ramirez, F. (1995) 'Developmental Expression of Fibrillin Genes Suggests Heterogeneity of Extracellular Microfibrils', *J Cell Biol*, 129(4), pp. 1165–1176.

Zócalo, Y. *et al.* (2013) 'Structural and Functional Properties of Venous Wall: Relationship between Elastin, Collagen, and Smooth Muscle Components and Viscoelastic Properties', *ISRN Physiology*, 2013, pp. 1–9.

Appendixes

Appendix A – List of Materials used and Respective Details

Table 8 – List of some of the materials used for both immunohistochemical and biochemical analysis with details regarding the supplier, catalogue and batch numbers.

Product	Supplier	Catalogue Number	Batch Number
Immunohistochemical Analysis			
Isotype Control Mouse IgG1	Sigma	M5284 - 1mg	066M4750V
Alexa Fluor 488 Goat Anti rabbit	Life Technologies	A11008	1678787
Alexa Fluor 555 Goat Anti-Mouse IgG	Life Technologies	A21424	1691772
Hyaluronidase from Bovine	Sigma	H3884-100mg	SLBL6343V
OCT	Thermo Scientific	LAMB/OCT	3803431
ProLong Gold antifade reagent with DAPI	Life Technologies	P36931	1506916
Mowiol 4-88	Sigma	81381-50g	BCBL8261V
Biochemical Analysis			
Elastase	Elastin Products Company	EC134	1335
Soybean Trypsin Inhibitor	Roche Diagnostics GmbH	10109886001	19752620
Complete Mini Protease Inhibitor Cocktail	Roche Diagnostics GmbH	11836153001	10948000
DESMOSINE ELISA Kit	B.I.T.S.	BDEXV1	MJ311016
Papain from papaya latex	Sigma	P3125-100mg	SLB6471V
Guanidine Hydrochloride	Sigma	G3272-100g	SLBJ2599V
L-Cysteine Hydrochloride	Sigma	C7477-25g	1436197

Appendix B - Protocols

B1. Fastin Elastin Assay – Finalised Protocol

Tendon elastin was quantified using the FASTIN^{TM} Elastin Assay (Biocolor, UK). Before the assay could be performed, the native hydrophobic elastin in the powdered, lyophilised samples (~3 mg dry weight) required conversion into the water soluble derivate α-elastin. The conversion was achieved by heating the samples to 100 °C for 2 one hour periods with 750 µl of 0.25 M oxalic acid to guarantee complete solubilisation of the tissue elastin. Preliminary tests were performed to determine that two extractions were sufficient to solubilise all elastin. After each test sample extraction, the tubes were allowed to cool down for about 10 min and then centrifuged at 10000rpm for 10 min. The supernatant was then pipetted off to a 1.5ml Eppendorf. Tubes were weighted before and after the liquid removal. As explained before, to the residual tissue in the tubes was added a further 750µl of 0.25M oxalic acid and another extraction was performed.

After the extractions, the tissue elastin was in the form of α-elastin, which has a molecular weight range of 60-84 KDa. Thus, the extract (supernatant) could be directly assayed using the procedure described for soluble elastin (Fastin Elastin Assay Kit, Biocolour, UK). α-elastin standards, with concentrations from 0-90 µg/ml, were prepared in duplicate using a 1mg/ml α-elastin standard solution (Biocolor, UK). To each tube, including test samples, sample blank and standards, was added an equal volume of Elastin Precipitating Reagent.

Tubes were briefly vortex to mix contents and left for 15 minutes to complete the precipitation of –αelastin. Then, tubes were centrifuge at 9500 rpm for 10 min and the liquid was drained into a beaker. After removing the majority of the liquid by inverting the tubes, the remaining liquid was removed from each tube using thin strips of filter paper. Then, to each tube 1.00 ml of Dye Reagent was added and tubes were briefly vortex and placed on a mechanical shaker for 90 min to allow reaction between the –αelastin and the dye. Once again, tubes were then centrifuge at 9500 rpm for 10 min. All tubes were drained from unbound dye by inverting the tube and the remaining liquid was removed as previously described, by using thin strips of filter paper. The elastin-dye complex could be observed as a reddish-brown deposit in the bottom and inside lower wall of the tubes. Finally, to each tube was then added 250µl of

Dissociation Reagent. Tubes were vortexed twice every 10 min to ensure that all bound dye has passed into solution. The tube's content was transferred (200μl) to a 96 well flat bottom microwell plate, placed into a Spectrophotometer (SPECTROstar Nano) and absorbance was measured at 513 nm. Elastin concentration was calculated by comparison to a standard curve, generated by the α-elastin standards and it was expressed as a percentage of dry weight tendon tissue.

B2. Preparation of Mowiol Mounting Medium

For the preparation of the Mowiol mounting medium, a 50ml plastic centrifuge tube was used. 6g of glycerol and 2.4g of Mowiol 4-88 were mixed together, using a stirrer. While stirring, 6ml of distilled water was added and the solution was left stirring for 2hours at room temperature. 12ml 0.2M Tris (pH 8.5) was added to the mixture and incubated in a hot water bath (50-60°C) for 10 minutes. The solution was centrifuged for 15min at 5000g to remove any undissolved solid parts, transferred to 1ml aliquots, and stored in the freezer until required. When required, tubes were removed from the freezer and allowed to thaw at room temperature.

B3. Elastin Immunostaining – Finalised Protocol

For elastin immunostaining, previously prepared longitudinal and transverse cryosections (Chapter 2), were allowed to thaw for 1 minute, before fixing with ice-cold methanol (−20 °C) for 20 minutes. Slides were rinsed 3 times in phosphate-buffered saline (PBS), treated with hyaluronidase (Sigma, H3884) (4800 units/ml in PBS containing protease inhibitor cocktail (complete mini, Roche)) to increase tissue permeability (Csóka et al. 1997), and incubated over night at room temperature. Cryosections were washed 3 times in PBS and incubated in blocking buffer (10% goat serum in PBS) for 1 hour at room temperature. They were then drained and incubated in the primary antibody. Elastin primary antibody ab9519 (Abcam Cambridge, UK) was diluted in 5% goat serum in PBS (1:100) and applied to different sections (approximately 100ul of antibody per section) before incubation overnight at 4 °C. After overnight incubation, sections were washed in PBS and incubated with Alexa Fluor 555 Goat anti-Mouse IgG Secondary Antibody diluted in 5% goat serum (1:500 dilution) for 1 h at room temperature (protected from light). Finally, sections were washed and mounted with ProLong Gold Antifade reagent with 4′,6-diamidino-2-phenylindole (DAPI), and allowed to cure overnight, at 4 °C in the dark, before being sealed with nail polish and imaged. Imaging was performed on a confocal microscope (Leica TCS SP2) using × 40 (oil) objective.

Appendix C – MATLAB Code

C1 – IFM recoil ability – Angle Deviation Calculation

C1.1 MATLAB code "Find_Marker"

Credit to Dr. Wing Keung Cheung (Screen's Group)

```
function [crop_A, Label, s] = find_marker(Image)
A = imread(Image);
 crop_A = rgb2gray(A);
 crop_A = imgaussfilt(crop_A, 1,'FilterSize',[3 3]);
BW = imbinarize(crop_A,'adaptive','ForegroundPolarity','dark','Sensitivity',0.1);
 BW = abs(int8(BW)-1);
CC = bwconncomp(BW);
numPixels = cellfun(@numel,CC.PixelIdxList);
for i=1:length(numPixels)
    if (numPixels(i)<=25)
        BW(CC.PixelIdxList{i}) = 0;
    end
end
[Label,Total]=bwlabel(BW,8);
marker_margin = 10;
check_merge = 1;
while (check_merge == 1)
    check_merge = 0;
    s = regionprops(Label,'BoundingBox');
    boundingboxes = cat(1, s.BoundingBox);
    paired_index = [];
    total_merge = 0;
    for (i=1:Total)
        for (j=i+1:Total)
            check_margin = (boundingboxes(j,1) - boundingboxes(i,1)) -
boundingboxes(i,3);
            if (check_margin <= marker_margin)
                paired_index = [paired_index; [i j]];
                total_merge = total_merge + 1;
                check_merge = 1;
            end
        end
    end
    if (total_merge > 0)
        for (k=1:size(paired_index,1))
            Label = changem(Label,paired_index(k,1),paired_index(k,2));
        end
        Total = Total - total_merge;
    end
end
s = regionprops(Label,'all');
checkloop = size(s,1);
i=1;
while (i <= checkloop)
    for (j=1:size(s,1))
        if (s(j).Area == 0)
            s(j) = [];
            break;
        end
    end
    i=i+1;
end
centroids = cat(1, s.Centroid);
boundingboxes = cat(1, s.BoundingBox);
for (jj=1:size(s,1))
    idx = s(jj).PixelList;
    sorted_idx = sortrows(idx,2);
    check_value = sorted_idx(1,2);
    counter = 0;
    sum_x = 0;
    avg_x = [];
    for ii=1:length(sorted_idx)
```

```
        if (check_value == sorted_idx(ii,2))
            sum_x = sum_x + sorted_idx(ii,1);
            counter = counter + 1;
        else
            avg_x = [avg_x ; [sorted_idx(ii-1,2) sum_x/counter]];
            check_value = sorted_idx(ii,2);
            counter = 1;
            sum_x = sorted_idx(ii,1);
        end
        if (ii == length(sorted_idx))
            avg_x = [avg_x ; [sorted_idx(ii,2) sum_x/counter]];
        end
    end
    p = polyfit(avg_x(:,1),avg_x(:,2),1);
    min_x = min(avg_x(:,1));
    max_x = max(avg_x(:,1));
    x_range = min_x:0.5:max_x;
    x_range = x_range';
    interpolated_x = [x_range x_range*p(1)+p(2)];
    s(jj).average_x = avg_x;
    s(jj).slope = -p(1);
    s(jj).interpolated_x = interpolated_x;
end
```

C1.2. MATLAB Code "Image_Analysis"

Credit to Dr. Wing Keung Cheung (Screen's Group)

```
clear;
folder_name = uigetdir;
imagefiles = dir(fullfile(folder_name, '*.jpg'));
nfiles = length(imagefiles);
 for ii=1:nfiles
    currentfilename = imagefiles(ii).name;
    result(ii).name =  currentfilename;
    [result(ii).image, result(ii).label, result(ii).all] =
find_marker(fullfile(folder_name,currentfilename));
end
average_displacement_deviation = zeros(nfiles-1,size(result(ii).all,1));
displacement_deviation = zeros(nfiles-1,size(result(ii).all,1));
slope_deviation = zeros(nfiles-1,size(result(ii).all,1));
angle_deviation = zeros(nfiles-1,size(result(ii).all,1));
 for ii=1:nfiles
    for jj=1:size(result(ii).all,1)
        min_y(ii,jj) = result(ii).all(jj).interpolated_x(1,1);
        max_y(ii,jj) = result(ii).all(jj).interpolated_x(end,1);
    end
end
 sorted_min_y = sort(min_y);
sorted_max_y = sort(max_y);
 marker_min_y = sorted_min_y(end,:);
marker_max_y = sorted_max_y(1,:);
 for ii=2:nfiles
    for jj=1:size(result(ii).all,1)

        ref_min_y_indices = find(result(1).all(jj).interpolated_x(:,1)==
marker_min_y(jj));
        ref_max_y_indices = find(result(1).all(jj).interpolated_x(:,1)==
marker_max_y(jj));

        min_y_indices = find(result(ii).all(jj).interpolated_x(:,1)==
marker_min_y(jj));
        max_y_indices = find(result(ii).all(jj).interpolated_x(:,1)==
marker_max_y(jj));

        total_rows = max_y_indices-min_y_indices+1;

        displacement_deviation(ii-1,jj) =
sum(abs(result(ii).all(jj).interpolated_x(min_y_indices:max_y_indices,2)-
result(1).all(jj).interpolated_x(ref_min_y_indices:ref_max_y_indices,2)));

        average_displacement_deviation(ii-1,jj) = displacement_deviation(ii-1,jj) /
total_rows;

        slope_deviation(ii-1,jj) = (result(ii).all(jj).slope -
result(1).all(jj).slope);

        angle_deviation(ii-1,jj) = (rad2deg(atan(result(ii).all(jj).slope)) -
rad2deg(atan(result(1).all(jj).slope)));
    end
end

average_displacement_deviation
displacement_deviation
slope_deviation
angle_deviation

figure;
for ii=1:nfiles


    subplot(3,nfiles, ii),
    imagesc(result(ii).image);
    title(result(ii).name, 'Interpreter', 'none');
    colormap('gray');

    subplot(3,nfiles, ii+(nfiles)),
    imagesc(result(ii).label);
```

```
    title('Average X position', 'Interpreter', 'none');

    hold on

    centroids = cat(1, result(ii).all.Centroid);
    boundingboxes = cat(1, result(ii).all.BoundingBox);

    plot(centroids(:,1),centroids(:,2), 'r*');

    for k = 1:size(boundingboxes,1)

        rectangle('position',boundingboxes(k,:),'Edgecolor','y');

        plot(result(ii).all(k).average_x(:,2),result(ii).all(k).average_x(:,1), '.g')

    end
    hold off

    subplot(3,nfiles,ii+(2*nfiles)),
    imagesc(result(ii).label);
    title('Interpolated Line', 'Interpreter', 'none');

    hold on

    plot(centroids(:,1),centroids(:,2), 'r*')

    for k = 1:size(result(ii).all,1)

        rectangle('position',boundingboxes(k,:),'Edgecolor','y'

plot(result(ii).all(k).interpolated_x(:,2),result(ii).all(k).interpolated_x(:,1), '-
b')

    end

    hold off

end

figure;
for ii=2:nfiles

    subplot(nfiles-1,1,ii-1),
    [m,n]= size(result(1).image);
    set(gca,'Color','k')
    set(gca,'Ydir','reverse');
    xlim([0 n]);
    ylim([0 m]);
    set(gca,'XTick',(0:50:n));
    set(gca,'YTick',(0:20:m));

    [B] = bwboundaries(result(1).label);
    hold on
    for k = 1:length(B)
        boundary = B{k};
        plot(boundary(:,2),(boundary(:,1)), 'r', 'LineWidth', 1);
    end

    [B] = bwboundaries(result(ii).label);
    for k = 1:length(B)
        boundary = B{k};
        plot(boundary(:,2),(boundary(:,1)), 'b', 'LineWidth', 1);
    end

    figure_number = ii-1;
    title(['Overlaid Interpolated Line (Ref [red] vs Set ',num2str(figure_number),'
[blue])']);

    hold on

    for k = 1:size(result(ii).all,1)

plot(result(ii).all(k).interpolated_x(:,2),result(ii).all(k).interpolated_x(:,1), '-
b')

    end
```

```
    for k = 1:size(result(1).all,1)
plot(result(1).all(k).interpolated_x(:,2),result(1).all(k).interpolated_x(:,1), '-r')
    end
    hold off
end
```